Spreading Speeds and Travelling Waves in Integrodifference Equations with Overcompensatory Dynamics

Adèle Bourgeois

Thesis submitted to the Faculty of Graduate and Postdoctoral Studies in partial fulfillment of the requirements for the degree of
Master of Science in Mathematics[1]

Department of Mathematics and Statistics
Faculty of Science
University of Ottawa

[1]The M.Sc. program is a joint program with Carleton University, administered by the Ottawa-Carleton Institute of Mathematics and Statistics

Abstract

We consider integrodifference equations (IDEs), which are of the form

$$N_{t+1}(x) = \int K(x-y)F(N_t(y))dy,$$

where K is a probability distribution and F is a growth function. It is already known that for monotone growth functions, solutions of the IDE will have spreading speeds and are sometimes in the form of travelling waves. We are interested in the case where F has a stable 2-point cycle, namely for the Ricker function and the logistic function [22]. It was claimed in [14] that the solution of this IDE alternates between two profiles, all the while moving with a certain speed. However, simulations revealed that not only do the profiles alternate, but the solution is a succession of two travelling objects with different speeds. Using the theory from [31], we can prove the existence of two speeds and establish their theoretical formulas. To explain the succession of travelling objects, we relate to the concept of dynamical stabilization [19].

Dedications

To my family, who has always believed in me and encouraged me.

Acknowledgement

I would like to thank my supervisors, Frithjof Lutscher and Victor LeBlanc, for their guidance and support.

Contents

Abbreviations

We provide a small list of abbreviations that are used in the figure and table descriptions in the subsequent pages.

DDE : Delay Differential Equation

DDS : Discrete Dynamical System

FFT : Fast Fourier Transform

IDE : Integrodifference Equation

ODE: Ordinary Differential Equation

List of Figures

List of Tables

Biological Terminology

Population biology is concerned with understanding and predicting how the density of a population changes over time and space. Such predictions can be obtained through a model, such as an integrodifference equation. In this section, we define keywords that are required to define this model. Firstly, we need terminology that describes the said population:

Overlapping generations: Population with more than one breeding generation present at any time.

Non-overlapping generations: Population with only one breeding generation present at any time.

The integrodifference equation takes into account the different aspects of the life cycle for the species studied, as well as environmental limitations, namely:

Growth phase: Period of time during which the individuals of a population reproduce, grow, die.

Intrinsic growth rate: Maximum rate of reproduction per individual in a generation.

Dispersal phase: Period of time during which the individuals of a population relocate from their birth site to their breeding site.

Carrying capacity: The maximum number of individuals that can be supported by the environment.

We also have terminology to describe the way the population grows during the growth phase:

Overcompensation: When after a certain density, the population at the next generation is described by a decreasing function with respect to the current population.

Allee effect: If given low densities, the population at the next generation is described by a convex function with respect to the current population.

Strong Allee effet: When the Allee effect introduces a population threshold, which must be surpassed for the population to grow.

Weak Allee effect: When the Allee effect does not introduce a population growth threshold.

The outcomes of these models can allow to explain certain biological phenomena:

Spread: When the environment occupied by a species is increased due to dispersal.

Speed of spatial spread: Rate at which the spreading of a species occurs.

Invasive species: Species that is not native to the habitat and that causes harm to the environment, human economy and human health by spreading.

Chapter 1

Introduction

Integrodifference equations are discrete-time models that can be used to describe the temporal dynamics of the spatial density of a biological population [15]. These models then allow us to make predictions about the spatial spread of a population. More specifically, integrodifference equations apply to species with non-overlapping generations and distinct growth and dispersal phases (see "Biological Terminology"), which include annual plants and many insects. We denote the spatial density of such a population at the beginning of the t-th generation by $N_t(x)$. The model we will be studying in this thesis describes the dynamics from one generation to the next by:

$$N_{t+1}(x) = \int_{-\infty}^{\infty} K(x-y)F(N_t(y))dy,$$

where K is a distribution kernel that describes the dispersal phase, and F is a function that describes the growth phase. A more detailed explanation of this model will be provided in section 2.2, after reviewing some key concepts from the theory of discrete dynamical systems in section 2.1.

Understanding the mathematical properties of such a model can help with the management and control of invasive species. Such species spread into a habitat, in which they were previously absent. Invasive species can thus cause harm to the environment, human economy and human health by crowding out or devastating native species and their ecosystems. In Canada, and particularly in Ontario, the problem of invasive species is a reality. In fact, according to the Invasive Species Center [1], a Canadian non-profit organization, they represent one of Canada's greatest threats to the survival of wildlife. Among such species, we can find the dog-strangling vine, the zebra mussel and the emerald ash borer. The impact that invasive species have on the environment include irreversible damage to the ecosystem and a loss of biodiversity. There are also economical consequences due to losses in forestry, agriculture, fisheries, and other industries. Estimated annual costs can reach

millions or even billions of dollars per species in Canada alone [4]. Field experiments to study the spread of such species can be tricky, given the temporal and spatial scales, as well as the risks associated to expeditions in the wild. Modeling and understanding population spread is thus an important problem in applied ecology. For this reason, it is of great importance to understand the mathematical properties of integrodifference equations.

It is already known that under certain conditions, solutions of the integrodifference equation can have spreading speeds and appear in the form of travelling waves (topics that are discussed generally in section 2.3 and applied to integrodifference equations in section 2.4), which would translate to invasions in ecology. In particular, these results are observed when the growth function F has two steady states, which after rescaling we can assume are $N = 0$ and $N = 1$, and where the former is unstable and the latter is stable. In this thesis, we will study the case where F is a function with overcompensatory dynamics, i.e. 2-point cycles, 4-point cycles and even chaotic behavior can arise for certain parameter values of the growth function. Such is the case for the Ricker function and the logistic function.

This topic was first introduced in [14], where the solution of an integrodifference equation was plotted with F being the logistic function with a stable 2-point cycle (see figure 1.1). It was said that the solution of this integrodifference equation was alternating between two profiles (one for the even values of t, and another for the odd values of t) while moving to the left and was thus described as a travelling two-cycle.

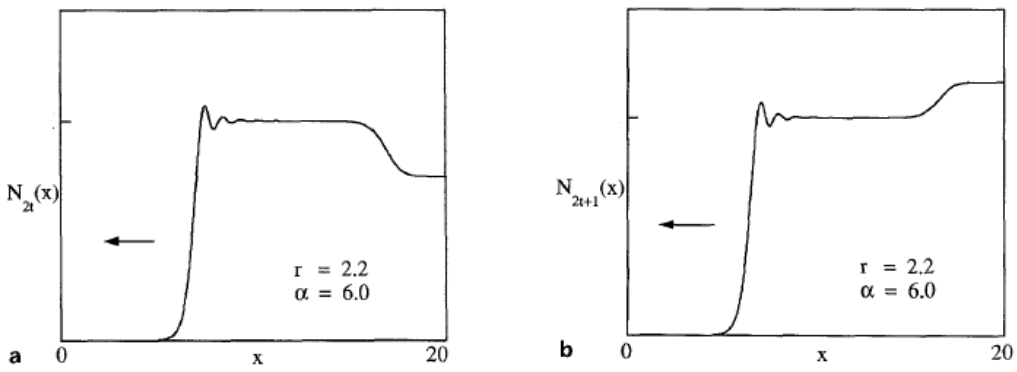

Figure 1.1: Fig. 9a,b from [14]. Solution of an integrodifference equation, where r is the parameter of the logistic function and α is the parameter of the Laplace kernel.

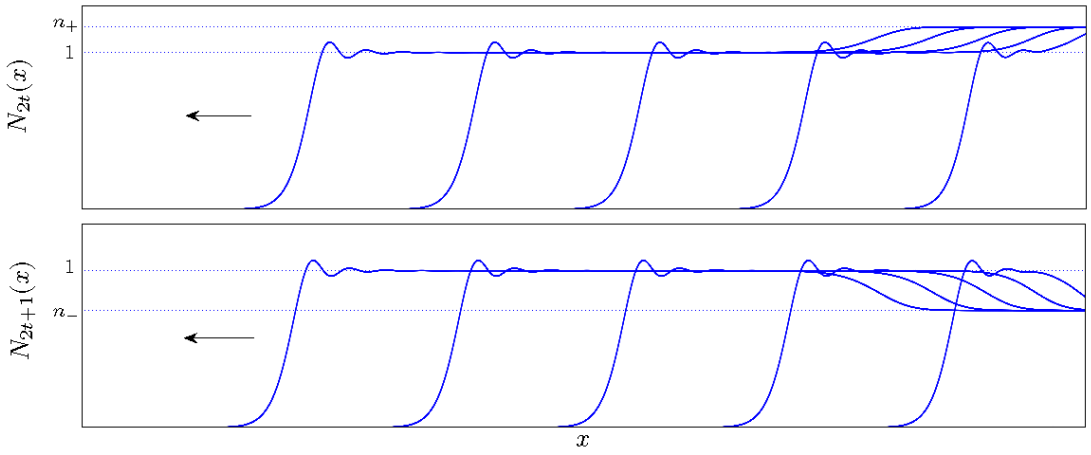

Figure 1.2: Solution of the integrodifference equation, where F is the logistic function with $r = 2.2$, K is the Laplace kernel with $a = 6$ and $N_0 = n_+\chi_{[x\geq 10]}$ is the initial condition, plotted for even (top panel) and odd (bottom panel) generations every 10 time steps. n_- and n_+ are the values that form the 2-point cycle.

However, when running the simulation in MATLAB®, we see that the solution is not exactly a travelling two-cycle, as not all parts move at the same speed (see figure 1.2). Instead, we observe that there are two different travelling profiles, the first one being the connection from $N = 0$ to $N = 1$ and the second being the connection between $N = 1$ and $N = n_+$ ($N = n_-$) in the case of even (odd) time steps, as illustrated in figure 1.2.

Thus, the following question arises: can we show the existence of two different spreading speeds within the different parts of the solution? In order to answer this question, we will start by reviewing the known literature for the connection from $N = 0$ to $N = 1$ in chapter 2. We will then proceed to studying the connection between $N = 1$ and $N = n_+$ in the solution for the even time steps in chapter 3. This will require generalizing some of the concepts of chapter 2 and proving new results. The presence of two spreading speeds within the same equation will then lead to the concept of *dynamical stabilization* [19, 20]. This topic will be studied in chapter 4 and will allow us to provide a summary of the behavior for the solution of the integrodifference equation. Finally, in chapter 5, we will discuss the results and their biological implications, as well future projects that could follow from this work.

Chapter 2

Literature Review

In this chapter, we will summarize the existing literature regarding the solutions of integrodifference equations. In order to do so, we will first review fundamental concepts on discrete dynamical systems, which will allow us to define the integrodifference equation model. We will then introduce the theory about the existence of a spreading speed and travelling wave solutions for a given recursion and apply these results to integrodifference equations. The results regarding the existence of a spreading speed and travelling waves in integrodifference equations will allow us to understand the connection between the states 0 and 1 that was observed during simulations, as shown in figure 1.2.

2.1 Discrete Dynamical Systems

In this section, we will review the fundamental concepts of one-dimensional discrete dynamical systems. For more details, one can consult [10]. We will also explore the properties of two functions with overcompensatory dynamics, namely the Ricker function and the logistic function.

Definition 2.1.1. *Let $F : \mathbb{R} \to \mathbb{R}$ be a continuously differentiable function. We say that the iteration defined by*

$$N_{t+1} = F(N_t) \tag{2.1.1}$$

is a discrete dynamical system and that the function F is the first iterate map.

Given an initial condition N_0, one can iteratively calculate the terms of the

sequence $\{N_t\}$ using equation (2.1.1):

$$\begin{aligned}
N_1 &= F(N_0),\\
N_2 &= F(N_1) = F(F(N_0)) = F^2(N_0),\\
N_3 &= F(N_2) = F(F(N_1)) = F(F^2(N_0)) = F^3(N_0),\\
&\vdots\\
N_t &= F^t(N_0),
\end{aligned}$$

where F^t is the t-fold composition of F. We call F^t the t-th iterate map of F.

When a discrete dynamical system is defined, a cobweb diagram can be used to determine the long-term behavior of solutions. This method allows us to see graphically whether the sequence $\{N_t\}$ converges to a particular point. The first step to drawing a cobweb diagram is to plot the identity line and the function F that defines the iteration sequence. Then, starting with the point N_0 on the x-axis, its image on the graph of F will give us N_1. Projecting N_1 horizontally onto the identity line, we get the next input value for F to get N_2. We continue in the same manner until we can see whether or not the sequence converges. For example, given the function $F(N) = \sqrt{N}$ as in figure 2.1, we can see that if we start with an initial condition near 0 the sequence converges to the point N^*.

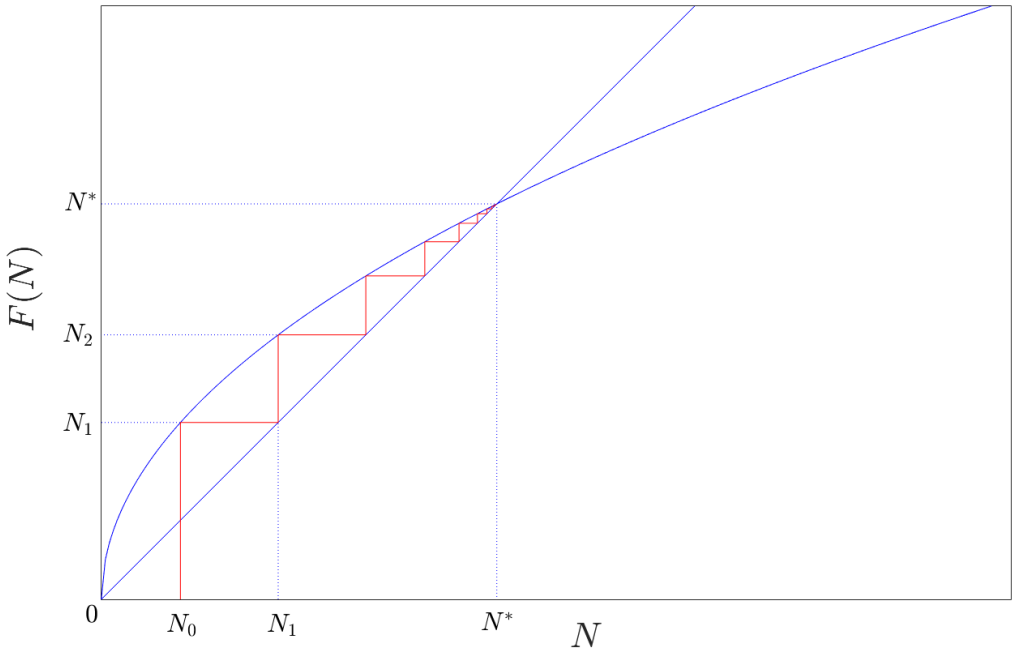

Figure 2.1: Cobweb diagram of a discrete dynamical system.

One can also determine many aspects of the long-term behavior of a discrete dynamical system analytically by studying the fixed points, also called steady states, and their stability.

Definition 2.1.2. *We say that N^* is a fixed point of (2.1.1) if $F(N^*) = N^*$. N^* is said to be globally (asymptotically) stable if*

$$\lim_{t\to\infty} N_t = N^* \text{ for all } N_0 \in \mathbb{R}$$

and locally (asymptotically) stable if

$$\lim_{t\to\infty} N_t = N^* \text{ for all } N_0 \in \mathbb{R} \text{ such that } |N_0 - N^*| < \epsilon \text{ for some } \epsilon > 0.$$

We say that N^* is stable if it is at least locally stable. We also say that N^* is unstable if it is not locally stable.

Cobwebbing allows us to graphically determine whether the fixed points are stable. In figure 2.1, we can see that $N = 0$ is an unstable fixed point whereas $N = N^*$ is a stable fixed point. We also have the following proposition that allows us to determine the stability of a fixed point:

Proposition 2.1.3 (Proposition 1.9 of [10])**.** *Let F be the function that defines the discrete dynamical system (2.1.1), and N^* be a steady state.*

$$\begin{aligned} &\text{If } |F'(N^*)| < 1 \text{ then } N^* \text{ is locally stable, and} \\ &\text{if } |F'(N^*)| > 1 \text{ then } N^* \text{ is unstable.} \end{aligned}$$

Fixed points are not the only objects that can be studied in a discrete dynamical system. Depending on the nature of the first iterate map, one can sometimes observe p-point cycles.

Definition 2.1.4. *A p-point cycle is a series of p distinct points N_1^*, N_2^*, ..., N_p^* such that $F(N_i^*) = N_{i+1}^*$ for $i = 1, 2, ..., p-1$ and $F(N_p^*) = N_1^*$.*

From the previous definition, it follows that the points forming the p-point cycle are fixed points of the p-th iterate map. Figure 2.2 illustrates a discrete dynamical system with a 2-point cycle along with its second iterate map. Since p-point cycles correspond to fixed points of the p-th iterate map, we can also define their stability.

Definition 2.1.5. *A p-point cycle is said to be stable if $N_1^*, N_2^*, ..., N_p^*$ are stable fixed points of the p-th iterate map. The p-point cycle is unstable if $N_1^*, N_2^*, ..., N_p^*$ are unstable fixed points of the p-th iterate map.*

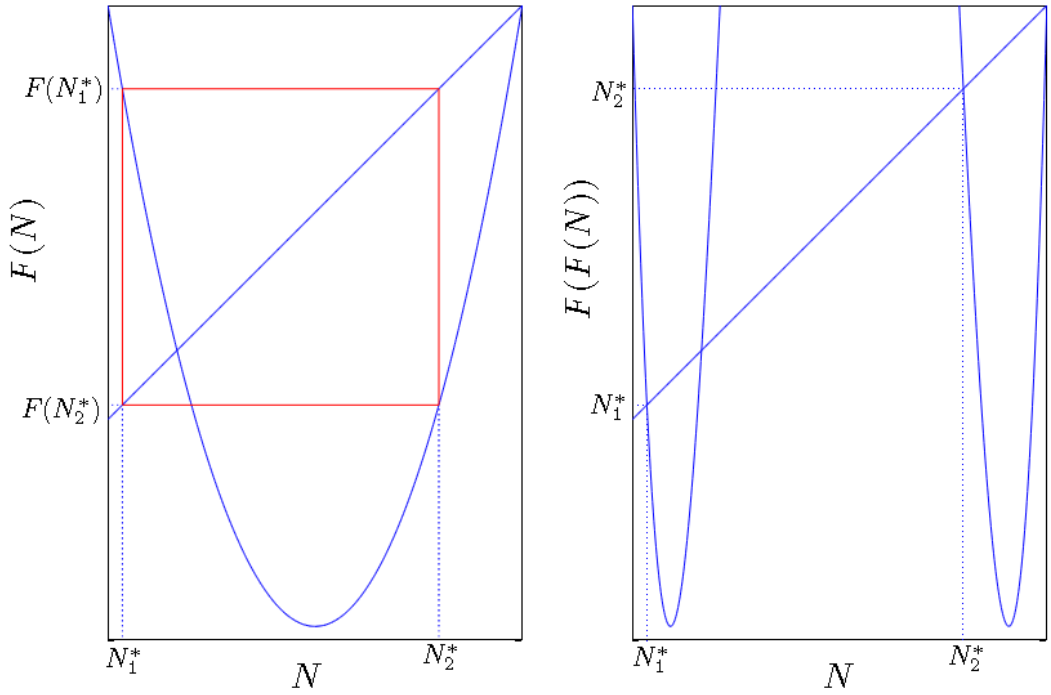

Figure 2.2: Illustration of a 2-point cycle for a discrete dynamical system with $F(N) = N^2 - 6$ (left) and its second iterate map (right).

The theory of discrete dynamical systems can be applied to study the dynamics of biological populations for species with non-overlapping generations.

Definition 2.1.6. *Let N_t be the number or density of individuals of a given population in generation t. If $N_{t+1} = F(N_t)$ is a discrete dynamical system that describes the total production of individuals in the next generation, then we say that F is a growth function. In order for the solution of the system to be biologically relevant, we restrict the range of F to the interval $[0, \infty)$. In this case, studying the fixed points and p-point cycles of F allows to predict future population dynamics.*

2.1.1 Ricker Function

A function that is often used to model population growth in biology is the Ricker function. This model was introduced to describe the stock and recruitment in fisheries [26]. Its expression is given by

$$F(N) = Ne^{r(1-N/C)}, \tag{2.1.2}$$

where $r > 0$, e^r is the intrinsic growth rate and C is the carrying capacity (see "Biological Terminology"). By rescaling variables, we can assume that $C = 1$. The fixed points of the Ricker function are thus $N = 0$ and $N = 1$. Figure 2.3 illustrates the Ricker map for various values of r.

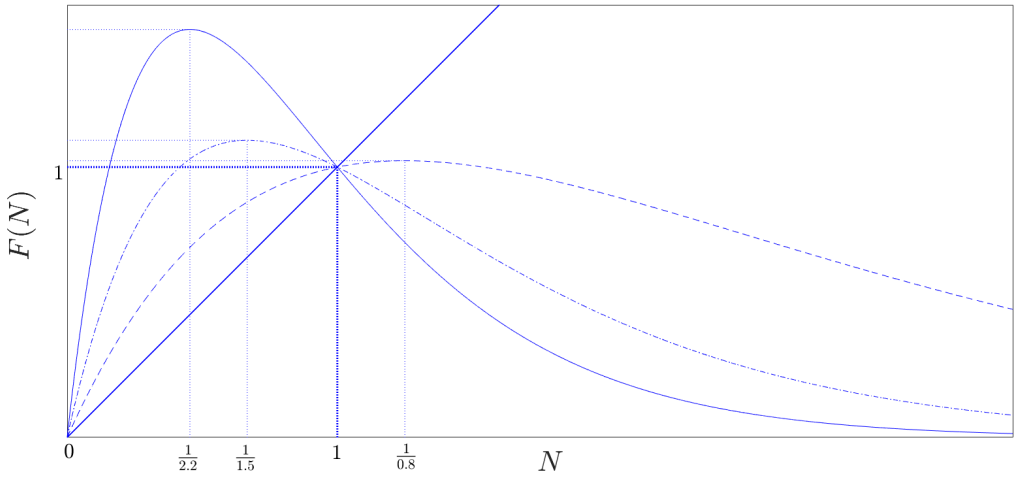

Figure 2.3: Plot of the Ricker function for $r = 0.8$ (dashed curve), $r = 1.5$ (dash-dot curve) and $r = 2.2$ (full curve). The full line is the identity line.

We have that $F'(N) = (1 - rN)e^{r(1-N)}$, which implies that the global maximum is attained at $N = 1/r$. We can also calculate the higher order derivatives using the following formula:

$$F^{(n)}(N) = (-1)^n r^{n-1}(rN - n)e^{r(1-N)}. \tag{2.1.3}$$

In fact, since this formula is true for $n = 1$, we proceed by induction and assume that the formula holds for some k. Then we calculate

$$\begin{aligned} F^{(k+1)}(N) &= \left[(-1)^k r^{k-1}(rN - k)e^{r(1-N)}\right]' \\ &= (-1)^k r^{k-1}\left[re^{r(1-N)} + (rN - k)e^{r(1-N)}(-r)\right] \\ &= (-1)^k r^k e^{r(1-N)}((k+1) - rN) \\ &= (-1)^{k+1} r^k (rN - (k+1))e^{r(1-N)}. \end{aligned}$$

These derivatives can be used to determine the stability of the fixed points of the Ricker map.

When $r \leq 1$, the Ricker function is increasing on $[0, 1]$, which is no longer the case when $r > 1$ (see figure 2.3). Also, for different values of r, the dynamical behavior of solutions changes, but $N = 0$ always remains unstable for $r > 0$ (see table 2.1).

Value of r	Dynamical Behaviour
$0 < r < 2$	Globally stable equilibrium point ($N = 1$)
$2 < r < 2.526$	Globally stable 2-point cycle ($N = 1$ is unstable)
$2.526 < r < 2.656$	Globally stable 4-point cycle (2-point cycle is unstable)
$2.656 < r < 2.692$	Stable cycle, period 8, giving way in turn to cycles of period 16, 32, etc., as r increases.
$r > 2.692$	Chaos (cycles of arbitrary period, or aperiodic behavior, depending on the initial condition)

Table 2.1: Dynamics of a population described by the Ricker function as seen in [22]. The threshold values for r are rounded to 4 digits.

For the remainder of this work, we will denote by n_- and n_+ the values of the 2-point cycle, and n_-^-, n_-^+, n_+^- and n_+^+ the values of the 4-point cycle when these exist. The stable 2-point cycle is illustrated in figure 2.4 for $r = 2.2$. The values of the 2-point cycle are stable fixed points of the second iterate map, as observed in figure 2.5. In the case of a stable 4-point cycle in the first iterate map (see figure 2.6), there will be two stable 2-point cycles in the second iterate map, as illustrated in figure 2.7.

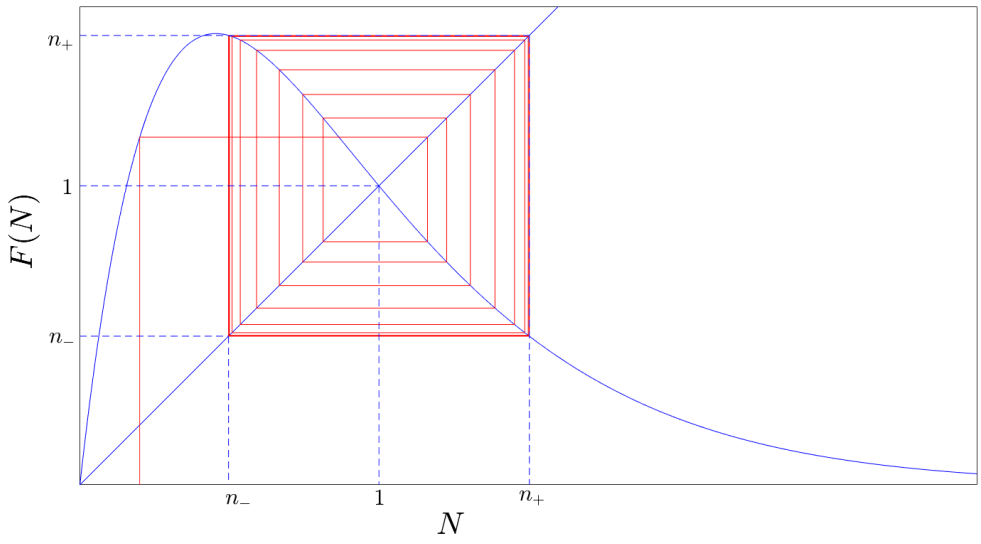

Figure 2.4: Cobweb diagram of the Ricker function for $r = 2.2$.

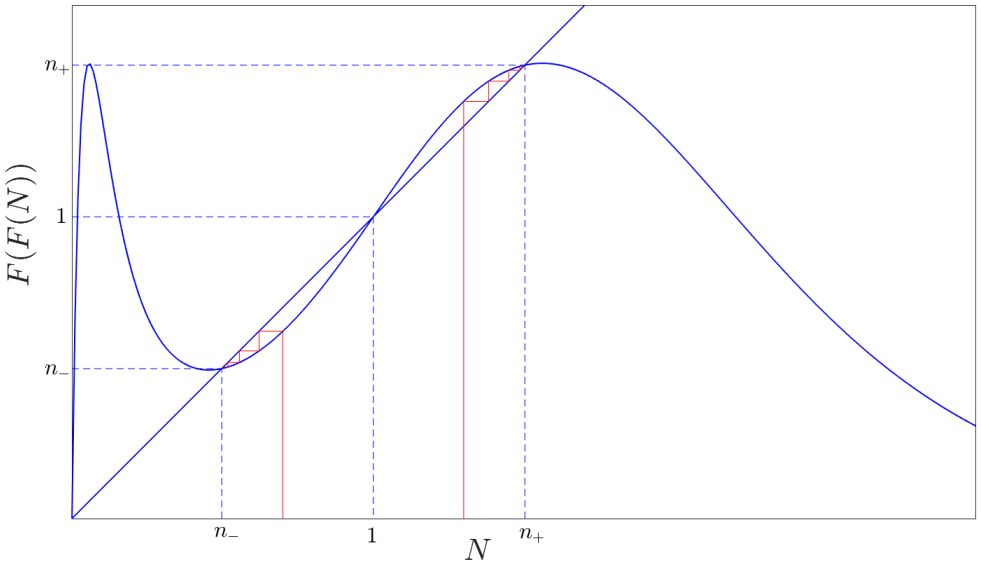

Figure 2.5: Cobweb diagram of the second iterate map of the Ricker function for $r = 2.2$.

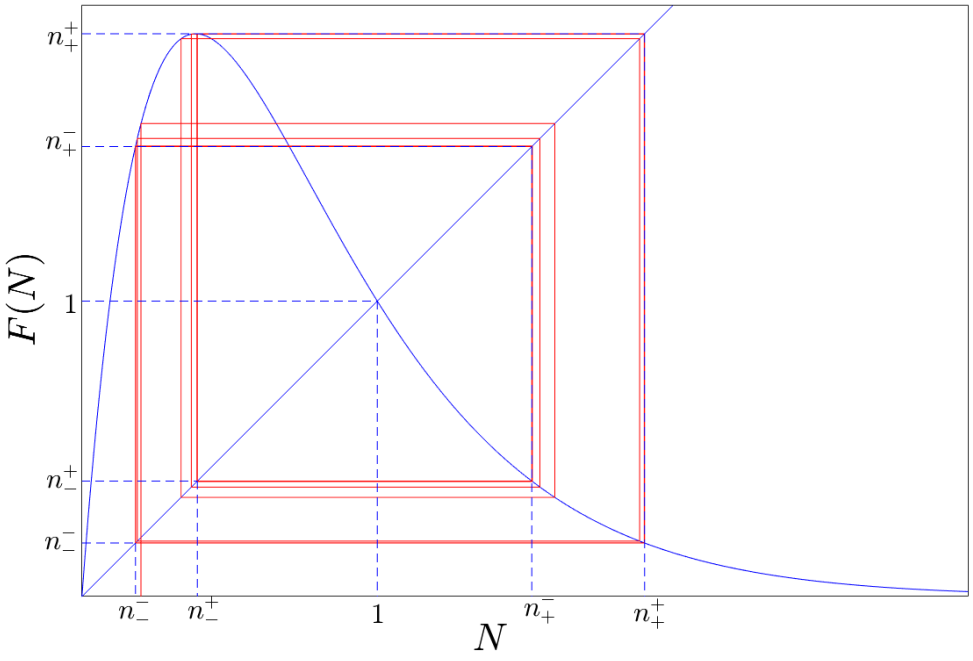

Figure 2.6: Cobweb diagram of the Ricker function for $r = 2.6$.

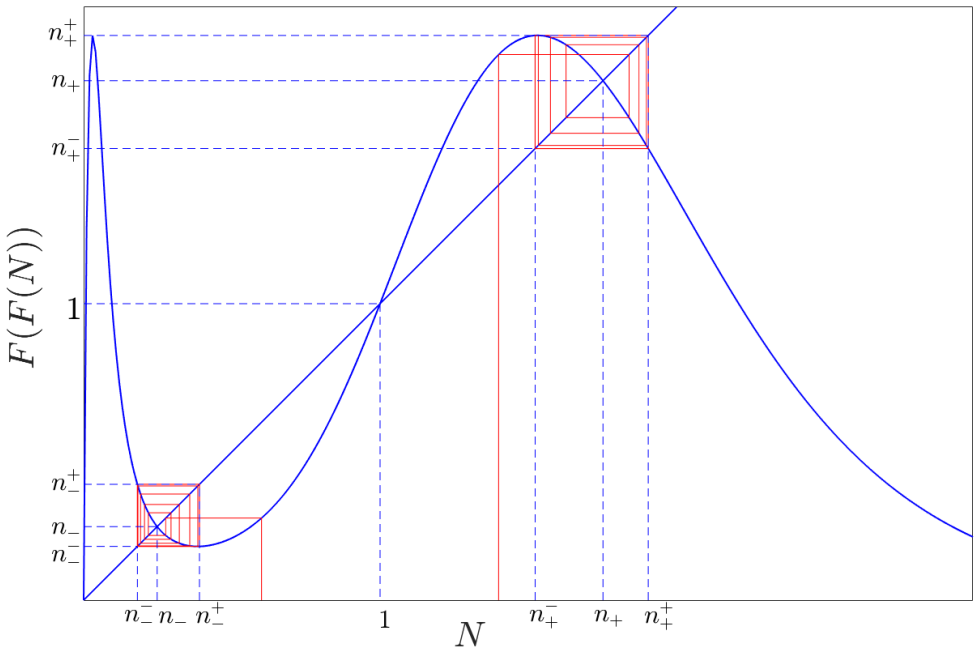

Figure 2.7: Cobweb diagram of the second iterate map of the Ricker function for $r = 2.6$.

We can implicitly define the non-trivial fixed points of the p-th iterate map for the Ricker function. This characterization can then be useful to determine the values of the p-point cycle numerically (when p is even):

$$\begin{aligned}
N = F^p(N) &\Rightarrow N = F(F^{p-1}(N)) \\
&\Rightarrow N = F^{p-1}(N)e^{r(1-F^{p-1}(N))} \\
&\Rightarrow N = F(F^{p-2}(N))e^{r(1-F^{p-1}(N))} \\
&\Rightarrow N = F^{p-2}(N)e^{r(1-F^{p-2}(N))}e^{r(1-F^{p-1}(N))} \\
&\vdots \\
&\Rightarrow N = Ne^{r(1-N)}e^{r(1-F(N))}\dots e^{r(1-F^{p-2}(N))}e^{r(1-F^{p-1}(N))} \\
&\Rightarrow 1 = e^{r(p-N-F(N)-\dots-F^{p-2}(N)-F^{p-1}(N))} \\
&\Rightarrow N + \sum_{i=1}^{p-1} F^i(N) - p = 0. \qquad (2.1.4)
\end{aligned}$$

Thus, we can apply Newton's method for finding roots of equation (2.1.4) (see MATLAB® code in table D.1). Alternatively, we can also use a cobwebbing algorithm

to find the values of the p-point cycle (see MATLAB® code in table D.2 that generated figures 2.4, 2.5, 2.6 and 2.7). In the case of the stable 2-point cycle, we can find the value of r for which the Ricker function is decreasing on $[n_-, n_+]$, a property that will be important in a later chapter. Numerically, we find that the Ricker function is decreasing on $[n_-, n_+]$ for $2 < r < 2.2564$, and non-decreasing for $r > 2.2565$ by solving $n_- \geq 1/r$. (see MATLAB® code in table D.3).

2.1.2 Logistic Function

The logistic function is another function that can be used to model population dynamics in ecology. For example, it can model the population of *Paramecium Aurelia*, which is a unicellular organism found in freshwater ponds, as done in section 2.2.1 of [6]. Its expression is given by

$$F(N) = (1 + r)N - rN^2/C, \tag{2.1.5}$$

where $r > 0$, $1 + r$ is the intrinsic growth rate and C is the carrying capacity (see "Biological Terminology"). By rescaling variables, we can assume that $C = 1$. Similarly to the Ricker function, $N = 0$ and $N = 1$ are fixed points of the logistic function (see figure 2.8). One must be careful when using the logistic function as a biological model, because it only preserves positivity for $N > \frac{1+r}{r}$.

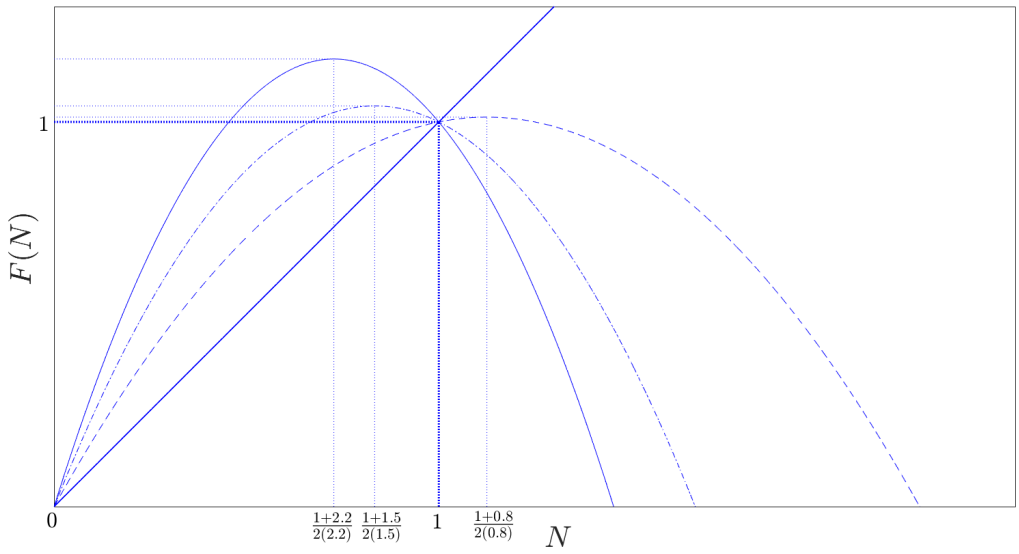

Figure 2.8: Plot of the logistic function for $r = 0.8$ (dashed curve), $r = 1.5$ (dash-dot curve) and $r = 2.2$ (full curve). The full line is the identity line.

We have $F'(N) = (1 + r) - 2rN$, which implies that the global maximum is attained at $N = \frac{1+r}{2r}$, as illustrated in figure 2.8 for various values of r. As for the Ricker function, we have that the logistic function is increasing on $[0, 1]$ when $r \leq 1$, and non-increasing when $r > 1$ (see figure 2.8). Also, the dynamical behavior of solutions changes for different values of r, with $N = 0$ always being unstable (see table 2.2).

Value or r	Dynamical Behaviour
$0 < r < 2$	Globally stable equilibrium point ($N = 1$)
$2 < r < 2.449$	Globally stable 2-point cycle ($N = 1$ is unstable)
$2.449 < r < 2.544$	Globally stable 4-point cycle (2-point cycle is unstable)
$2.544 < r < 2.570$	Stable cycle, period 8, giving way in turn to cycles of period 16, 32, etc., as r increases.
$r > 2.570$	Chaos (cycles of arbitrary period, or aperiodic behavior, depending on the initial condition)

Table 2.2: Dynamics of a population described by the logistic function as seen in [22].

A stable 2-point cycle is illustrated in figure 2.9 for $r = 2.2$. The values of the 2-point cycle are stable fixed points of the second iterate map, as shown in figure 2.10. In the case of a stable 4-point cycle in the first iterate map (see figure 2.11), there will be two stable 2-point cycles in the second iterate map (see figure 2.12).

Unlike the case of the Ricker function, we do not obtain a compact and nice formula to determine the fixed points of the p-th iterate map. However, we still derive the formula for the second iterate map in order to calculate the values of the 2-point cycle:

$$\begin{aligned} N = (F \circ F)(N) &\Rightarrow N = (1 + r)F(N) - r[F(N)]^2 \\ &\Rightarrow N = (1 + r)[(1 + r)N - rN^2] - r[(1 + r)N - rN^2]^2 \\ &\Rightarrow N = (1 + r)^2N - r(1 + r)(2 + r)N^2 + 2r^2(1 + r)N^3 - r^3N^4 \\ &\Rightarrow [(1 + r)^2 - 1]N - r(1 + r)(2 + r)N^2 + 2r^2(1 + r)N^3 - r^3N^4 = 0. \end{aligned}$$

Since $N = 0$ and $N = 1$ are known fixed points, we divide the last polynomial by N and $N - 1$ to obtain a polynomial of degree 2:

$$r^2N^2 - (r^2 + 2r)N + r + 2 = 0. \tag{2.1.6}$$

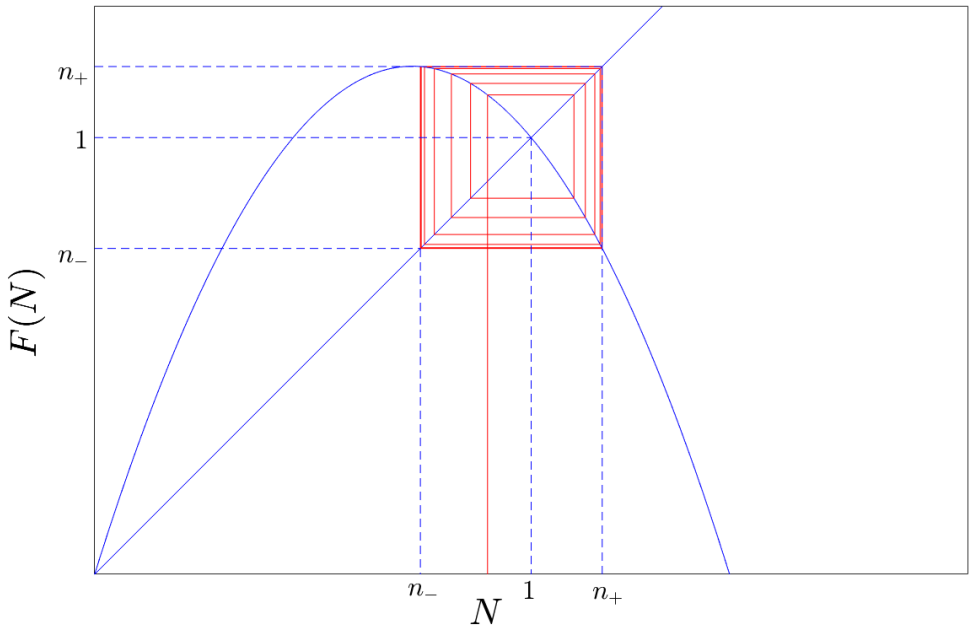

Figure 2.9: Cobweb diagram of the logistic function for $r = 2.2$.

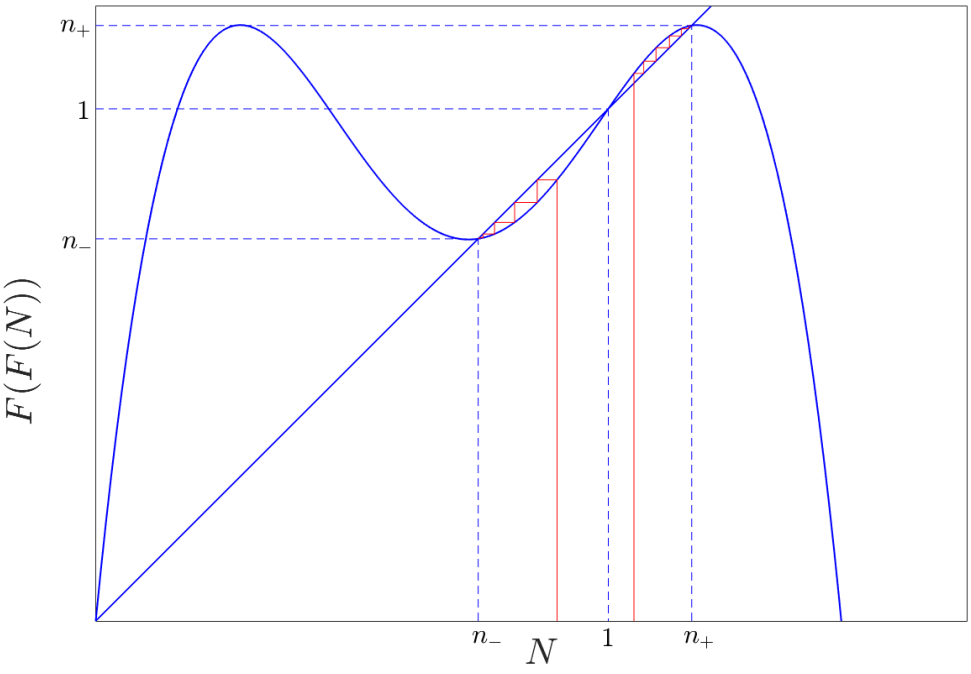

Figure 2.10: Cobweb diagram of the second iterate map of the logistic function for $r = 2.2$.

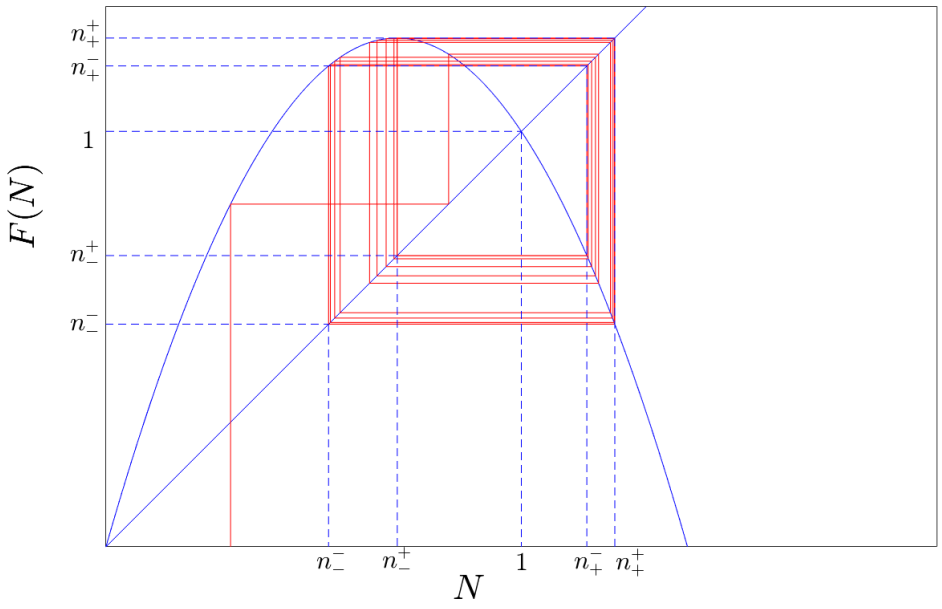

Figure 2.11: Cobweb diagram of the logistic function for $r = 2.5$.

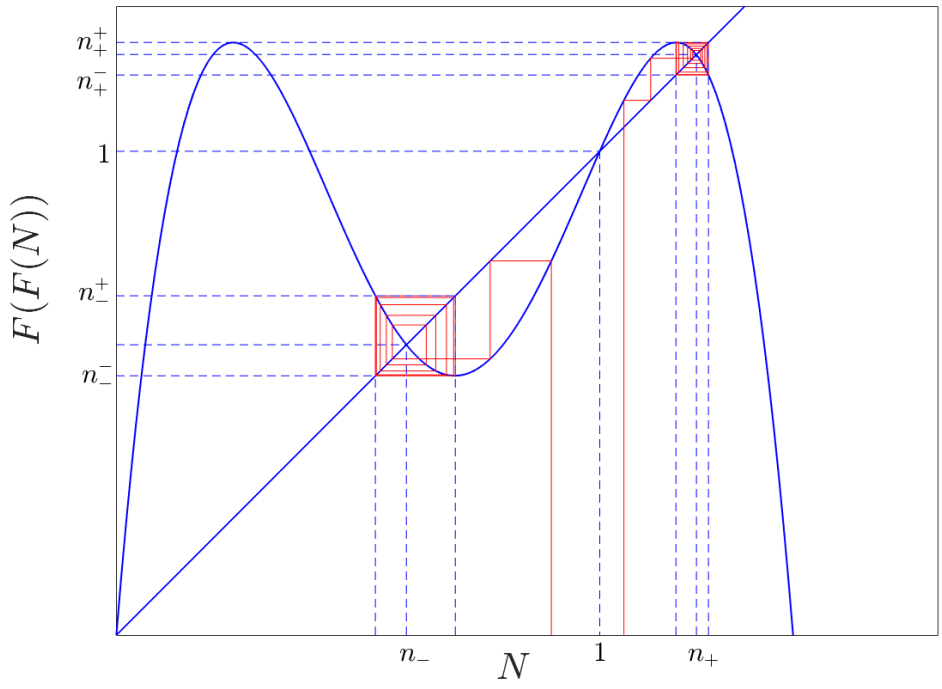

Figure 2.12: Cobweb diagram of the second iterate map of the logistic function for $r = 2.5$.

The roots of equation (2.1.6) are thus obtained with the quadratic formula and represent the values of n_- and n_+:

$$\begin{aligned} n_\pm &= \frac{r^2 + 2r \pm \sqrt{(r^2+2r)^2 - 4r^2(r+2)}}{2r^2} \\ &= \frac{r + 2 \pm \sqrt{r^2 - 4}}{2r} \end{aligned}$$

We see from this last equation that n_- and n_+ exist if and only if $r > 2$.

For the values of the 4-point cycle, we use a cobwebbing algorithm, as it would require solving a polynomial of order 4 to get the values of n_-^-, n_-^+, n_+^- and n_+^+. The MATLAB® code used is similar to the one for the Ricker function in table D.2 and plots figures 2.9, 2.10, 2.11 and 2.12. In the case of the stable 2-point cycle, we can also find the value of r for which the logistic function is decreasing on $[n_-, n_+]$, a property that will important in a later chapter. Using MATLAB® we find that the logistic function is decreasing on $[n_-, n_+]$ for $2 < r < 2.2361$, and non-decreasing for $r > 2.2361$ by solving $n_- \geq \frac{1+r}{2r}$ (see code in table D.3).

2.2 Integrodifference equations

Discrete dynamical systems of the previous form, when viewed as models for population dynamics, are non-spatial, as they do not relate individuals to their position in space. From these models, we can build integrodifference equations, which are spatial. This method is appropriate when modelling the spatial distribution of a species with non-overlapping generations and distinct growth and dispersal phases [15]. In this section, we explain how to construct this model and show how solutions can behave.

Let x denote a spatial variable taken in $\mathbb{R}$. Let $N_t(x)$ be the spatial density of the population of a species with non-overlapping growth and dispersal phases at the beginning of generation t. The population at generation $t+1$ is the population resulting after one growth and one dispersal phase.

The growth phase is modeled by a discrete map $N_t \mapsto F(N_t)$, where F is called the growth function. If F is homogeneous on the environment, then this is analogous to the iterate map of a discrete dynamical system with respect to N_t. This discrete map is applied to every x in $\mathbb{R}$. Thus, after the growth phase, the spatial density of the population is given by $F(N_t(x))$.

The dispersal phase is described by using a distribution kernel, that defines the

probability of an individual to move from some location y to some location x in $\mathbb{R}$. Assuming that movement depends on relative distance rather than absolute location, we can denote the distribution kernel by $K(x-y)$. The probability that an individual moves from the interval $[y, y+\Delta y)$ to location x is $K(x-y)\Delta y$. The number of individuals that move from the interval $[y, y+\Delta y)$ to location x during the dispersal phase is thus given by $K(x-y)F(N_t(y))\Delta y$.

The density of the population after the dispersal phase is thus the sum of the individuals that came from all the possible locations y, which leads to the integrodifference equation:

$$N_{t+1}(x) = \int_{-\infty}^{\infty} K(x-y)F(N_t(y))dy. \tag{2.2.1}$$

We shall omit the boundaries of integration hereafter when the domain is $\mathbb{R}$. We assume that there is no loss or gain of individuals during dispersal, so that $\int K(x)dx = 1$. We will also assume that the distribution kernel is symmetric, i.e. $K(-x) = K(x)$.

Examples of such kernels include the Gaussian kernel and the Laplace kernel. When K is the Gaussian kernel, we have

$$K(x) = \frac{1}{\sqrt{2\pi\sigma^2}} e^{-\frac{x^2}{2\sigma^2}}, \tag{2.2.2}$$

where σ^2 is the variance.
When K is the Laplace kernel,

$$K(x) = \frac{a}{2} e^{-a|x|}, \tag{2.2.3}$$

where $a = \sqrt{\frac{2}{\sigma^2}}$ and σ^2 is the variance.

The question on how the dynamics of (2.2.1) depend on the chosen growth function and distribution kernel has been studied widely in the literature [12, 14, 15, 17, 18, 29, 30, 33]. We shall review some of this literature in section 2.4. One particular focus is the conditions under which the population can spread spatially when introduced locally; the speed at which it spreads and the shape and qualitative behavior of the spreading density profile. We illustrate one possible spreading scenario in figure 2.13. After a while, we observe a fixed monotone density profile that moves to the left by a constant distance per generation. The MATLAB® code can be found in appendix D.

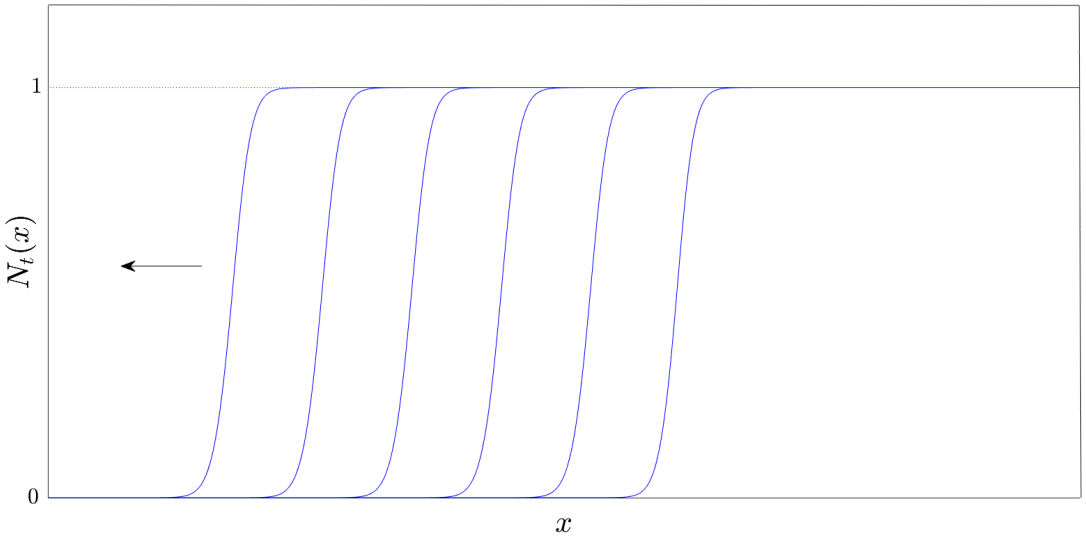

Figure 2.13: Solution of the integrodifference equation, where K is the Laplace kernel with $a = 15$, F is the Ricker function with $r = 0.8$ and $N_0 = \chi_{[x\geq 10]}$, plotted every 10 time steps. The fixed profile moves left, in the direction of the arrow.

The next section will introduce the two most important concepts for this thesis: the spreading speed and a travelling wave solution. These concepts relate to the speed of spatial spread of the population and its density profile. Before proceeding, we point out that in figure 2.13, the parameter in the growth function is chosen such that F is monotone between its steady states $N = 0$ and $N = 1$, where $N = 1$ is stable. In this case, we shall see that the theory is well developed. The novel part of this thesis (chapters 3 and 4) will be to study the case when F is not monotone and the fixed point $N = 1$ is unstable. In particular, we study the Ricker function (2.1.2) and the logistic function (2.1.5).

2.3 Existence of Spreading Speeds and Travelling Waves

In order to have a better understanding of the observed phenomenon in figure 2.13, we need to get familiarized with some theory on the existence of a spreading speed and travelling wave solutions in a more general setting. The main results of this theory can be found in [31], but we will provide a summary in this section.

Definition 2.3.1. *Let $C_{[0,\beta]}$ denote the set of continuous functions on $\mathbb{R}$ with values in the interval $[0,\beta]$, where $\beta > 0$. Let $R : C_{[0,\beta]} \to C(\mathbb{R})$, where $C(\mathbb{R})$ is the set of continuous functions with real values. We shall refer to R as an operator on $C_{[0,\beta]}$. We define the following recursion:*

$$u_{t+1} = R[u_t]. \tag{2.3.1}$$

Definition 2.3.2. *The value c^* is called the rightward asymptotic spreading speed of R on $[0,\beta]$ if the following conditions hold:*

i) For any $u_0 \in C_{[0,\beta]}$ with compact support,

$$\lim_{t\to\infty} \sup_{x\geq ct} u_t(x) = 0 \text{ for all } c > c^*. \tag{2.3.2}$$

ii) For any $u_0 \in C_{[0,\beta]}\backslash\{0\}$,

$$\lim_{t\to\infty} \inf_{x\leq ct} u_t(x) = \beta \text{ for all } c \in (0, c^*). \tag{2.3.3}$$

We can interpret this last definition in terms of population biology. A population introduced in a confined environment is said to spread with speed c^* if an observer who moves at a speed $c > c^*$ is eventually ahead of said population, whereas an observer who moves at a speed $c < c^*$ is eventually surrounded. In [31], it was shown that if R satisfies some predetermined conditions, then a spreading speed exists. Those conditions are listed in the next theorem.

Theorem 2.3.3. *Assume the following hypotheses on the operator R that defines a recursion like (2.3.1):*

1. *Translation invariance: $R[u(\cdot - a)](x) = R[u](x - a)$.*
2. *Invariance on $C_{[0,\beta]}$: $u \in C_{[0,\beta]} \Rightarrow R[u] \in C_{[0,\beta]}$.*
3. *Fixed points:*
   a) *$R[0](x) = 0$, where 0 denotes the constant function with value 0,*
   b) *$R[\beta](x) = \beta$, where β denotes the constant function with value β,*
   c) *$R[\alpha](x) > \alpha$ for any constant function $\alpha \in C_{(0,\beta)}$.*
4. *Monotonicity: $0 \leq u \leq w \leq \beta \Rightarrow R[u] \leq R[w]$.*
5. *Continuity: If $\{f_t\} \subset C_{[0,\beta]}$ and $f_t \to f$ uniformly on compact subsets of $\mathbb{R}$ then $R[f_t] \to R[f]$ pointwise as $t \to \infty$.*

Then there exists a spreading speed c^* for the operator R on the interval $[0, \beta]$.

When a spreading speed c^* exists, we can calculate its value with the following theorem.

Theorem 2.3.4 (Corollary of Theorems 6.3 and 6.4 from [31] and Theorems 2.1 and 2.2 from [32])**.** *Let R be an operator that satisfies the five hypotheses of Theorem 2.3.3. Let g be a bounded non-negative measurable function on $\mathbb{R}$ with the following properties:*

1. *for all $u \in C_{[0,\beta]}$*

$$R[u](x) \leq \int u(x-y)g(y)dy,$$

2. *for all $\delta > 0$, there exists $\epsilon > 0$ such that when $0 \leq u \leq \epsilon$*

$$R[u](x) \geq (1-\delta) \int u(x-y)g(y)dy.$$

Then, the value of c^* is given by

$$c^* = \inf_{s \in \Omega} \frac{1}{s} \log \left(\int e^{sx} g(x)dx \right), \tag{2.3.4}$$

where Ω represents the values of $s > 0$ for which the integral converges. If $\int e^{sx} g(x)dx = \infty$ for all $s > 0$, then $c^* = \infty$.

By definition, the integral term in equation (2.3.4) is the *moment-generating function* of g and its domain consists of all s for which the integral converges (see appendix A). Now that some existence conditions have been established for the spreading speed, we can determine the conditions for the existence of travelling wave solutions in the recursion defined by expression (2.3.1).

Theorem 2.3.5 (Theorem 6.6 of [31])**.** *Let R be an operator that satisfies the hypotheses of Theorem 2.3.3. Assume that every sequence $\{v_t\}$ of functions in $C_{[0,\beta]}$ has a subsequence $\{v_{t_i}\}$ such that $\{R[v_{t_i}]\}$ converges uniformly on every bounded subset of $\mathbb{R}$. Then for all $c \geq c^*$, there exists a non-increasing function W such that $u_t(x) = W(x - tc)$ satisfies (2.3.1), $W(-\infty) = \beta$ and $W(\infty) = 0$. We refer to W as a monotone travelling wave solution of the recursion.*

Note that the previous result states that the spreading speed c^* of the operator R corresponds to the minimal wave speed. In the following result, c^* is interpreted as such.

Proposition 2.3.6. *Let g be a bounded non-negative function on $\mathbb{R}$ and R be the operator on $C_{[0,\infty)}$ defined by $R[u](x) = \int u(x-y)g(y)dy$. Then the spreading speed c^* of R is given by equation (2.3.4), assuming that the moment-generating function of g exists for some $s > 0$. If $\int e^{sx}g(x)dx = \infty$ for all $s > 0$, then $c^* = \infty$.*

Proof: Assume that the recursion defined by the operator R has a solution in the form of a travelling wave:

$$u_{t+1}(x) = u_t(x-c) = \int g(x-y)u_t(y)dy.$$

We then apply the exponential transform:

$$\int e^{sx}u_t(x-c)dx = \int\int g(x-y)u_t(y)e^{sx}dydx.$$

Letting $w = x - c$ on the left-hand side and $z = x - y$ on the right-hand side, we get

$$\begin{aligned}
&\int e^{s(w+c)}u_t(w)dw = \int\int g(z)u_t(y)e^{s(z+y)}dydz \\
&\Rightarrow e^{sc} = \int e^{sz}g(z)dz \\
&\Rightarrow c(s) = \frac{1}{s}\log\left(\int e^{sx}g(x)dx\right).
\end{aligned}$$

The minimum speed c^* of the travelling front is thus given by equation (2.3.4) in the positive direction. If g is symmetric, then this value of c^* is also the minimum wave speed in the negative direction and therefore corresponds to the spreading speed by definition. ∎

Let R be an operator with spreading speed c^* given by equation (2.3.4). We would like to compute the value c^* as easily as possible. We thus seek an equivalent and simpler representation. Assume $g(x) = \mu\tilde{g}(x)$ for some constant $\mu > 0$. Define

$$c(s) := \frac{1}{s}\log\left(\mu\int e^{sx}\tilde{g}(x)dx\right) = \frac{1}{s}\log\left(\mu M_{\tilde{g}}(s)\right), \tag{2.3.5}$$

where is the moment-generating function of $\tilde{g}$.

If the global minimum of $c(s)$ exists for some $s \in \Omega$, then $c^* = \min_{s\in\Omega} c(s)$. If that minimum is also local, then we can obtain a parametric representation for c^*:

$$\begin{aligned} c'(s) = 0 \Rightarrow -\frac{1}{s^2}\log(\mu M_{\tilde{g}}(s)) + \frac{M'_{\tilde{g}}(s)}{sM_{\tilde{g}}(s)} = 0 \\ \Rightarrow c(s) = \frac{M'_{\tilde{g}}(s)}{M_{\tilde{g}}(s)}. \end{aligned} \tag{2.3.6}$$

Replacing this last expression into equation (2.3.5), we obtain

$$\mu = \frac{e^{sM'_{\tilde{g}}(s)/M_{\tilde{g}}(s)}}{M_{\tilde{g}}(s)}. \tag{2.3.7}$$

The parametric representation of c^* is then described by equations (2.3.6) and (2.3.7).

Proposition 2.3.7 (Lemma 4.1 of [30])**.** *Let Ω denote the values of $s > 0$ for which the moment-generating function of $\tilde{g}$ exists. The function c defined by equation* (2.3.5) *has no local maximum and has at most one local minimum.*

In order to prove this proposition, we will need the result of the following lemma.

Lemma 2.3.8. *Let c be a differentiable function defined for $s \in \Omega \subset \mathbb{R}^+$. Assume that the function s^2c', where c' denotes the derivative of c, is increasing on Ω. Then c has no local maximum on Ω.*

Proof: We have that s^2c' is increasing, which implies that for all $s \in \Omega$

$$(s^2c')'(s) = 2sc'(s) + s^2c''(s) > 0 \Rightarrow c'(s) > -\frac{s}{2}c''(s). \tag{2.3.8}$$

Assume that there exists $s_0 \in \Omega$ such that $c(s_0)$ is a local maximum. Then, replacing s_0 in equation (2.3.8), we get

$$0 > -\frac{s_0}{2}c''(s_0).$$

Hence $c''(s_0) > 0$, which contradicts the assumption that s_0 is a local maximum. Thus, the function c has no local maximum. ∎

Proof: (**Proof of Proposition 2.3.7**)
We follow the steps from [30] and consider the following function:

$$\Psi(s) = \frac{\int xe^{sx}\tilde{g}(x)dx}{\int e^{sx}\tilde{g}(x)dx}. \tag{2.3.9}$$

We can then differentiate the functions c and Ψ:

$$\begin{aligned} c'(s) &= -\frac{1}{s^2}\log\left(\mu\int e^{sx}\tilde{g}(x)dx\right) + \frac{1}{s}\frac{\int xe^{sx}\tilde{g}(x)dx}{\int e^{sx}\tilde{g}(x)dx} \\ &= -\frac{1}{s}[c(s) - \Psi(s)], \end{aligned} \tag{2.3.10}$$

$$\begin{aligned} \Psi'(s) &= \frac{\int x^2e^{sx}\tilde{g}(x)dx}{\int e^{sx}\tilde{g}(x)dx} - [\Psi(s)]^2 \\ &= \frac{\int x^2e^{sx}\tilde{g}(x)dx}{\int e^{sx}\tilde{g}(x)dx} - 2[\Psi(s)]^2 + [\Psi(s)]^2 \\ &= \frac{\int x^2e^{sx}\tilde{g}(x)dx - 2\Psi(s)\int xe^{sx}\tilde{g}(x)dx + [\Psi(s)]^2\int e^{sx}\tilde{g}(x)dx}{\int e^{sx}\tilde{g}(x)dx} \\ &= \frac{\int[x-\Psi(s)]^2e^{sx}\tilde{g}(x)dx}{\int e^{sx}\tilde{g}(x)dx}. \end{aligned} \tag{2.3.11}$$

It follows that

$$c''(s) = \frac{1}{s^2}[c(s) - \Psi(s)] - \frac{1}{s}[c'(s) - \Psi'(s)]. \tag{2.3.12}$$

Substituting equation (2.3.10) into equation (2.3.12) and multiplying the result by s^2, we obtain

$$[s^2c']'(s) = s\Psi'(s). \tag{2.3.13}$$

By (2.3.11), we conclude that the function s^2c' is increasing. It follows by Lemma 2.3.8 that c has no local maximum. We also have that Ω is connected. In fact, if $s_1, s_2 \in \Omega$ with $s_1 > s_2$, then $[s_1, s_2] \subset \Omega$ by the comparison test for integrals since $\tilde{g}$ is non-negative. This implies that there is at most one local minimum, which is also the global minimum. ∎

The result of Proposition 2.3.7 ensures us that there is at most one value of s that can satisfy equation (2.3.7). Hence, we will have a global minimum when we can solve for s in equation (2.3.7). In this case, solving for c^* can then be done by replacing the obtained value for s in (2.3.6).

2.4 Spreading Speeds and Travelling Waves in IDEs

Now that we are equipped with the main results for the existence of a spreading speed and travelling wave solutions in a given recursion, we can apply them to integrodifference equations. By doing so, we will gain insight on the solution behavior observed in figure 1.2.

Definition 2.4.1. *Let F be a growth function (see definition 2.1.6) and K be a continuous and symmetric distribution kernel of an integrodifference equation. We define the operator Q as follows:*

$$Q[N](x) = \int K(x-y)F(N(y))dy. \tag{2.4.1}$$

By definition, integrodifference equation (2.2.1) becomes a recursion as in (2.3.1), namely

$$N_{t+1}(x) = Q[N_t](x). \tag{2.4.2}$$

In order to establish the existence of a spreading speed, we require this operator to satisfy the hypotheses of Theorem 2.3.3. We will start this section by proving that Q satisfies the continuity property (hypothesis 5).

Proposition 2.4.2. *Let Q be the operator as defined by expression (2.4.1). Assume that F is bounded by M and Lipschitz continuous with constant L. Then $Q[f_t] \to Q[f]$ pointwise given $f_t \to f$ uniformly on compact subsets of $\mathbb{R}$ as $t \to \infty$.*

Proof: For all $m > 0$, we have the following estimate:

$$\begin{aligned}
|Q[f_t](x) - Q[f](x)| &= \left| \int K(x-y)\left[F(f_t(y)) - F(f(y))\right] dy \right| \\
&\leq \int\limits_{|y|>m} K(x-y)\left|F(f_t(y)) - F(f(y))\right| dy + \int\limits_{|y|\leq m} K(x-y)\left|F(f_t(y)) - F(f(y))\right| dy \\
&\leq 2M \int\limits_{|y|>m} K(x-y)dy + L \int\limits_{|y|\leq m} K(x-y)\left|f_t(y) - f(y)\right| dy
\end{aligned}$$

The hypothesis of uniform convergence on compact subsets of $\mathbb{R}$ implies that for all $m > 0$ and for all $\epsilon > 0$, there exists $P > 0$ such that the following holds:

$$\sup_{x\in[-m,m]} |f_t(x) - f(x)| < \epsilon \text{ when } t > P.$$

Hence, the result follows by choosing P and m large enough to get

$$|f_t(y) - f(y)| < \frac{\epsilon}{L} \text{ and } \int\limits_{|y|>m} K(x-y)dy < \frac{\epsilon}{2M}.$$

∎

To establish the existence of travelling waves, we also require Q to satisfy the compactness property described by Theorem 2.3.5. This leads to the next proposition.

Proposition 2.4.3. *Let Q be the operator as defined by expression (2.4.1), where F and K are continuous and bounded functions. Every sequence $\{v_t\}$ of functions in $C_{[0,\beta]}$ has a subsequence $\{v_{t_i}\}$ such that $\{Q[v_{t_i}]\}$ converges uniformly on every bounded subset of $\mathbb{R}$.*

In order to prove Proposition 2.4.3, we will need the results of the following lemma as well as the Arzelà-Ascoli theorem.

Lemma 2.4.4. *Let G be a non-negative bounded function defined on $\mathbb{R}$. Then for all $\epsilon > 0$ there exists $m_\epsilon > 0$ such that for all x*

$$\int\limits_{\mathbb{R}\setminus(-m_\epsilon, m_\epsilon)} K(x-y)G(y)dy < \epsilon.$$

Proof: We have that

$$\int\limits_{\mathbb{R}} K(x-y)dy = 1.$$

Also, since G is bounded, there exists a constant $M > 0$ such that $G(x) \leq M$ for all $x \in \mathbb{R}$. Since the integral of K is finite, for $\epsilon > 0$, choose m_ϵ such that

$$\int\limits_{-m_\epsilon}^{m_\epsilon} K(x-y)dy > 1 - \frac{\epsilon}{M}.$$

It follows that

$$\int\limits_{\mathbb{R}\setminus(-m_\epsilon, m_\epsilon)} K(x-y)G(y)dy < M\frac{\epsilon}{M} = \epsilon.$$

∎

Theorem 2.4.5 (Arzelà-Ascoli [11]). *Let $\{f_t\}$ be a sequence of continuous functions on an interval $I = [a, b]$. Assume that $\{f_t\}$ is uniformly bounded, i.e. there exists $M > 0$ such that $|f_t(x)| \leq M$ for all t. We also assume that $\{f_t\}$ is equicontinuous, i.e. for all $\epsilon > 0$ there exists $\delta > 0$ such that $|f_t(x) - f_t(y)| < \epsilon$ provided $|x - y| < \delta$, where x, $y \in I$. Then there exists a subsequence $\{f_{t_i}\}$ that converges uniformly on I.*

Proof: (**Proof of Proposition 2.4.3**)
Take $m > 0$ and $\{v_t\} \subset C_{[0,\beta]}$. Let

$$f_t(x) = \int_{-m}^{m} K(x - y)F(v_t(y))dy.$$

We consider the sequence $\{f_t\}$ on the interval $I = [a, b]$ for a, $b \in \mathbb{R}$. Since F is bounded, there exists $M > 0$ such that $|F(v_t)| \leq M$. Also, K is bounded, so there exists $B > 0$ such that $|K(x)| \leq B$. For $x \in [a, b]$

$$\begin{aligned} |f_t(x)| &= \left| \int_{-m}^{m} K(x - y)F(v_t(y))dy \right| \\ &\leq \int_{-m}^{m} |K(x - y)F(v_t(y))| \, dy \\ &\leq 2mBM. \end{aligned}$$

Hence, $\{f_t\}$ is uniformly bounded. We also have that $\{f_t\}$ is equicontinuous. In fact, since K is continuous on $\mathbb{R}$, it will be uniformly continuous on compact sets (see Theorem 4.37 in [16]). In particular, K is uniformly continuous on I. Hence, for every $\epsilon > 0$, there exists $\delta > 0$ such that for all $x_1, x_2 \in I$, $|K(x_1) - K(x_2)| < \frac{\epsilon}{2Mm}$ provided $|x_1 - x_2| < \delta$. It thus follows that for x_1, $x_2 \in I$ such that $|x_1 - x_2| < \delta$,

$$\begin{aligned} |f_t(x_1) - f_t(x_2)| &= \left| \int_{-m}^{m} [K(x_1 - y) - K(x_2 - y)]F(v_t(y))dy \right| \\ &\leq M \int_{-m}^{m} |K(x_1 - y) - K(x_2 - y)|dy \\ &< 2mM \frac{\epsilon}{2mM} = \epsilon. \end{aligned}$$

By the Arzelà-Ascoli theorem, it follows that there exists a subsequence $\{f_{t_i}\}$ that converges uniformly on I to some function f^m (the same argument can be applied

when integrating over any finite domain). This implies that for every $\epsilon_0 > 0$ there exists $P_0 > 0$ such that for $t_i > P_0$

$$\sup_{x\in I}\left|\int_{-m}^{m} K(x-y)F(v_{t_i}(y))dy - f^m(x)\right| < \epsilon_0.$$

Now, for a given $\epsilon > 0$, we let $\epsilon = \epsilon_1 + \epsilon_2$, where ϵ_1, $\epsilon_2 > 0$. Since F is continuous and v_{t_i} is bounded, there exists $m_{\epsilon_1} > 0$ such that

$$\int_{\mathbb{R}\setminus(-m_{\epsilon_1},m_{\epsilon_1})} K(x-y)F(v_{t_i}(y))dy < \epsilon_1.$$

by Lemma 2.4.4.
From what precedes, we also have that there exists $P > 0$ such that for $t_i > P$

$$\sup_{x\in I}\left|\int_{-m_{\epsilon_1}}^{m_{\epsilon_1}} K(x-y)F(v_{t_i}(y))dy - f^{m_{\epsilon_1}}(x)\right| < \epsilon_2.$$

Thus, for $t_i > P$, we have

$$\begin{aligned}
&\sup_{x\in I}|Q[v_{t_i}](x) - f^{m_{\epsilon_1}}(x)| = \sup_{x\in I}\left|\int K(x-y)F(v_{t_i}(y))dy - f^{m_{\epsilon_1}}(x)\right| \\
&\leq \sup_{x\in I}\left(\left|\int_{-m_{\epsilon_1}}^{m_{\epsilon_1}} K(x-y)F(v_{t_i}(y))dy - f^{m_{\epsilon_1}}(x)\right| + \int_{\mathbb{R}\setminus(-m_{\epsilon_1},m_{\epsilon_1})} K(x-y)F(v_{t_i}(y))dy\right) \\
&< \epsilon_1 + \epsilon_1 = \epsilon.
\end{aligned}$$

Thus, $Q[v_{t_i}]$ converges uniformly on bounded subsets of $\mathbb{R}$. ∎

Note that in the previous proof, we can replace the interval $[0, \beta]$ by $[\pi_0, \pi_1]$, where $0 \leq \pi_0 < \pi_1$, as we only require the sequence v_t to be bounded.

2.4.1 Monotone Growth Functions on $[0, \beta]$

Now that we know that Q satisfies the continuity and compactness properties required for the existence of a spreading speed and travelling wave solutions, we must verify

that it also satisfies the other four hypotheses of Theorem 2.3.3. In the next theorem, we will see that the existence of a spreading speed depends on the characteristics of the growth function F. The case where F is non-decreasing on $[0, \beta]$, where 0 and β are the fixed points of F, is the easiest to study, and the results have been known for some time. In fact, it was first explored in [30] before the model was termed as an integrodifference equation. In this section, we will state the results for this case and use the theorems and propositions from section 2.3 to prove them.

Theorem 2.4.6. *Let F be a growth function (see definition 2.1.6) that satisfies the following conditions:*

i) F is bounded and Lipschitz continuous,

ii) $F(0) = 0$ and $F(\beta) = \beta$ are the only two fixed points of F on $[0, \beta]$,

iii) $F'(0) > 1$,

iv) F is non-decreasing on $[0, \beta]$.

Then, there exists a spreading speed c^* for the operator Q defined by equation (2.4.1) *on the interval $[0, \beta]$.*

Proof: In order to show the existence of a spreading speed for the operator Q on the interval $[0, \beta]$, it suffices to show that Q respects the five hypotheses of Theorem 2.3.3 on $[0, \beta]$.

1. Translation invariance:

$$\begin{aligned} Q[N(\cdot - a)](x) &= \int K(x - y)F(N(y - a))dy \\ &= \int K((x - a) - (y - a))F(N(y - a))dy \\ &= \int K((x - a) - y)F(N(y))dy \\ &= Q[N](x - a). \end{aligned}$$

2. Invariance on $[0, \beta]$: (follows from ii), iv) and the fact that K integrates to 1)

$$\begin{aligned} 0 \leq N \leq \beta &\Rightarrow 0 \leq F(N) \leq \beta \\ &\Rightarrow 0 \leq Q[N] \leq \beta. \end{aligned}$$

3. Fixed points (follows from ii), iii) and the fact that K integrates to 1):
   a) $Q[0](x) = 0$ since $F(0) = 0$.
   b) $Q[\beta](x) = \int \beta K(x-y)dy = \beta$.
   c) For $\alpha \in (0,1)$, $F(\alpha) > \alpha$ since $F'(0) > 1$ and $N = \beta$ is the only fixed point on $(0, \beta]$, thus $Q[\alpha](x) > \alpha$.
4. Monotonicity: Similarly to the proof of invariance, monotonicity follows from the hypothesis that F is non-decreasing on $[0, \beta]$.
5. Continuity: See Proposition 2.4.2.

∎

Since K is symmetric, the value c^* from the previous theorem is the spreading speed for the operator Q in both left and right directions. Applying this result in combination with definitions (2.3.2) and (2.3.3), we have the following:

i) For any $N_0 \in C_{[0,\beta]}$ with compact support, the solution of (2.4.2) satisfies

$$\lim_{t\to\infty} \sup_{|x|\geq ct} N_t(x) = 0 \text{ for all } c > c^*. \tag{2.4.3}$$

ii) For any $N_0 \in C_{[0,\beta]}\backslash\{0\}$, the solution of (2.4.2) satisfies

$$\lim_{t\to\infty} \inf_{|x|\leq ct} N_t(x) = \beta \text{ for all } c \in (0, c^*). \tag{2.4.4}$$

The result of the next theorem allows us to calculate the value of c^*, given that the growth function F satisfies an additional condition.

Theorem 2.4.7. *Let F be a function that satisfies the hypotheses of Theorem 2.4.6. If $F(N) \leq F'(0)N$ on $[0, \beta]$, then the spreading speed of Q is given by*

$$c^* = \inf_{s\in\Omega} \frac{1}{s} \log\left(F'(0)\int e^{sx}K(x)dx\right), \tag{2.4.5}$$

where Ω denotes the values of $s > 0$ for which the moment-generating function of K exists. If $\int e^{sx}K(x)dx = \infty$ for all $s > 0$, then $c^* = \infty$.

Proof: Since $F(N) \leq F'(0)N$ on $[0, \beta]$, we have that

$$Q[N](x) \leq \int F'(0)K(y)N(x-y)dy$$

for all $N \in C_{[0,\beta]}$. Now, take $\delta > 0$. We distinguish two cases for δ:

1) If $\delta \geq 1 - 1/F'(0)$, then $(1-\delta)F'(0) \leq 1$. Since $F(N) \geq N$ on $[0, \beta]$, it follows that $F(N) \geq (1-\delta)F'(0)N$ for all $N \in [0, \beta]$.

2) If $0 < \delta < 1 - 1/F'(0)$, then $1 < (1-\delta)F'(0) < F'(0)$. Define G to be the function on $[0, \beta]$ given by the expression

$$G(N) = \begin{cases} F'(0) & \text{if } N = 0, \\ F(N)/N & \text{if } N \in (0, \beta]. \end{cases}$$

We have that $G(\beta) = 1$ and $G(N)$ is continuous on the interval $[0, \beta]$ since $F'(0) = \lim_{N \to 0^+} F(N)/N$. By the intermediate value theorem, for all $\alpha \in (1, F'(0))$, there exists $M \in (0, \beta)$ such that $G(M) = F(M)/M = \alpha$. Hence, there exists $M \in (0, \beta)$ such that $F(M) = (1-\delta)F'(0)M$. Let ϵ be the smallest such M. Since $F'(0) > (1-\delta)F'(0)$, it follows that $F(N) \geq (1-\delta)F'(0)N$ on $[0, \epsilon]$.

Hence, for all $\delta > 0$, there exists $\epsilon > 0$ such that $F(N) \geq (1-\delta)F'(0)N$ on $[0, \epsilon]$. Thus, for all $\delta > 0$, there exists $\epsilon > 0$ such that

$$Q[N](x) \geq (1-\delta) \int F'(0)K(y)N(x-y)dy$$

when $0 \leq N \leq \epsilon$. Using the result of Theorem 2.3.4, we get the formula for c^*. ∎

Note that if we linearize the function F in the operator Q around $N = 0$, we get the following:

$$\begin{aligned} Q[N](x) &= \int K(x-y)F(N(y))dy \\ &\approx \int K(x-y)[F(0) + F'(0)N(y)]dy \\ &= \int F'(0)K(x-y)N(y)dy. \end{aligned}$$

By Theorem 2.3.6, the spreading speed of the operator $\tilde{Q}$ defined by

$$\tilde{Q}[N](x) = \int F'(0)K(x-y)N(y)dy$$

is given by equation (2.4.5).

Definition 2.4.8. *If the spreading speed of Q corresponds to the spreading speed of the operator $\tilde{Q}$ that results from linearizing F at 0 in Q, then we say that c^* is linearly determined.*

Proposition 2.4.9. *Let F be a function that satisfies the hypotheses of Theorem 2.4.6. If $F''(N) \leq 0$ on $[0, \beta]$, then the spreading speed c^* of the operator Q on $[0, \beta]$ is linearly determined.*

Proof: Let $N \in (0, \beta]$. Since F is differentiable (see definition 2.1.6), it follows by the mean value theorem that there exists $c \in (0, N)$ such that

$$F'(c) = \frac{F(N) - F(0)}{N - 0}.$$

Since $F''(N) \leq 0$ on $[0, \beta]$, it follows that $F'(0) \geq F'(c)$. Hence, $F(N) \leq F'(0)N$ for all $N \in [0, \beta]$. The result then follows from Theorem 2.4.7. ∎

Using the results of Theorem 2.3.3 and Proposition 2.4.3, we can also establish the existence of travelling wave solutions for the operator Q.

Theorem 2.4.10. *Let F be a function that satisfies the hypotheses of Theorem 2.4.6. Then for all $c \geq c^*$, there exists a monotone travelling wave solution connecting 0 to β for the recursion defined by equation (2.4.2).*

Proof: By the result of Theorem 2.4.6, we have the existence of a spreading speed c^* for the operator Q. By Proposition 2.4.3, we also have that every sequence $\{v_t\}$ of functions in $C_{[0,\beta]}$ has a subsequence $\{v_{t_i}\}$ such that $\{Q[v_{t_i}]\}$ converges on every bounded subset of $\mathbb{R}$. Hence, applying the result of Theorem 2.3.5, for all $c \geq c^*$ there exists a non-increasing function W such that $N_t(x) = W(x - tc)$ satisfies equation (2.4.2), $W(-\infty) = \beta$ and $W(\infty) = 0$. By symmetry of the distribution kernel K, for all $c \geq c^*$ there exists a non-decreasing function $\tilde{W}$ such that $N_t(x) = \tilde{W}(x+tc)$ satisfies equation (2.4.2), $\tilde{W}(-\infty) = 0$ and $\tilde{W}(\infty) = \beta$. ∎

The Ricker function and the logistic function satisfy the hypotheses of Theorem 2.3.3 with $\beta = 1$ when $r \leq 1$ (see subsections 2.1.1 and 2.1.2). We are able to simulate a travelling wave solution connecting 0 to 1 for the integrodifference equation with those growth functions (see figure 2.13).

2.4.2 Non-Monotone Growth Functions on $[0, \beta]$

In the case of the Ricker function and logistic function, when r exceeds 1, all the hypotheses of Theorem 2.4.6, except monotonicity on $[0, 1]$, are still met. In this section, we will see that even when the growth function F is not monotone on $[0, 1]$, a spreading speed and travelling wave solutions can still exist when $N = 1$ is a stable fixed point (i.e. for $r \leq 2$). We illustrate this in figure 2.14 when F is the Ricker function with $r = 1.5$. These results are demonstrated in [12] and [17], based on ideas that were developped in [27]. We will present and provide proofs for these results by using the methods in [12] and [17].

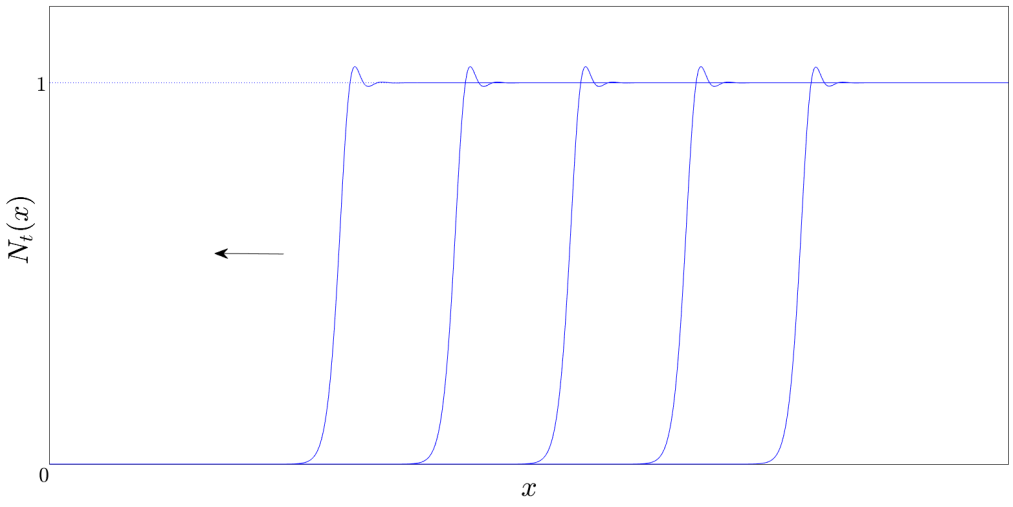

Figure 2.14: Solution of the integrodifference equation, where K is the Laplace kernel with $a = 15$, F is the Ricker function with $r = 1.5$ and $N_0 = \chi_{[x \geq 10]}$, plotted every 10 time steps.

Definition 2.4.11. *Let F be a growth function (see definition 2.1.6) such that*

i) F satisfies the first three hypotheses of Theorem 2.4.6,

ii) there exists $b > \beta$ such that $F([0, b]) = [0, b]$ and $0 < F(N) < N$ on $(\beta, b]$,

iii) $F(N) \leq F'(0)N$ *on* $[0, b]$.

We define functions F^- *and* F^+ *as follows:*

$$F^+(N) := \max_{0 \leq n \leq N} F(n)$$
$$F^-(N) := \min_{N \leq n \leq b} F(n), \text{ for } 0 \leq N \leq b.$$

Define the fixed point of $F^\pm$ as $\tilde{n}^\pm$, i.e. $F^\pm(\tilde{n}^\pm) = \tilde{n}^\pm$. Note that the existence and uniqueness of the fixed points $\tilde{n}^+$ and $\tilde{n}^-$ follow from the intermediate value theorem, the properties of F and the definitions of F^+ and F^-. The functions F^+ and F^- are illustrated in figure 2.15 for the Ricker function, where $b = F(1/r)$, $\tilde{n}^+ = b$, $\tilde{n}^- = F(b)$. Note that $F^-(N) \leq F(N) \leq F^+(N)$ on $[0, b]$. Also, since F is continuous, $F(0) = 0$ and $F(b) > 0$, there exists $\delta \in (0, b]$ such that $F^-(N) = F(N) = F^+(N)$ on $[0, \delta]$.

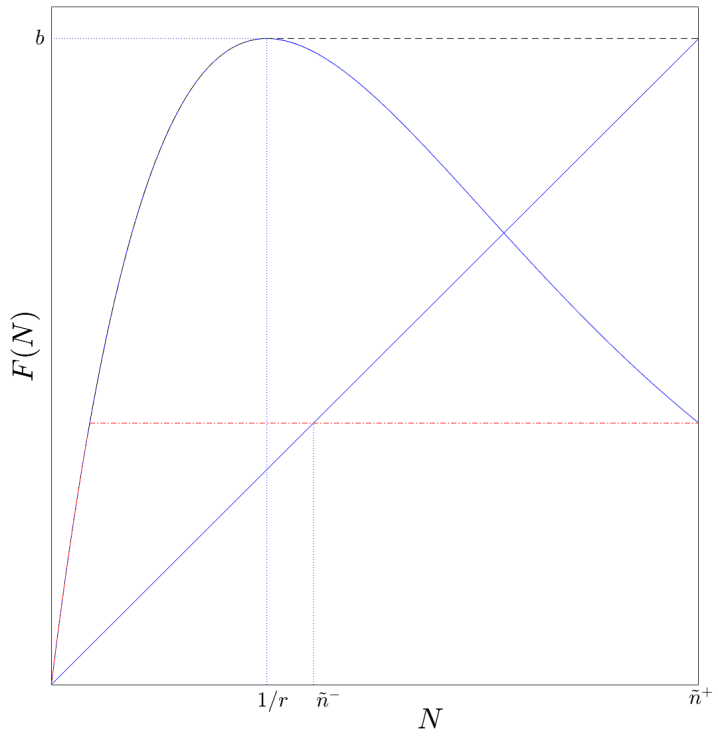

Figure 2.15: Illustration of F^+ and F^- for the Ricker function. The dashed (dash-dot) horizontal line with the increasing portion of the Ricker function is the function F^+ (F^-).

Theorem 2.4.12 (Theorem 2.2 of [12] and Proposition 3.1 of [17]). *Let F be a function that satisfies the hypotheses of the previous definition, and define F^+, F^-, $\tilde{n}^+$ and $\tilde{n}^-$ as previously. Then, assuming that the moment-generating function of K exists for some $s > 0$, the value c^* given by equation* (2.4.5) *is the spreading speed for Q as in (2.4.1) in the following sense:*

i) For any $N_0 \in C_{[0,\tilde{n}^+]}$ with compact support, the solution of (2.4.2) satisfies

$$\lim_{t\to\infty} \sup_{|x|\geq ct} N_t(x) = 0 \text{ for all } c > c^*.$$

ii) For any $N_0 \in C_{[0,\tilde{n}^+]}\backslash\{0\}$, the solution of (2.4.2) satisfies

$$\tilde{n}^- \leq \lim_{t\to\infty} \inf_{|x|\leq ct} N_t(x) \leq \tilde{n}^+.$$

We will require the comparison principle in our proof.

Proposition 2.4.13 (Comparison Principle: Proposition 4.1 in [31]). *Let R be an operator on $C_{[0,\infty)}$. Assume that R is order preserving in the sense that $v \geq w \Rightarrow R[v] \geq R[w]$. If the sequence $\{v_n\}$ satisfies the inequality $v_{n+1} \geq R[v_n]$ while the sequence $\{u_n\}$ satisfies $u_{n+1} \leq R[u_n]$, and if $v_0 \geq u_0$, then $v_n \geq u_n$ for all n.*

Proof: (**Proof of Theorem 2.4.12**)
F^- and F^+ are non-decreasing functions on $[0, b]$. We define operators Q^+ and Q^- by:

$$Q^+[N](x) = \int K(x-y)F^+(N(y))dy,$$
$$Q^-[N](x) = \int K(x-y)F^-(N(y))dy.$$

We have that

$$Q^-[N](x) \leq Q[N](x) \leq Q^+[N](x) \tag{2.4.6}$$

for $0 \leq N \leq b$. Since the functions F^+ and F^- satisfy the hypotheses of Theorem 2.4.6 for $\beta = \tilde{n}^+$ and $\beta = \tilde{n}^-$, respectively, it follows that there exist spreading speeds c^*_+ and c^*_- for operators Q^+ and Q^- on $[0, \tilde{n}^+]$ and $[0, \tilde{n}^-]$, respectively. Since $F^{\pm}(N) \leq F'(0)N$ on $[0, b]$ and $F^-(N) = F(N) = F^+(N)$ near 0, we find $c^*_+ = c^*_- := c^*$ by Theorem 2.3.6. We now proceed to proving i) and ii) from the statement.

i) Let $N_0 \in C_{[0,\tilde{n}^+]}$ with compact support. If $N_t = Q^t(N_0)$ and $N_t^+ = (Q^+)^t(N_0)$, then by the comparison principle,

$$0 \leq N_t(x) \leq N_t^+(x).$$

Applying equation (2.4.3) to the previous inequality gives us the result.

ii) Let $N_0 \in C_{[0,\tilde{n}^+]}\backslash\{0\}$ and $M_0 = \min\{N_0, \tilde{n}^-\}$. It follows that $M_0 \leq N_0$ and $M_0 \in C_{[0,\tilde{n}^-]}\backslash\{0\}$. Since F^- is non-decreasing, $(Q^-)^t(M_0) \leq (Q^-)^t(N_0)$. If $M_t^- = (Q^-)^t(M_0)$, $N_t = Q^t(N_0)$ and $N_t^+ = (Q^+)^t(N_0)$, then by the comparison principle

$$0 \leq M_t^- \leq N_t \leq N_t^+.$$

We get our result by applying equation (2.4.4) with $\beta = \tilde{n}^-$ on the sequence $\{M_t^-\}$ and $\beta = \tilde{n}^+$ on the sequence $\{N_t^+\}$.

∎

The previous theorem does not provide a spreading speed in the same sense as definition 2.4.4, as ii) provides bounds rather than an exact value. However, it was shown in [12] that given additional conditions on F, c^* is then a spreading speed in the sense of definition 2.4.4.

Theorem 2.4.14 (Theorem 2.2(3) of [12])**.** *Let F be a growth function (see definition 2.1.6) that satisfies the hypotheses of Theorem 2.4.12, and let $F^\pm$ and $\tilde{n}^\pm$ be defined as previously. If in addition,*

i) $F(N)/N$ is strictly decreasing for $N \in (0, b]$,

ii) for any $N_1, N_2 \in (0, b]$ satisfying $N_1 < \beta < N_2$, $N_1 > F(N_2)$ and $N_2 < F(N_1)$, we have $N_1 = N_2$,

then for any $N_0 \in C_{[0,\tilde{n}^+]}\backslash\{0\}$, the solution of (2.4.2) satisfies

$$\lim_{t\to\infty} \inf_{|x|\leq ct} N_t(x) = \beta \text{ for all } c \in (0, c^*). \tag{2.4.7}$$

The existence of travelling wave solutions was also shown in [12] and [17], and is stated in the next theorem.

Theorem 2.4.15 (Theorems 3.1 and 3.2 of [12] and Theorem 4.1 of [17]). *Let F be a function that satisfies the hypotheses of Theorem 2.4.12. Let c^* denote the spreading speed of the operator Q, and let $\tilde{n}^-$ and $\tilde{n}^+$ be defined as in the proof of Theorem 2.4.12. Then, for any $c \geq c^*$, equation (2.4.2) has a travelling wave solution $N_t(x) = W(x + tc)$ with $W(x) \leq \tilde{n}^+$ for all x, $W(-\infty) = 0$ and $\limsup_{x\to\infty} W(x) \geq \tilde{n}^-$.*

As stated in Theorems 3.1 and 3.2 in [12], if in addition to the hypotheses of Theorem 2.4.12, F respects the two additional conditions stated in Theorem 2.4.14, then $W(\infty) = \beta$.

In the case of the Ricker function and the logistic function, it was stated in [12] that F satisfies the hypotheses of Theorem 2.4.14 when $r \leq 2$ for $b = F(1/r)$ and $b = F((1 + r)/2r)$, respectively. We illustrated the shape of a travelling wave connecting 0 to 1 in this case in figure 2.14. When $r > 2$, the steady state $N = 1$ is unstable and the solution we observe during simulation (figure 2.16) is not in the form of a travelling wave. However, there is a spreading speed c^* in the sense of Theorem 2.4.12, as illustrated in figure 2.16. We observe that this value of c^* corresponds to the rate at which the connection between 0 and 1 moves in the solution.

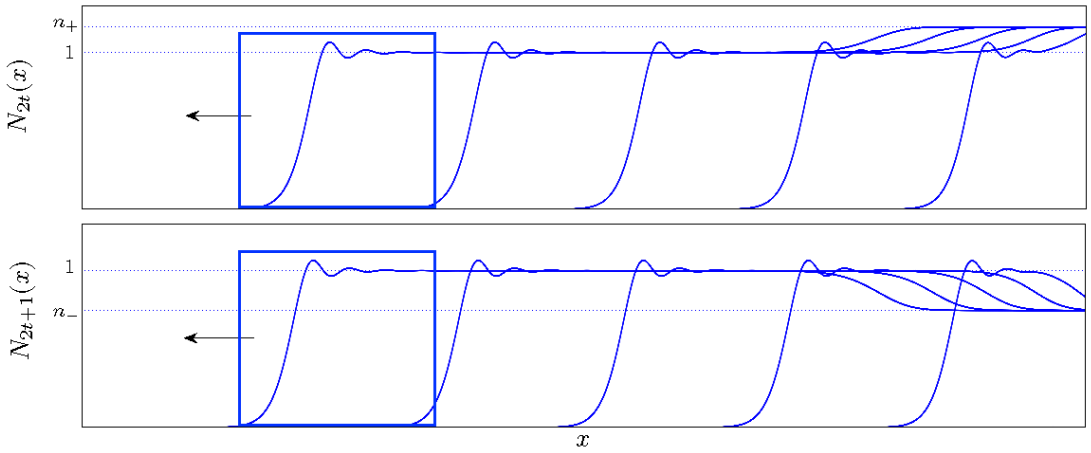

Figure 2.16: (Reminder of figure 1.2.) Solution of the integrodifference equation, where F is the logistic function with $r = 2.2$, K is the Laplace kernel with $a = 6$ and $N_0 = n_+\chi_{[x\geq 10]}$, plotted for even (top panel) and odd (bottom panel) generations every 10 time steps. n_- and n_+ are the values that form the 2-point cycle. The box in the plot represents the portion of the solution with speed c^*.

2.4.3 Calculating the Spreading Speed

The spreading speed c^* on $[0,1]$ for an integrodifference equation with a Ricker function or logistic function is determined by equation (2.4.5), regardless of whether the growth function is monotone on $[0,1]$. From equations (2.3.6) and (2.3.7), the value of c^* can be obtained by using the following parametrization:

$$c = \frac{M_K'(s)}{M_K(s)} \tag{2.4.8}$$

and

$$F'(0) = \frac{e^{sM_K'(s)/M_K(s)}}{M_K(s)}, \tag{2.4.9}$$

assuming equation (2.4.9) can be solved for s. As usual, M_K denotes the moment-generating function of K. In this section, we will show how to calculate the well-known spreading speed for an integrodifference equation when K is the Gaussian kernel. We will also express the spreading speed when K is the Laplace kernel in terms of the Lambert W function, something that has not yet been done in the literature.

Gaussian kernel: Let K be defined by equation (2.2.2). We have that $M_K(s) = e^{\sigma^2 s^2/2}$ (see appendix A.1.1). It follows that $M_K'(s) = \sigma^2 s M_K(s)$. Replacing the two expressions in equations (2.4.8) and (2.4.9), we find

$$c = \sigma^2 s, \tag{2.4.10}$$

$$F'(0) = e^{\sigma^2 s^2/2}. \tag{2.4.11}$$

We solve for s in equation (2.4.11):

$$F'(0) = e^{\sigma^2 s^2/2} \Rightarrow s = \sqrt{\frac{2}{\sigma^2}\log(F'(0))}.$$

Thus, replacing s into equation (2.4.10), we get the value of c^*:

$$c^* = \sqrt{2\sigma^2 \log(F'(0))}. \tag{2.4.12}$$

Note that if $F'(0)$ increases with r, then c^* is an increasing function with respect to r. In the case of the Ricker function, we will have

$$c^* = \sqrt{2\sigma^2 r},$$

whereas in the case of the logistic function, we will have

$$c^* = \sqrt{2\sigma^2 \log(1+r)}.$$

Laplace kernel: Let K be defined by equation (2.2.3). We have that $M_K(s) = \frac{a^2}{a^2-s^2}$ for $|s| < a$. (see appendix A.1.2) It follows that $M'_K(s) = \frac{2s}{a^2-s^2} M_K(s)$. Replacing the two expressions in equations (2.4.8) and (2.4.9), we get:

$$c = \frac{2s}{a^2 - s^2}, \tag{2.4.13}$$

$$F'(0) = \frac{a^2 - s^2}{a^2} \exp\left(\frac{2s^2}{a^2 - s^2}\right). \tag{2.4.14}$$

In order to get the value of c^*, we use the Lambert W function as described in appendix B. We solve for s in equation (2.4.14):

$$\begin{aligned} F'(0) = \frac{a^2 - s^2}{a^2} \exp\left(\frac{2s^2}{a^2 - s^2}\right) &\Rightarrow F'(0)\frac{a^2}{a^2 - s^2} = \exp\left(\frac{2s^2}{a^2 - s^2}\right) \\ &\Rightarrow F'(0)\frac{a^2}{a^2 - s^2} = \exp\left(2\left(\frac{a^2}{a^2 - s^2} - 1\right)\right) \\ &\Rightarrow \frac{F'(0)e^2}{2}\frac{2a^2}{a^2 - s^2} = \exp\left(\frac{2a^2}{a^2 - s^2}\right). \end{aligned}$$

This expansion is an equation of the form $\rho x = e^x$, where $\rho = \frac{F'(0)e^2}{2}$ and $x = \frac{2a^2}{a^2-s^2}$. According to equation (B.1.1), it follows that

$$\frac{2a^2}{a^2 - s^2} = -W\left(-\frac{2}{F'(0)e^2}\right),$$

where W is the Lambert W function. Isolating s, we get

$$s = a\sqrt{\frac{2}{W\left(-\frac{2}{F'(0)e^2}\right)} + 1}.$$

In order for s to be a real positive number, we first need $W\left(-\frac{2}{F'(0)e^2}\right)$ to be real. We thus require the following condition (see appendix B):

$$-\frac{2}{F'(0)e^2} \geq -\frac{1}{e}.$$

The previous inequality is satisfied and $-\frac{1}{e} < -\frac{2}{F'(0)e^2} < 0$, since $F'(0) > 1$. As explained in appendix B, we have two real solutions, $W_0\left(-\frac{2}{F'(0)e^2}\right)$ and

$W_{-1}\left(-\frac{2}{F'(0)e^2}\right)$.
We also require that

$$\frac{2}{W\left(-\frac{2}{F'(0)e^2}\right)}+1\geq 0 \Rightarrow W\left(-\frac{2}{F'(0)e^2}\right)\leq -2.$$

This last condition cannot be satisfied by the function W_0 as its minimum is -1 (see figure B.1). However, it is satisfied by W_{-1} when $-\frac{2}{e^2}\leq -\frac{2}{F'(0)e^2}<0$ (see figure B.2), which is the case for all $r>0$, since $F'(0)>1$. Thus, we have

$$s=a\sqrt{\frac{2}{W_{-1}\left(-\frac{2}{F'(0)e^2}\right)}+1}. \tag{2.4.15}$$

By equation (2.4.13), it follows that

$$c^*=-\frac{1}{a}W_{-1}\left(-\frac{2}{F'(0)e^2}\right)\sqrt{\frac{2}{W_{-1}\left(-\frac{2}{F'(0)e^2}\right)}+1}. \tag{2.4.16}$$

Note that if $F'(0)$ increases with r, then c^* is an increasing function with respect to r. In fact, the expression in (2.4.13) is increasing with respect to s and expression (2.4.15) increases as $F'(0)$ increases since the Lambert W function is decreasing on $[-1/e,0]$ (see figure B.2). In the case of the Ricker function, we will have

$$c^*=-\frac{1}{a}W_{-1}\left(-\frac{2}{e^{r+2}}\right)\sqrt{\frac{2}{W_{-1}\left(-\frac{2}{e^{r+2}}\right)}+1}.$$

In the case of the logistic function, we will have

$$c^*=-\frac{1}{a}W_{-1}\left(-\frac{2}{(1+r)e^2}\right)\sqrt{\frac{2}{W_{-1}\left(-\frac{2}{(1+r)e^2}\right)}+1}.$$

Chapter 3

Second Iterate IDEs

The results from the previous chapter, more specifically sections 2.3 and 2.4, allow us to calculate a spreading speed for the connection from 0 to 1 that was observed in the solution of the integrodifference equation with a growth function that exhibits a stable 2-point cycle (see figure 2.16). In this chapter, we will go a step further and try to understand the connection from 1 to n_+ that we saw in the simulations, which in parallel will give us insight on the connection from 1 to n_-. In order to do so, we will first generalize the theory from section 2.3 and apply it to integrodifference equations with stable 2-point cycles. We will end the chapter with some calculations and simulations.

3.1 Generalizing Weinberger's Theory

The theory from [31] that we explored in section 2.3 allows us to define and show the existence of a spreading speed and travelling waves for solutions that connect from 0 to some $\beta > 0$ in a given recursion. In this section, we are going to show that these results can also be applied in a more general setting. More specifically, we will show that we can still define a spreading speed and travelling waves for solutions that connect from some $\pi_0 > 0$ to $\pi_1 > \pi_0$. Such a generalization was considered in the Corollary of Proposition 3 in [18], but we will provide the detailed proofs here. We will then use these results to study the connection from 1 to n_+ in the solution of the integrodifference equation with a stable 2-point cycle.

Definition 3.1.1. *Let $C_{[\pi_0,\pi_1]}$ denote the set of continuous functions on $\mathbb{R}$ with values on the interval $[\pi_0, \pi_1]$ where $\pi_1 > \pi_0 \geq 0$. Let R denote an operator on $C_{[\pi_0,\pi_1]}$. For*

$u_0 \in C_{[\pi_0,\pi_1]}$, we define the following recursion:

$$u_{t+1} = R[u_t]. \tag{3.1.1}$$

We start this section by generalizing the definition of a spreading speed.

Definition 3.1.2. *The value $c^*_{[\pi_0,\pi_1]}$ is called the rightward asymptotic spreading speed of R on $[\pi_0, \pi_1]$ if the following conditions hold:*

i) For any $u_0 \in C_{[\pi_0,\pi_1]}$ such that $u_0 - \pi_0$ has compact support,

$$\lim_{t\to\infty} \sup_{x\geq ct} u_t(x) = \pi_0 \text{ for all } c > c^*_{[\pi_0,\pi_1]}. \tag{3.1.2}$$

ii) For any $u_0 \in C_{[\pi_0,\pi_1]}\backslash\{\pi_0\} := \{u \in C_{[\pi_0,\pi_1]} : u - \pi_0 \neq 0\}$,

$$\lim_{t\to\infty} \inf_{x\leq ct} u_t(x) = \pi_1 \text{ for all } c \in (0, c^*_{[\pi_0,\pi_1]}). \tag{3.1.3}$$

With this generalized definition of a spreading speed, we will be able to show the existence of a spreading speed and travelling wave solutions for the operator R by translation of the construction in section 2.3. We start by establishing the conditions for the existence of a spreading speed.

Theorem 3.1.3. *Assume the following hypotheses on the operator R that defines a recursion like (3.1.1):*

1. *Translation invariance: $R[u(\cdot - a)](x) = R[u](x - a)$.*
2. *Invariance on $C_{[\pi_0,\pi_1]}$: $u \in C_{[\pi_0,\pi_1]} \Rightarrow R[u] \in C_{[\pi_0,\pi_1]}$.*
3. *Fixed points:*
   a) *$R[\pi_0](x) = \pi_0$, where π_0 denotes the constant function with value π_0,*
   b) *$R[\pi_1](x) = \pi_1$, where π_1 denotes the constant function with value π_1,*
   c) *$R[\alpha](x) > \alpha$ for any constant function $\alpha \in C_{(\pi_0,\pi_1)}$.*
4. *Monotonicity: $\pi_0 \leq u \leq w \leq \pi_1 \Rightarrow R[u] \leq R[w]$.*
5. *Continuity: If $\{f_t\} \subset C_{[\pi_0,\pi_1]}$ and $f_t \to f$ uniformly on compact subsets of $\mathbb{R}$ then $R[f_t] \to R[f]$ pointwise as $t \to \infty$.*

Then there exists a spreading speed $c^*_{[\pi_0,\pi_1]}$ for the operator R on the interval $[\pi_0, \pi_1]$.

Proof: Let $\tilde{R}$ be the operator defined by

$$\tilde{R}[u] = R[u + \pi_0] - \pi_0. \tag{3.1.4}$$

$\tilde{R}$ is thus an operator on $C_{[0,\pi_1-\pi_0]}$ that defines the following recursion:

$$u_{t+1} = \tilde{R}[u_t], \tag{3.1.5}$$

for $u_0 \in C_{[0,\pi_1-\pi_0]}$. We will show that $\tilde{R}$ satisfies the hypotheses of Theorem 2.3.3 with $\beta = \pi_1 - \pi_0$.

1. Translation invariance:

$$\begin{aligned}\tilde{R}[u(\cdot - a)](x) &= R[(u + \pi_0)(\cdot - a)](x) - \pi_0 \\ &= R[u + \pi_0](x - a) - \pi_0 \\ &= (R[u + \pi_0] - \pi_0)(x - a) \\ &= \tilde{R}[u](x - a)\end{aligned}$$

2. Invariance on $C_{[0,\pi_1-\pi_0]}$:

$$\begin{aligned}u \in C_{[0,\pi_1-\pi_0]} &\Rightarrow u + \pi_0 \in C_{[\pi_0,\pi_1]} \\ &\Rightarrow R[u + \pi_0] \in C_{[\pi_0,\pi_1]} \\ &\Rightarrow \tilde{R}[u] = R[u + \pi_0] - \pi_0 \in C_{[0,\pi_1-\pi_0]}\end{aligned}$$

3. Fixed points:

   a) $\tilde{R}[0](x) = R[\pi_0](x) - \pi_0 = \pi_0 - \pi_0 = 0$

   b) $\tilde{R}[\pi_1 - \pi_0](x) = R[\pi_1](x) - \pi_0 = \pi_1 - \pi_0$

   c) For any constant function $\alpha \in C_{(0,\pi_1-\pi_0)}$,
   $\tilde{R}[\alpha](x) = R[\alpha + \pi_0](x) - \pi_0 > \alpha + \pi_0 - \pi_0 = \alpha$.

4. Monotonicity:

$$\begin{aligned}0 \le u \le w \le \pi_1 - \pi_0 &\Rightarrow \pi_0 \le u + \pi_0 \le w + \pi_0 \le \pi_1 \\ &\Rightarrow \tilde{R}[u] = R[u + \pi_0] - \pi_0 \le R[w + \pi_0] - \pi_0 = \tilde{R}[w]\end{aligned}$$

5. Continuity:

$$\begin{aligned}f_t \to f \text{ uniformly} &\Rightarrow f_t + \pi_0 \to f + \pi_0 \text{ uniformly} \\ &\Rightarrow R[f_t + \pi_0] \to R[f + \pi_0] \text{ pointwise} \\ &\Rightarrow \tilde{R}[f_t] \to \tilde{R}[f] \text{ pointwise}\end{aligned}$$

We conclude that there exists a spreading speed c^* for the operator $\tilde{R}$ on $[0, \pi_1 - \pi_0]$. Thus, equations (2.3.2) and (2.3.3) are satisfied with $\beta = \pi_1 - \pi_0$ for the solution of (3.1.5). This implies that equations (3.1.2) and (3.1.3) are satisfied for the solution of equation (3.1.1) with $c^*_{[\pi_0,\pi_1]} = c^*$, which concludes the proof. ∎

When a spreading speed $c^*_{[\pi_0,\pi_1]}$ exists for the operator R, the following theorem allows us to calculate its value.

Theorem 3.1.4. *Let R be an operator that satisfies the hypotheses of Theorem 3.1.3. Let g be a bounded non-negative measurable function on $\mathbb{R}$ with the following properties:*

1. *for all $u \in C_{[\pi_0,\pi_1]}$*

$$R[u](x) \leq \int (u(x-y) - \pi_0) g(y) dy + \pi_0,$$

2. *for all $\delta > 0$, there exists $\epsilon > 0$ such that when $\pi_0 \leq u \leq \pi_0 + \epsilon$*

$$R[u](x) \geq (1-\delta) \int (u(x-y) - \pi_0) g(y) dy + \pi_0.$$

Then, the value of $c^*_{[\pi_0,\pi_1]}$ is given by

$$c^*_{[\pi_0,\pi_1]} = \inf_{s \in \Omega} \frac{1}{s} \log \left(\int e^{sx} g(x) dx \right), \tag{3.1.6}$$

where Ω represents the values of $s > 0$ for which the moment-generating function of g exists. If $\int e^{sx} g(x) dx = \infty$ for all $s > 0$, then $c^*_{[\pi_0,\pi_1]} = \infty$.

Proof: Let $\tilde{R}$ be the operator defined by equation (3.1.4). We can easily verify that $\tilde{R}$ satisfies the hypotheses of Theorem 2.3.4 for $\beta = \pi_1 - \pi_0$. Hence, the speed c^* of $\tilde{R}$ is given by equation (3.1.6), which in turn corresponds to the speed $c^*_{[\pi_0,\pi_1]}$ of R, as shown in the proof of Theorem 3.1.3. ∎

Now that we have established the existence of a spreading speed for an operator R on $[\pi_0, \pi_1]$, we can provide conditions for the existence of travelling wave solutions for the recursion defined by expression (3.1.1).

Theorem 3.1.5. *Let R be an operator on $C_{[\pi_0,\pi_1]}$ that satisfies the hypotheses of Theorem 3.1.3. Assume that every sequence $\{v_t\}$ of functions in $C_{[\pi_0,\pi_1]}$ has a subsequence $\{v_{t_i}\}$ such that $\{R[v_{t_i}]\}$ converges uniformly on every bounded subset of $\mathbb{R}$. Then for all $c \geq c^*_{[\pi_0,\pi_1]}$, there exists a non-increasing function W such that $U_t(x) = W(x - tc)$ satisfies (3.1.1), $W(-\infty) = \pi_1$ and $W(\infty) = \pi_0$. We refer to W as a monotone travelling wave solution of the recursion.*

Proof: Let $\tilde{R}$ be the operator defined by equation (3.1.4). We have that $\tilde{R}$ satisfies the hypotheses of Theorem 2.3.3 with $\beta = \pi_1 - \pi_0$. Let $\{v_t\}$ be a sequence in $C_{[0,\pi_1-\pi_0]}$. Then $\{v_t + \pi_0\}$ is a sequence in $C_{[\pi_0,\pi_1]}$. By assumption, there exists a subsequence $\{v_{t_i} + \pi_0\}$ such that $\{R[v_{t_i} + \pi_0]\}$ converges uniformly on bounded subsets of $\mathbb{R}$. It thus follows that $\{\tilde{R}[v_{t_i}]\}$ converges uniformly on bounded subsets of $\mathbb{R}$. Since $\tilde{R}$ satisfies the compactness property of Theorem 2.3.5, there exists a non-increasing function w such that for all $c \geq c^* = c^*_{[\pi_0,\pi_1]}$ the function $u_t = w(x-tc)$ satisfies (3.1.5), $w(-\infty) = \pi_1 - \pi_0$ and $w(\infty) = 0$. Let $W(x) := w(x) + \pi_0$. W is a non-increasing function such that for all $c \geq c^*_{[\pi_0,\pi_1]}$, the function $U_t = W(x - tc)$ satisfies equation (3.1.1). We also have that $W(-\infty) = \pi_1$ and $W(\infty) = \pi_0$, which concludes the proof. ∎

Finally, we generalize the result of Proposition 2.3.6, by seeing that the spreading speed $c^*_{[\pi_0,\pi_1]}$ corresponds to the minimal wave speed.

Proposition 3.1.6. *Let g be a bounded non-negative function on $\mathbb{R}$ and R be the operator on $C_{[0,\infty)}$ defined by $R[u](x) = \int (u(x-y)-\pi_0)g(y)dy+\pi_0$. Then the spreading speed $c^*_{\pi_0}$ of R is given by equation* (3.1.6)*, assuming that the moment-generating function of g exists for some $s > 0$. If $\int e^{sx}g(x)dx = \infty$ for all $s > 0$, then $c^*_{\pi_0} = \infty$.*

Proof: Similarly to the previous proofs, we construct the operator $\tilde{R}$ (3.1.4), whose spreading speed is given by the result of Proposition 2.3.6. ∎

Note that we do not refer to the spreading speed of R as $c^*_{[\pi_0,\pi_1]}$ in the previous proposition since the operator may not satisfy the hypotheses of Theorem 3.1.3, namely hypothesis 2. Instead, we refer to the spreading speed as being the minimal wave speed, and we denote it by $c^*_{\pi_0}$ since π_0 is a fixed point of R. Also, since the formulas for the spreading speed are the same as in section 2.3, we can apply Proposition 2.3.7 to find a parametric representation of $c^*_{[\pi_0,\pi_1]}$ by using equations (2.3.6) and (2.3.7).

3.2 Spreading Speed and Travelling Waves in Second Iterate IDEs

Now that we have established the criteria for the existence of a spreading speed and travelling wave solutions that connect two positive numbers, we will apply those results to integrodifference equations. More specifically, we will justify the presence of a connection between 1 and n_+ (similarly between 1 and n_-) observed when the growth function exhibits a 2-point cycle. To do so, we first construct an operator q. In order to capture the behavior of this connection, this operator needs to describe the solution of the integrodifference equation every other time step (see figure 3.1).

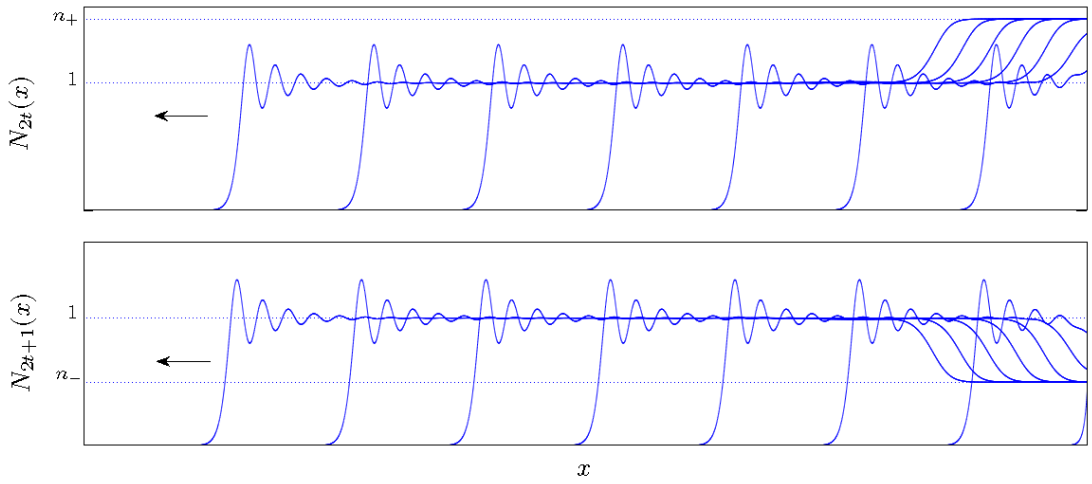

Figure 3.1: Solution of the integrodifference equation, where F is the Ricker function with $r = 2.2$, K is the Laplace kernel with $a = 15$ and $N_0 = n_+\chi_{[x\geq 10]}$, plotted for even (top panel) and odd (bottom panel) generations every 10 time steps. n_- and n_+ are the values that form the 2-point cycle.

Definition 3.2.1. *Let F be a growth function (see definition 2.1.6) and K be a continuous and symmetric distribution kernel of an integrodifference equation. We define the operator q as follows:*

$$\begin{aligned} q[N](x) &:= (Q \circ Q)[N](x) \\ &= \int K(x-y)F(Q[N](y))dy \\ &= \int K(x-y)F\left(\int K(y-z)F(N(z))dz\right)dy, \end{aligned} \tag{3.2.1}$$

where Q is the operator defined in (2.4.1).

By the previous definition, if $N_{t+1}(x) = Q[N_t](x)$, then

$$N_{t+2}(x) = q[N_t](x).$$

Thus, q represents the solution of the integrodifference equation at every other time step. Using a change of indices, we write

$$\tilde{N}_{t+1}(x) = q[\tilde{N}_t](x). \tag{3.2.2}$$

We will drop tildes hereafter if no confusion can arise.

In order to establish the existence of a spreading speed, we require this operator to satisfy the hypotheses of Theorem 3.1.3. We will start this section by proving that q satisfies the continuity property (hypothesis 5).

Proposition 3.2.2. *Let q be the operator defined in expression (3.2.1). Assume F is bounded by M and Lipschitz continuous with constant L. Then $q[f_t] \to q[f]$ pointwise given $f_t \to f$ uniformly on compact subsets of $\mathbb{R}$ as $t \to \infty$.*

To prove this result, we apply the dominated convergence theorem (see [9]).

Theorem 3.2.3 (Dominated convergence theorem for real-valued functions)**.** *Let $\{f_t\}$ be a sequence of real-valued continuous functions on $\mathbb{R}$. Suppose that the sequence is dominated by an integrable function g, i.e. $|f_t| < g$ with $\int g(x)dx < \infty$ for all t. If $\{f_t\}$ converges pointwise to a function f, then*

$$\lim_{t\to\infty} \int f_t(x)dx = \int f(x)dx.$$

Proof: (**Proof of Proposition 3.2.2**)
We assume that $f_t \to f$ uniformly on compact subsets of $\mathbb{R}$. By definition (3.2.1),

$$q[f_t](x) = Q[Q[f_t]](x) = \int K(x-y)F\left(Q[f_t](y)\right)dy.$$

Using the result of Proposition 2.4.2, we have that $Q[f_t] \to Q[f]$ pointwise. By the continuity of F, $K(x-y)F\left(Q[f_t](y)\right) \to K(x-y)F\left(Q[f](y)\right)$ pointwise. Since F is bounded by M, it follows that $|K(x-y)F\left(Q[f_t](y)\right)| \leq K(x-y)M$, with $\int K(x-y)Mdx < \infty$. Thus, we can apply the dominated convergence theorem to get the result. ∎

To establish the existence of travelling waves, we also require q to satisfy the compactness property described by Theorem 3.1.5. This leads to the next proposition.

Proposition 3.2.4. *Let q be the operator defined in expression (3.2.1), where F and K are continuous functions, and F is bounded by M. Every sequence $\{v_t\}$ of functions in $C_{[\pi_0,\pi_1]}$ has a subsequence $\{v_{t_i}\}$ such that $\{q[v_{t_i}]\}$ converges uniformly on every bounded subset of $\mathbb{R}$.*

Proof: Take $\{v_t\} \subset C_{[\pi_0,\pi_1]}$. Let $u_t = Q[v_t]$, where Q is the operator defined in (2.4.1). We have that $\{u_t\}$ is continuous and bounded since F and K are continuous, F is bounded and K integrates to 1. From Theorem 2.4.3, there exists a subsequence $\{u_{t_i}\}$ such that $\{Q[u_{t_i}]\}$ converges uniformly on bounded subsets of $\mathbb{R}$. Since $q[v_t] = Q[Q[v_t]] = Q[u_t]$, we conclude that there exists a subsequence $\{v_{t_i}\}$ such that $\{q[v_{t_i}]\}$ converges uniformly on bounded subsets of $\mathbb{R}$. ∎

Now that we have established some properties of q, we are ready to apply the results of section 3.1. In particular, we are looking at integrodifference equations for which the growth function exhibits a stable 2-point cycle, whose values are denoted by n_- and n_+. We wish to study the existence of a spreading speed and travelling wave solutions between a fixed point β of F, where $n_- < \beta < n_+$, and n_+. In order to do so, we will start by studying growth functions that are monotone on the interval $[n_-, n_+]$.

3.2.1 Non-Increasing Functions on $[n_-, n_+]$

We begin this section by establishing the existence of a spreading speed on $[\beta, n_+]$ for the operator q in the case where F is non-increasing on the interval $[n_-, n_+]$. When F is the Ricker function or the logistic function with a 2-point cycle, we take $\beta = 1$ to study the connection between 1 and n_+ that was observed during simulations.

Theorem 3.2.5. *Let F be a growth function (see definition 2.1.6) that satisfies the following conditions:*

i) F is bounded and Lipschitz continuous,

ii) F has exactly one stable 2-point cycle, i.e. there exist n_- and n_+ such that $0 < n_- < n_+$, and $F(n_-) = n_+$ and $F(n_+) = n_-$,

iii) $N = \beta$ is the only fixed point of F on the interval $[n_-, n_+]$,

iv) $F'(\beta) < -1$,

v) F is non-increasing on the interval $[n_-, n_+]$.

Then, there exists a spreading speed $c^*_{[\beta,n_+]}$ for the operator q defined by equation (3.2.1) *on the interval $[\beta, n_+]$.*

Proof: In order to show the existence of a spreading speed for the operator q on the interval $[\beta, n_+]$, it suffices to show that q satisfies the five hypotheses of Theorem 3.1.3 on $[\beta, n_+]$.

1. Translation invariance: (follows from the translation invariance of Q)

$$\begin{aligned} q[N(\cdot - a)](x) &= Q[Q[N(\cdot - a)]](x) \\ &= \int K(x-y)F\left(Q[N(\cdot - a)](y)\right) dy \\ &= \int K(x-y)F\left(Q[N](y-a)\right) dy \\ &= \int K((x-a)-(y-a))F\left(Q[N](y-a)\right) dy \\ &= \int K((x-a)-y)F\left(Q[N](y)\right) dy \\ &= q[N](x-a). \end{aligned}$$

2. Invariance on $[\beta, n_+]$: (follows from ii), v) and the fact that K integrates to 1)

$$\begin{aligned} \beta \leq N \leq n_+ &\Rightarrow n_- \leq F(N) \leq \beta \\ &\Rightarrow n_- \leq Q[N] \leq \beta \\ &\Rightarrow \beta \leq F(Q[N]) \leq n_+ \\ &\Rightarrow \beta \leq Q[Q[N]] \leq n_+. \end{aligned}$$

3. Fixed points: (follows from ii), iii), iv) and the fact that K integrates to 1)
   a) $q[\beta](x) = \beta$ since $N = \beta$ is a fixed point of the second iterate map of F.
   b) $q[n_+](x) = n_+$ since $N = n_+$ is a fixed point of the second iterate map of F.
   c) Since $F'(\beta) < -1$, it follows that $(F \circ F)'(\beta) > 1$. Thus, for $\alpha \in (\beta, n_+)$, $F(F(\alpha)) > \alpha$ since there are no fixed points between β and n_+, which implies $q[\alpha](x) > \alpha$.

4. Monotonicity: Similarly to the proof of invariance, monotonicity follows from the hypothesis that F is non-increasing on $[n_-, n_+]$.

5. Continuity: See Proposition 3.2.2.

∎

Since K is symmetric, the value $c^*_{[\beta,n_+]}$ from the previous theorem is the spreading speed for the operator q in both left and right directions. Applying this result in combination with definitions (3.1.2) and (3.1.3), we have the following:

i) For any $N_0 \in C_{[\beta,n_+]}$ such that $N_0 - \beta$ has compact support, the solution of (3.2.2) satisfies

$$\lim_{t\to\infty} \sup_{|x|\geq ct} N_t(x) = \beta \text{ for all } c > c^*_{[\beta,n_+]}. \tag{3.2.3}$$

ii) For any $N_0 \in C_{[\beta,n_+]}\backslash\{\beta\} := \{N \in C_{[\beta,n_+]} : N - \beta \neq 0\}$, the solution of (3.2.2) satisfies

$$\lim_{t\to\infty} \inf_{|x|\leq ct} N_t(x) = n_+ \text{ for all } c \in (0, c^*_{[\beta,n_+]}). \tag{3.2.4}$$

Using the results of Theorem 3.2.5 and Proposition 3.2.4, we can also establish the existence of travelling wave solutions for the operator q.

Theorem 3.2.6. *Let F be a function that satisfies the hypotheses of Theorem 3.2.5. Then for all $c \geq c^*_{[\beta,n_+]}$, there exists a monotone travelling wave solution connecting β to n_+ for the recursion defined by equation* (3.2.2).

Proof: By the result of Theorem 3.2.5, we have the existence of a spreading speed $c^*_{[\beta,n_+]}$ for the operator q. By Proposition 3.2.4, we also have that every sequence $\{v_t\}$ of functions in $C_{[\beta,n_+]}$ has a subsequence $\{v_{t_i}\}$ such that $\{q[v_{t_i}]\}$ converges on every bounded subset of $\mathbb{R}$. Hence, applying the result of Theorem 3.1.5, for all $c \geq c^*_{[\beta,n_+]}$ there exists a non-increasing function W such that $N_t(x) = W(x - tc)$ satisfies equation (3.2.2), $W(-\infty) = n_+$ and $W(\infty) = \beta$. By symmetry of the distribution kernel K, for all $c \geq c^*_{[\beta,n_+]}$ there exists a non-decreasing function $\tilde{W}$ such that $N_t(x) = \tilde{W}(x + tc)$ satisfies equation (3.2.2), $\tilde{W}(-\infty) = \beta$ and $\tilde{W}(\infty) = n_+$. ∎

The Ricker function and the logistic function satisfy the hypotheses of Theorem 3.2.5 with $\beta = 1$ when $2 < r < 2.2564$ and $2 < r < 2.2361$, respectively, as

explained at the end of subsections 2.1.1 and 2.1.2. We illustrate the solution of Q for even and odd time steps in figure 3.2 for this case. The top panel illustrates the travelling wave solution of q connecting 1 and n_+ for an initial condition on $[1, n_+]$. We have an analogous result for the interval $[n_-, 1]$, as the simulation suggests in the bottom panel of figure 3.2. We will further discuss the connection between 1 and n_- in section 5.1.

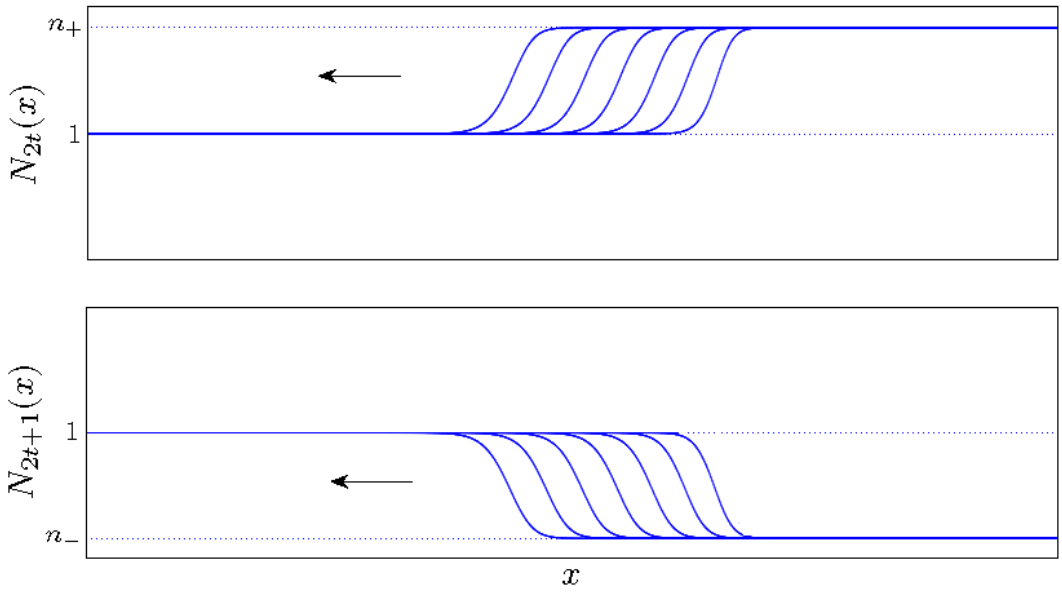

Figure 3.2: Solution of the integrodifference equation, where F is the Ricker function with $r = 2.2$, K is the Laplace kernel with $a = 15$ and $N_0 = \chi_{[x<10]} + n_+\chi_{[x\geq 10]}$, plotted for even (top panel) and odd (bottom panel) generations every 10 time steps. n_- and n_+ are the values that form the 2-point cycle.

Now that we know under what conditions $c^*_{[\beta,n_+]}$ exists for the operator q, we would like to know how to calculate its value. However, given the more complicated nature of q due to the presence of an integral inside the function F, it is very difficult to find a property of F that allows us to bound q in a similar way as done in the proof of Theorem 2.4.7. Instead, we will assume that the spreading speed is linearly determined to obtain the formula in the next proposition. At the end of this chapter, we will then provide some justification as to why we can use this assumption in the case of the Ricker function and the logistic function with the help of numerical simulations.

Proposition 3.2.7. *Assume that F satisfies the hypotheses of Theorem 3.2.5. If the*

spreading speed $c^*_{[\beta,n_+]}$ *of* q *is linearly determined, i.e. it corresponds to the spreading speed of the operator resulting from linearizing* F *at* $N = \beta$ *in* q*, then*

$$c^*_{[\beta,n_+]} = \inf_{s\in\Omega} \frac{1}{s} \log\left([F'(\beta)]^2 \int e^{sx}(K * K)(x)dx \right), \tag{3.2.5}$$

where Ω *denotes the values of* $s > 0$ *for which the moment-generating function of* $K * K$ *exists, and* $K * K$ *denotes the convolution of* K *with itself. If* $\int e^{sx}(K * K)(x)dx = \infty$ *for all* $s > 0$*, then* $c^*_{[\beta,n_+]} = \infty$*.*

Proof: We formally derive the linearization of the operator q around $N = \beta$:

$$\begin{aligned}
q[N](x) &= \int K(x-y)F(Q[N](y))dy \\
&\approx \int K(x-y)[F(\beta) + F'(\beta)(Q[N](y) - \beta)]dy \\
&= \int K(x-y)[\beta + F'(\beta)(Q[N](y) - \beta)]dy \\
&= F'(\beta) \int K(x-y)(Q[N](y) - \beta)dy + \beta \\
&= F'(\beta) \int K(x-y) \left(\int K(y-z)F(N(z))dz - \beta \right) dy + \beta \\
&\approx F'(\beta) \int K(x-y) \left(\int K(y-z)[F(\beta) + F'(\beta)(N(z) - \beta)]dz - \beta \right) dy + \beta \\
&= [F'(\beta)]^2 \int K(x-y) \int K(y-z)(N(z) - \beta)dzdy + \beta \\
&= [F'(\beta)]^2 \int \left(\int K(x-y)K(y-z)dy \right) (N(z) - \beta)dz + \beta \\
&= [F'(\beta)]^2 \int (K * K)(x-z)(N(z) - \beta)dz + \beta.
\end{aligned}$$

Assuming the moment-generating function of $K * K$ exists for some $s > 0$, by Proposition 3.1.6, we have that the spreading speed of the operator $\tilde{q}$ defined by

$$\tilde{q}[N](x) = [F'(\beta)]^2 \int (K * K)(x-z)(N(z) - \beta)dz + \beta$$

is given by equation (3.2.5). ∎

3.2.2 Non-Monotone Growth Functions on $[n_-, n_+]$

In the case of the Ricker function and the logistic function, when r exceeds 2.2565 and 2.2361, respectively, all the hypotheses of Theorem 3.2.5, except monotonicity on $[n_-, n_+]$, are still met. Similarly to the ideas that were developped in [12] and [17] (see section 2.4.2), we would like to construct two new functions F^- and F^+ that satisfy all the hypotheses of Theorem 3.2.5 in order to bound the operator q by two new operators q^- and q^+. This will allow us to show the existence of a spreading speed for the operator q in the case where the growth function is not monotone on $[n_-, n_+]$. We begin by constructing the functions F^- and F^+.

Definition 3.2.8. *Let F be a function such that*

i) F satisfies the first four hypotheses of Theorem 3.2.5,

ii) F has one local maximum at $N = m$, with $F(m) = \tilde{n}$, that is also the global maximum, where $n_- < m < \beta$.

Let n^* be such that $n^* > m$ and $F(n^*) = F(F(\tilde{n}))$. Since F is unimodal, it follows that $n^* < \beta$. We define the functions F^+ and F^- as follows:

$$F^+(N) := \begin{cases} \tilde{n}, & 0 \le N \le m, \\ F(N), & N > m, \end{cases}$$

$$F^-(N) := \begin{cases} F(F(\tilde{n})), & 0 \le N \le n^*, \\ F(N), & N > n^*. \end{cases}$$

Figures 3.3 and 3.4 illustrate the first and second iterate maps of F^+ and F^-, where F is the Ricker function and $m = 1/r$. Note that $F^-(N) \le F(N) \le F^+(N)$ on $[F(\tilde{n}), \tilde{n}]$ and $F^-(N) = F(N) = F^+(N)$ for $N \ge n^*$.

By assumption, $(F \circ F)$ only has n_-, β and n_+ as its fixed points, with $(F \circ F)'(\beta) > 1$, which implies that $(F \circ F)(N) < N$ on (n_-, β). Since $n_- < m < n^* < \beta$, $F(\tilde{n}) = F(F(m)) < m$ and $F^3(\tilde{n}) = F(F(n^*)) < n^*$. We also have that $\tilde{n} > m$ and $(F \circ F)(\tilde{n}) > n^*$ since β is the only positive fixed point of F, F^+ and F^-. With this information, we can easily verify that the fixed points for the second iterate maps of F^+ and F^- are $N = F(\tilde{n})$, $N = \beta$ and $N = \tilde{n}$, and $N = F^3(\tilde{n})$, $N = \beta$ and $N = F(F(\tilde{n}))$, respectively, where $F(F(\tilde{n}))) \le n_+ \le \tilde{n}$. We now proceed to the construction of operators q^- and q^+ in the next theorem to show the existence of a spreading speed for q.

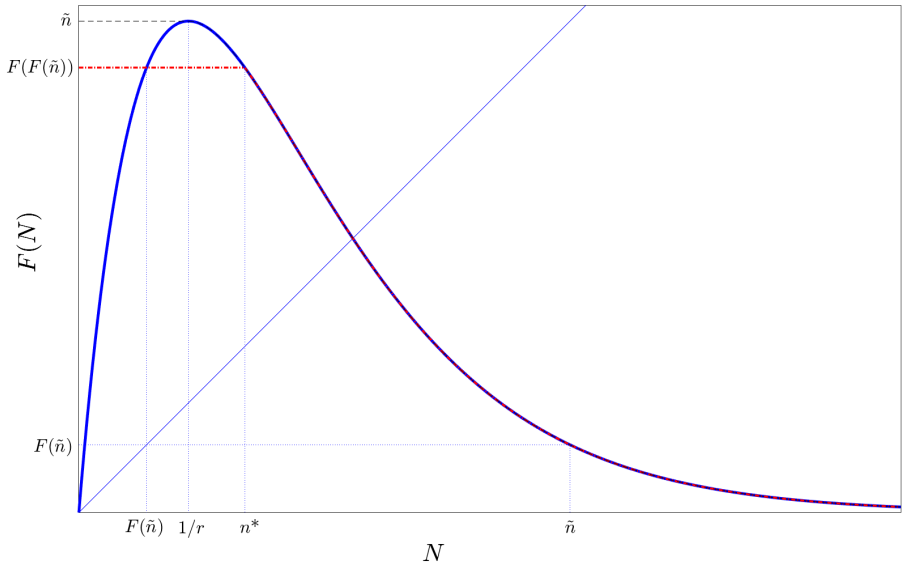

Figure 3.3: Illustration of F^+ and F^- for the Ricker function with $r = 2.5$. The dashed (dash-dot) line with the decreasing portion of the Ricker function is the function F^+ (F^-).

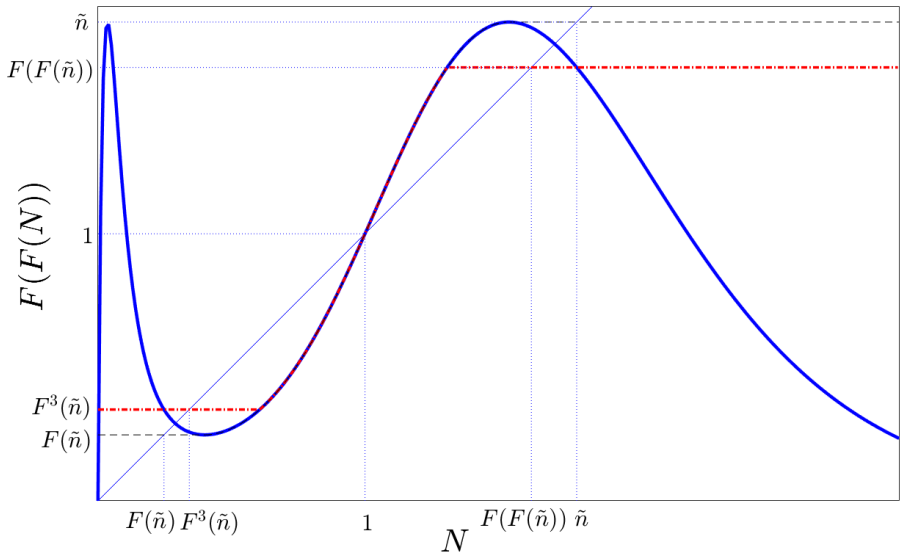

Figure 3.4: Second iterate maps of F^+ and F^- for the Ricker function with $r = 2.5$. The dashed (dash-dot) lines together with the mid-section of the second iterate Ricker map is the function F^+ (F^-).

Theorem 3.2.9. *Let F satisfy the hypotheses of the previous definition, and define F^+, F^- and $\tilde{n}$ as previously. Assume that the spreading speeds on $[\beta, n_+]$ of monotone operators on $[n_-, n_+]$ are linearly determined, i.e. the spreading speed corresponds to the spreading speed of the operator obtained by linearizing at $N = \beta$. Then, if the moment-generating function of $K * K$ exists for some $s > 0$, the value of $c^*_{[\beta,n_+]}$ given by equation (3.2.5) is a spreading speed for q in the following sense:*

i) For any $N_0 \in C_{[\beta,\tilde{n}]}$ such that $N_0 - \beta$ has compact support, the solution of (3.2.2) satisfies

$$\lim_{t\to\infty} \sup_{|x|\geq ct} N_t(x) = \beta \text{ for all } c > c^*_{[\beta,n_+]}.$$

ii) For any $N_0 \in C_{[\beta,\tilde{n}]}\backslash\{\beta\}$, the solution of (3.2.2) satisfies

$$F(F(\tilde{n})) \leq \lim_{t\to\infty} \inf_{|x|\leq ct} N_t(x) \leq \tilde{n} \text{ for all } c \in (0, c^*_{[\beta,n_+]}).$$

Proof: We proceed similarly to the proof of Theorem 2.4.12. F^+ and F^- are non-increasing functions on $[F(\tilde{n}), \tilde{n}]$. We now define the following operators:

$$q^+[N](x) = \int K(x-y)F^+\left(\int K(y-z)F^+(N(z))dz\right)dy,$$
$$q^-[N](x) = \int K(x-y)F^-\left(\int K(y-z)F^-(N(z))dz\right)dy.$$

By construction of F^+ and F^-, we have that

$$q^-[N](x) \leq q[N](x) \leq q^+[N](x) \tag{3.2.6}$$

for $\beta \leq N \leq \tilde{n}$. In fact, for $N \in [\beta, \tilde{n}]$, $\int K(y-z)F(N(z))dz \in [F(\tilde{n}), \beta]$. Thus,

$$F^-\left(\int K(y-z)F(N(z))dz\right) \leq F\left(\int K(y-z)F(N(z))dz\right)$$
$$\leq F^+\left(\int K(y-z)F(N(z))dz\right).$$

Since $F^-(N) = F(N) = F^+(N)$ for $N \geq \beta$, we have

$$F^-\left(\int K(y-z)F^-(N(z))dz\right) \leq F\left(\int K(y-z)F(N(z))dz\right)$$
$$\leq F^+\left(\int K(y-z)F^+(N(z))dz\right).$$

Since F^+ and F^- satisfy the hypotheses of Theorem 3.2.5 for $n_+ = \tilde{n}$ and $n_+ = F(F(\tilde{n}))$, respectively, there exist spreading speeds c^*_+ and c^*_- for the operators q^+ and q^- on $[1, \tilde{n}]$ and $[1, F(F(\tilde{n}))]$, respectively. Since $F^-(N) = F(N) = F^+(N)$ near $N = \beta$ and since we assume that the spreading speeds of q^+ and q^- are linearly determined, we have $c^*_+ = c^*_- = c^*_{[\beta, n_+]}$ by Proposition 3.2.7. We now proceed to proving i) and ii) from the statement.

i) Let $N_0 \in C_{[\beta,\tilde{n}]}$ such that $N_0 - \beta$ has compact support. If $N_t = q^t(N_0)$ and $N^+_t = (q^+)^t(N_0)$, then by the comparison principle (Proposition 2.4.13)

$$\beta \leq N_t(x) \leq N^+_t(x).$$

Applying equation (3.2.3) to the previous inequality gives us our result.

ii) Let $N_0 \in C_{[\beta,\tilde{n}]}\backslash\{\beta\}$ and $M_0 = \min\{N_0, F(F(\tilde{n}))\}$. It follows that $M_0 \leq N_0$ and $M_0 \in C_{[\beta,F(F(\tilde{n}))]}\backslash\{\beta\}$. Since F^- is non-increasing, $(q^-)^t(M_0) \leq (q^-)^t(N_0)$. If $M^-_t = (q^-)^t(M_0)$, $N_t = q^t(N_0)$ and $N^+_t = (q^+)^t(N_0)$, then by the comparison principle

$$\beta \leq M^-_t \leq N_t \leq N^+_t.$$

We get our result by applying equation (3.2.4) with $n_+ = F(F(\tilde{n}))$ to the sequence $\{M^-_t\}$ and $n_+ = \tilde{n}$ to the sequence $\{N^+_t\}$.

∎

We can illustrate the spreading speed on $[1, n_+]$ (and $[n_-, 1]$) as well as travelling wave solutions by numerical simulations. The solution of an integrodifference equation when the growth function is non-monotone on $[n_-, n_+]$ is plotted in figure 3.5 for $1 \leq N_0 \leq n_+$. Note that the sequence described by the operator q for this initial condition is then plotted at the top of the figure.

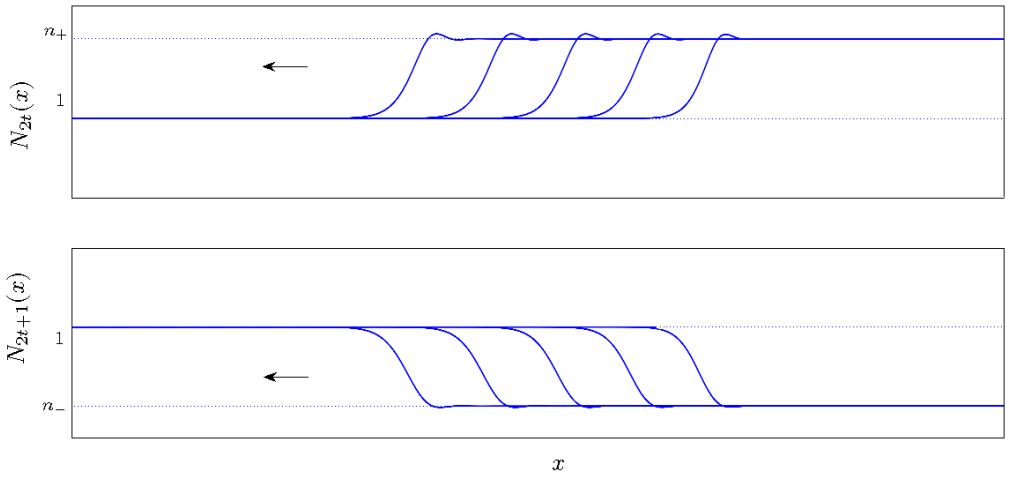

Figure 3.5: Solution of the integrodifference equation, where F is the Ricker function with $r = 2.5$, K is the Laplace kernel with $a = 15$ and $N_0 = \chi_{[x<10]} + n_+\chi_{[x\geq 10]}$, plotted for even (top panel) and odd (bottom panel) generations every 10 time steps. n_- and n_+ are the values that form the 2-point cycle. The top (bottom) panel corresponds to a solution of q for $1 \leq N_0 \leq n_+$ ($n_- \leq N_0 \leq 1$).

3.2.3 Simulations and Calculations

Previously, we constructed the theory assuming that the spreading speed of operator q is linearly determined. In this section, we will explain the motivation behind this assumption. Given that we cannot simulate an infinite domain in a numerical scheme, the solution generated during simulations starts with a compactly supported initial condition. Thus, when a travelling wave solution is simulated, its speed corresponds to the spreading speed (see definitions 2.3.2 and 3.1.2). In order to verify whether the spreading speed of q is linearly determined, we will compare the spreading speed predicted by the linearization with the one observed during numerical simulations.

If F is a growth function (see definition 2.1.6) that satisfies the hypotheses of Theorem 2.4.7, then $(F \circ F)$ also satisfies the same hypotheses on $[0, \beta]$. Let c^* denote the spreading speed of operator Q on $[0, \beta]$, given by equation (2.4.5). It follows that the spreading speed of operator q on $[0, \beta]$ is $2c^*$. We define operator q_2 as follows:

$$q_2[N](x) = \int (K * K)(x - y)(F \circ F)(N(y))dy, \tag{3.2.7}$$

where $K * K$ denotes the convolution product of K with itself. Since $(F \circ F)$ satisfies the hypotheses of Theorem 2.4.7 on $[0, \beta]$, a spreading speed c_2^* exists for the operator

q_2 on $[0, \beta]$ and is given by the following expression

$$c_2^* = \inf_{s \in \Omega} \frac{1}{s} \log \left((F \circ F)'(0) \int e^{sx} (K * K)(x) dx \right),$$

where Ω denotes the values of $s > 0$ for which the moment-generating function of $K * K$ exists. Since the moment-generating function of a convolution is the product of moment-generating functions (see appendix A.2.1), and since $F(0) = 0$,

$$c_2^* = \inf_{s \in \Omega} \frac{1}{s} \log \left(F'(0)^2 \left[\int e^{sx} K(x) dx \right]^2 \right) = 2c^*.$$

We thus conclude that operators q and q_2 have the same spreading speed on $[0, \beta]$.

Using the formulas from section 2.4.3, we compare the theoretical spreading speeds on $[0, 1]$ with numerical simulations for the Ricker function and the logistic function, with the Gaussian kernel and the Laplace kernel. We illustrate the results with the Ricker function in figures 3.6 and 3.7. We obtain similar plots for the logistic function (see figures C.1 and C.2 in appendix C).

Note that the results of the Gaussian kernel seem to be better due to the scaling of the plots. In both cases, the relative errors are less than 3%. We will discuss further the errors and limitations of our numerical schemes in section 5.6.

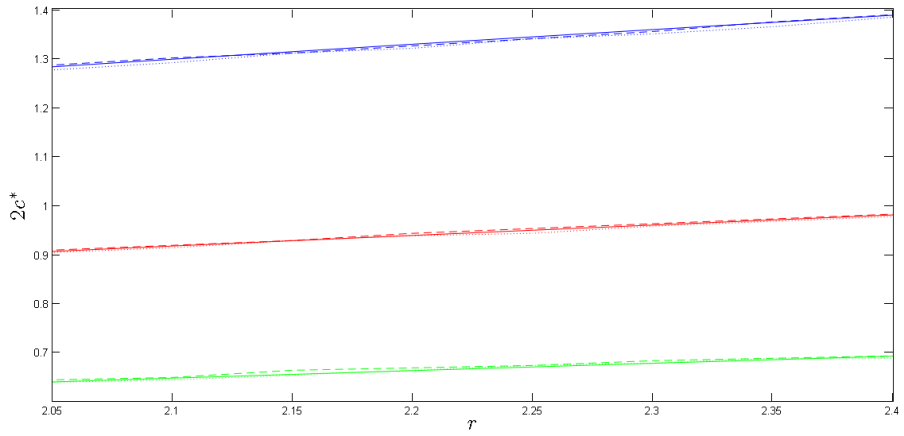

Figure 3.6: Theoretical (full line) and numerical speed of operators q (dashed line) and q_2 (dotted line) on $[0, 1]$ with Ricker function and Gaussian kernel for different values of σ^2 (top: $\sigma^2 = 0.1$, middle: $\sigma^2 = 0.05$, bottom: $\sigma^2 = 0.025$) with respect to the parameter r. The plot is generated with a scheme that uses the FFT algorithm, shown in table D.4, that is based on [25].

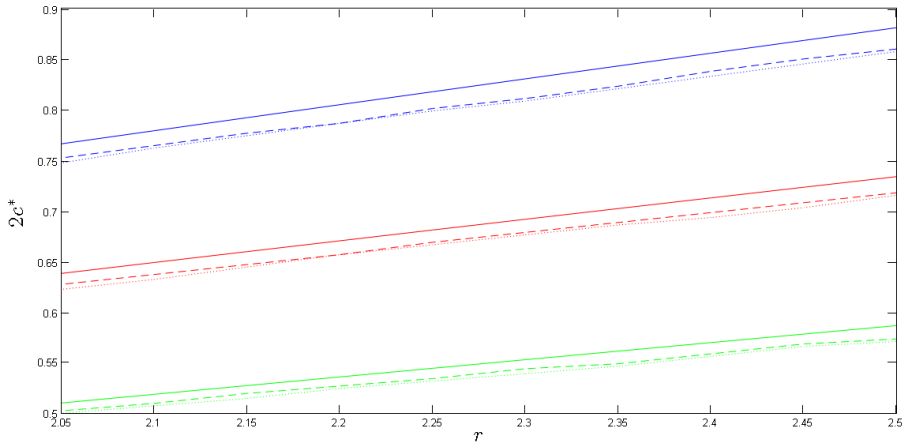

Figure 3.7: Theoretical (full line) and numerical speed of operators q (dashed line) and q_2 (dotted line) on $[0,1]$ with Ricker function and Laplace kernel for different values of a (top: $a = 10$, middle: $a = 12$, bottom: $a = 15$) with respect to the parameter r. The plot is generated with a scheme that uses the FFT algorithm, shown in table D.4, that is based on [25].

When F is a function that satisfies the hypotheses of Theorem 3.2.5, operators q and q_2 have spreading speeds on $[\beta, n_+]$, but operator Q does not since n_+ is not a fixed point of this operator (see Theorem 3.1.3). However, we can still expect operators q and q_2 to have the same spreading speed, as their linearization around β is the same. Thus, if the spreading speed of operator q_2 is linearly determined, it seems reasonable to expect that this would also be the case for operator q.

Assuming that the spreading speed of operators q and q_2 is linearly determined, the expression of $c^*_{[\beta,n_+]}$, from equation (3.2.5), is given by the following parametrization (see equations (2.3.6) and (2.3.7)):

$$c = \frac{M'_{K*K}(s)}{M_{K*K}(s)}, \tag{3.2.8}$$

$$[F'(\beta)]^2 = \frac{e^{sM'_{K*K}(s)/M_{K*K}(s)}}{M_{K*K}(s)}, \tag{3.2.9}$$

assuming equation (3.2.9) can be solved for s, and where M_{K*K} is the moment-generating function of the distribution kernel $K * K$. Since $K * K$ is the convolution of two kernels, its moment-generating function will be the product of both moment-generating functions (see appendix A.2.1). Thus,

$$M_{K*K}(s) = M_K(s)^2, \tag{3.2.10}$$

where M_K is the moment-generating function of the distribution kernel K. Substituting (3.2.10) into equations (3.2.8) and (3.2.9), we can rewrite the parametrization as follows:

$$c = \frac{2M'_K(s)}{M_K(s)}, \tag{3.2.11}$$

$$[F'(\beta)]^2 = \frac{e^{2sM'_K(s)/M_K(s)}}{M_K(s)^2}. \tag{3.2.12}$$

Since we will be doing the calculations for the Ricker function and the logistic function, we take $\beta = 1$.

Gaussian kernel: Let K be defined by equation (2.2.2). We have that $M_K(s) = e^{\sigma^2 s^2/2}$ (see appendix A.1.1). It follows that $M'_K(s) = \sigma^2 s M_K(s)$. Substituting these expressions into equation (3.2.12), we isolate for s:

$$[F'(1)]^2 = e^{\sigma^2 s^2} \Rightarrow s = \sqrt{\frac{\log[F'(1)]^2}{\sigma^2}}.$$

Thus, replacing s in equation (3.2.11), we get the value of $c^*_{[1,n_+]}$:

$$c^*_{[1,n_+]} = 2\sqrt{\sigma^2 \log[F'(1)]^2}.$$

Note that if $|F'(1)|$ increases with r, then $c^*_{[1,n_+]}$ is an increasing function with respect to r. When F is the Ricker function or the logistic function, we get

$$c^*_{[1,n_+]} = 2\sqrt{\sigma^2 \log[(1-r)^2]}. \tag{3.2.13}$$

Laplace kernel: Let K be defined by equation (2.2.3). We have that $M_K(s) = \frac{a^2}{a^2-s^2}$, provided that $|s| < a$. (see appendix A.1.2) It follows that $M'_K(s) = \frac{2s}{a^2-s^2} M_K(s)$. Replacing the two expressions in equation (3.2.11) and equation (3.2.12), we can rewrite the parametrization as follows:

$$c = \frac{4s}{a^2 - s^2}, \tag{3.2.14}$$

$$[F'(1)]^2 = \left(\frac{a^2 - s^2}{a^2}\right)^2 \exp\left(\frac{4s^2}{a^2 - s^2}\right). \tag{3.2.15}$$

In order to get the value of $c^*_{[1,n_+]}$, we use the Lambert W function, which is described in appendix B. We solve for s in equation (3.2.15):

$$\begin{aligned}
[F'(1)]^2 = \left(\frac{a^2-s^2}{a^2}\right)^2 \exp\left(\frac{4s^2}{a^2-s^2}\right) &\Rightarrow [F'(1)]^2\left(\frac{a^2}{a^2-s^2}\right)^2 = \exp\left(\frac{4s^2}{a^2-s^2}\right) \\
&\Rightarrow [F'(1)]^2\left(\frac{a^2}{a^2-s^2}\right)^2 = \exp\left(4\left(\frac{a^2}{a^2-s^2}-1\right)\right) \\
&\Rightarrow [F'(1)]^2 e^4\left(\frac{a^2}{a^2-s^2}\right)^2 = \exp\left(\frac{4a^2}{a^2-s^2}\right). \\
&\Rightarrow \frac{[F'(1)]^2 e^4}{16}\left(\frac{4a^2}{a^2-s^2}\right)^2 = \exp\left(\frac{4a^2}{a^2-s^2}\right).
\end{aligned}$$

This expansion is an equation of the form $\rho x^2 = e^x$, where $\rho = \frac{[F'(1)]^2 e^4}{16}$ and $x = \frac{4a^2}{a^2-s^2}$. According to equation (B.1.2), it follows that

$$\frac{4a^2}{a^2-s^2} = -2W\left(\pm\frac{2}{|F'(1)|e^2}\right).$$

We reject the solution

$$\frac{4a^2}{a^2-s^2} = -2W\left(\frac{2}{|F'(1)|e^2}\right).$$

In fact, $\frac{2}{|F'(1)|e^2} > 0$, which implies that in order to have real solutions, we must use the function W_0 to solve (see figures B.1 and B.2). It would then follow that

$$W\left(\frac{2}{|F'(1)|e^2}\right) > 0,$$

which would be a contradiction since $|s| < a$. Isolating for s in the remaining solution, we get

$$s = a\sqrt{\frac{2}{W\left(\frac{-2}{|F'(1)|e^2}\right)}+1}.$$

In order for s to be a real positive number, we first need $W\left(-\frac{2}{|F'(1)|e^2}\right)$ to be real. We thus require the following condition (see appendix B):

$$-\frac{2}{|F'(1)|e^2} \geq -\frac{1}{e} \Rightarrow r \geq \frac{2}{e}+1.$$

For $r > 2$, the previous inequality is satisfied and $-\frac{1}{e} < -\frac{2}{|F'(1)|e^2} < 0$, since $|F'(1)| > 1$. As explained in appendix B, we have two real solutions, $W_0\left(-\frac{2}{|F'(1)|e^2}\right)$ and $W_{-1}\left(-\frac{2}{|F'(1)|e^2}\right)$. We also require that

$$\frac{2}{W\left(-\frac{2}{|F'(1)|e^2}\right)} + 1 \geq 0 \Rightarrow W\left(-\frac{2}{|F'(1)|e^2}\right) \leq -2.$$

This last condition cannot be satisfied by the function W_0 as its minimum is -1 (see figure B.1). However, it is satisfied by W_{-1} when $-\frac{2}{e^2} \leq -\frac{2}{|F'(1)|e^2} < 0$ (see figure B.2), which is the case for all $r \geq 2$ since $|F'(1)| > 1$. Thus, we have

$$s = a\sqrt{\frac{2}{W_{-1}\left(-\frac{2}{|F'(1)|e^2}\right)} + 1}. \tag{3.2.16}$$

By equation (3.2.15), it follows that

$$c^*_{[1,n_+]} = -\frac{2}{a}W_{-1}\left(-\frac{2}{|F'(1)|e^2}\right)\sqrt{\frac{2}{W_{-1}\left(-\frac{2}{|F'(1)|e^2}\right)} + 1}.$$

Note that if $|F'(1)|$ increases with r, $c^*_{[1,n_+]}$ will be an increasing function with respect to r by a similar argument to the one done in section 2.4.3. When F is the Ricker function or the logistic function, we get

$$c^*_{[1,n_+]} = -\frac{2}{a}W_{-1}\left(-\frac{2}{(r-1)e^2}\right)\sqrt{\frac{2}{W_{-1}\left(-\frac{2}{(r-1)e^2}\right)} + 1}. \tag{3.2.17}$$

Now that we have calculated the spreading speed of operators q and q_2 under the assumption that they are linearly determined, we proceed to justifying why we make such an assumption for q_2 in the case of the Ricker function and the logistic function. We use the argument that operators q and q_2 have the same linearization to predict that the spreading speed of q is then also linearly determined.

Proposition 3.2.10. *Let F be the logistic function. Then the spreading speed of q_2 is linearly determined.*

Proof: We show that $(F \circ F)''(N) \leq 0$ on $[1, n_+]$. Indeed,

$$(F \circ F)(N) = (1+r)^2N - r(1+r)(2+r)N^2 + 2r^2(1+r)N^3 - r^3N^4$$

$$\Rightarrow (F \circ F)'(N) = (1+r)^2 - 2r(1+r)(2+r)N + 6r^2(1+r)N^2 - 4r^3N^3$$
$$\Rightarrow (F \circ F)''(N) = -2r(1+r)(2+r) + 12[r^2(1+r)N - r^3N^2]. \quad (3.2.18)$$

After simplification, the roots of (3.2.18) are given by the expression

$$N = \frac{3(1+r) \pm \sqrt{3(r^2-1)}}{6r}.$$

By solving the inequality

$$\frac{3(1+r) + \sqrt{3(r^2-1)}}{6r} - 1 < 0,$$

we conclude that both roots of (3.2.18) are less than 1 when $r > 2$. It follows that $(F \circ F)''(N) \leq 0$ for all $N \geq 1$, which implies that $(F \circ F)(N) \leq [F'(1)]^2(N-1)+1$ on $[1, n_+]$ (see proof of Proposition 2.4.9). Thus, the spreading speed of q_2 is linearly determined (similarly to the result of Theorem 2.4.7). ∎

With this information, we can then compare the numerical speed obtained for operator q_2 with the theoretical speed predicted by the linearization (formulas (3.2.13) and (3.2.17)). We also compare the numerical speed of operator q to these formulas when F is the logistic equation. Figures 3.8 and 3.9 illustrate these comparisons. We see that the spreading speeds of q and q_2 are very similar. Also, those values differ from the value predicted by the formulas obtained after linearization by a factor less than 5%. This result and the comparison of figures 3.8 and 3.9 to figures 3.6 and 3.7 gives us confidence in our hypothesis that the spreading speed of q on $[1, n_+]$ is linearly determined in the case where F is the logistic equation.

Now, let us consider the case where F is the Ricker function. Using the chain rule for derivation and equation (2.1.3), we have that

$$\begin{aligned}(F \circ F)''(1) &= F''(F(1))[F'(1)]^2 + F'(F(1))F''(1) \\ &= F''(1)[F'(1)]^2 + F'(1)F''(1) \\ &= F''(1)F'(1)(F'(1)+1) \\ &= r(r-2)(1-r)(2-r) \\ &= r(r-1)(r-2)^2 > 0.\end{aligned}$$

This inequality implies that for some $\alpha > 1$, we have $(F \circ F)(N) \geq [F'(1)]^2(N-1)+1$ on $[1, \alpha]$ (see proof of Proposition 2.4.9). We also have that $(F \circ F)'(1) > 1$. It follows that the function $(F \circ F)$ exhibits a weak Allee effect at $N = 1$ (see [28] for mathematical characterization and

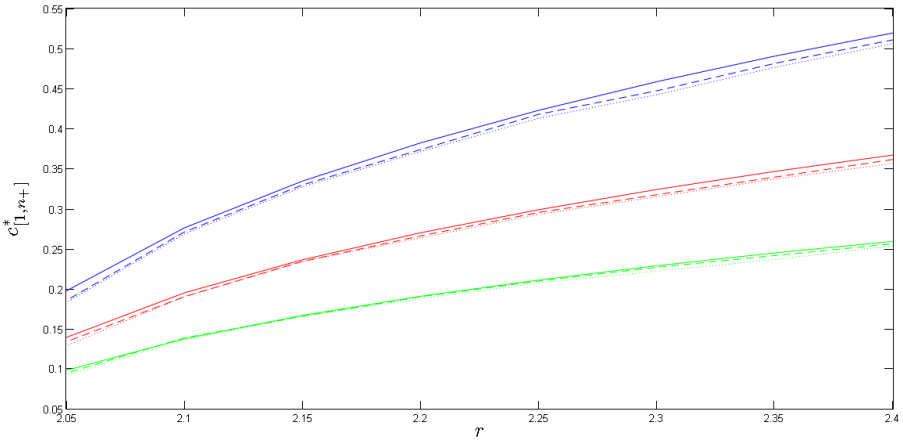

Figure 3.8: Theoretical (full line) and numerical speed of operators q (dashed line) and q_2 (dotted line) on $[1, n_+]$ with logistic function and Gaussian kernel for different values of σ^2 (top: $\sigma^2 = 0.1$, middle: $\sigma^2 = 0.05$, bottom: $\sigma^2 = 0.025$) with respect to the parameter r. The plot is generated with a scheme that uses the FFT algorithm, shown in table D.4, that is based on [25].

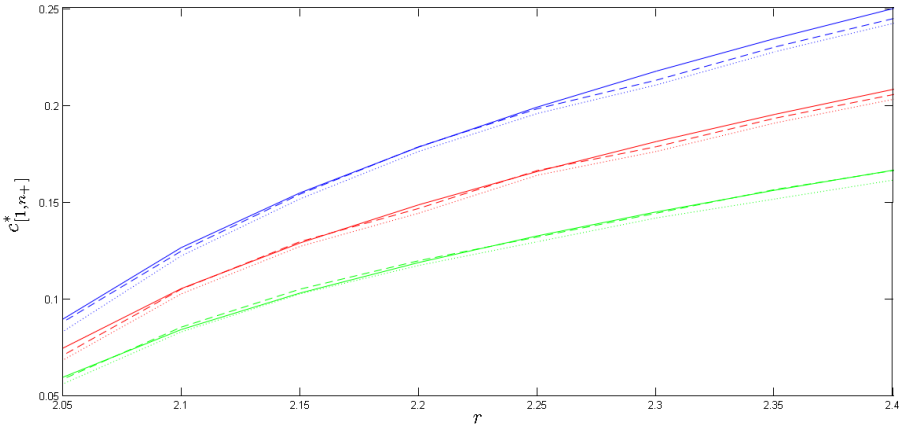

Figure 3.9: Theoretical (full line) and numerical speed of operators q (dashed line) and q_2 (dotted line) on $[1, n_+]$ with logistic function and Laplace kernel for different values of a (top: $a = 10$, middle: $a = 12$, bottom: $a = 15$) with respect to the parameter r. The plot is generated with a scheme that uses the FFT algorithm, shown in table D.4, that is based on [25].

"Biological Terminology" for ecological definition), and does not satisfy the condition for linearization provided by the result of Theorem 2.4.7. However, in the case of reaction-diffusion systems, it was shown that if the Allee effect is sufficiently weak, then the spreading speed is still linearly determined [28]. Although some analysis has been done regarding Allee effects in integrodifference equations (notably in [29]), it is unclear how to characterize an Allee effect as sufficiently weak. The results of our numerical simulations suggest that formulas (3.2.13) and (3.2.17) represent the value of $c^*_{[1,n_+]}$ for operators q_2 and q even with this Allee effect (see figures 3.10 and 3.11).

The figures that we showed so far in this section were obtained by using an FFT algorithm to calculate numerically the solution of q and q_2 at each iteration. The MATLAB® code for this numerical scheme can be found in table D.4. We also ran simulations where the integral is evaluated by direct integration with the trapezoid rule (see table D.5). This last scheme provided the same conclusions as the one that uses the FFT algorithm (see figures C.3 - C.10 in appendix C).

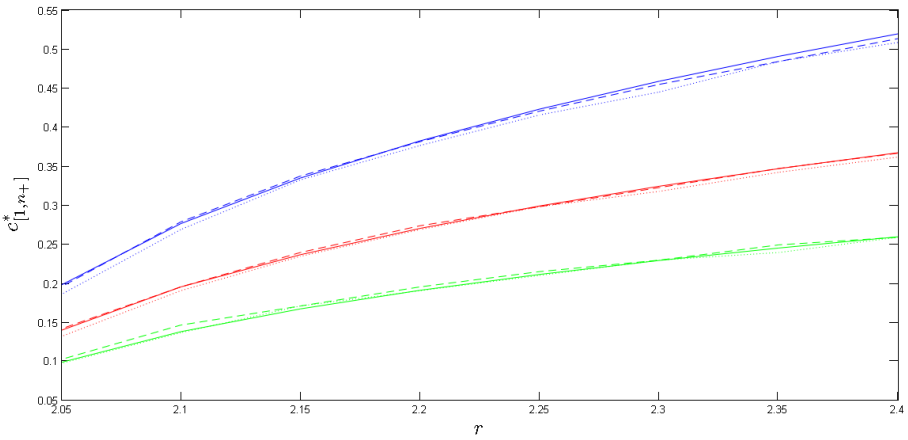

Figure 3.10: Theoretical (full line) and numerical speed of operators q (dashed line) and q_2 (dotted line) on $[1, n_+]$ with Ricker function and Gaussian kernel for different values of σ^2 (top: $\sigma^2 = 0.1$, middle: $\sigma^2 = 0.05$, bottom: $\sigma^2 = 0.025$) with respect to the parameter r. The plot is generated with a scheme that uses the FFT algorithm, shown in table D.4, that is based on [25].

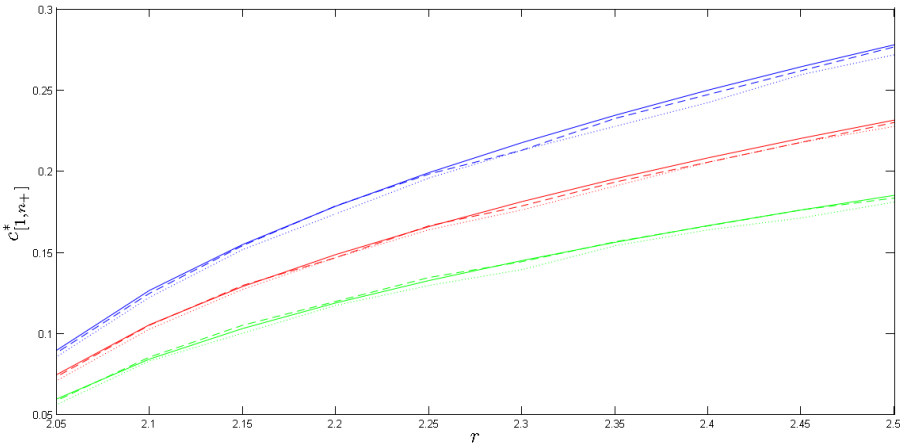

Figure 3.11: Theoretical (full line) and numerical speed of operators q (dashed line) and q_2 (dotted line) on $[1, n_+]$ with Ricker function and Laplace kernel for different values of a (top: $a = 10$, middle: $a = 12$, bottom: $a = 15$) with respect to the parameter r. The plot is generated with a scheme that uses the FFT algorithm, shown in table D.4, that is based on [25].

Chapter 4

Dynamical Stabilization

So far, we were able to show the existence of two spreading speeds for the operator q: one on the interval $[0, 1]$, that is obtained through the analysis of the operator Q, and another on the interval $[1, n_+]$. On each of these respective intervals, we can also establish the existence of travelling wave solutions. Now, we would like to explore the coexistence of both travelling waves in the same solution, as we observe two successive travelling profiles during simulations when there is a stable 2-point cycle. The shape of the solution of the second iterate integrodifference equation exhibits the same type of behavior that was observed in a reaction-diffusion system described in [19]. In this chapter, we will briefly describe the observations in [19] and then relate them to the solution of the second iterate integrodifference equation to provide an argument for the existence of two successive travelling objects in this solution.

4.1 A Predator-Prey Model

In [19], a reaction-diffusion system describing a predator-prey interaction was studied. For the one-dimensional case, the system is given by

$$\begin{aligned} u_t &= u_{xx} + u(1-u) - \frac{u}{u+h}v, \\ v_t &= v_{xx} + k\frac{u}{u+h}v - mv, \end{aligned} \tag{4.1.1}$$

where u is the density of the prey, v is the density of the predator, x is the spatial variable, t is the temporal variable, and h, k and m are positive constants. Note that the subscripts t and xx denote the partial derivative with respect to t and the second

order partial derivative with respect to x, respectively. The non-spatial model that corresponds to system (4.1.1) is

$$\begin{aligned} u_t &= u(1-u) - \frac{u}{u+h}v, \\ v_t &= k\frac{u}{u+h}v - mv. \end{aligned} \tag{4.1.2}$$

One can easily see that $(0,0)$ and $(1,0)$ are steady states of (4.1.2), corresponding to the trivial extinction and the predator extinction, respectively. There is also a non-trivial steady state when $h < \frac{k-m}{m}$, given by (u^*, v^*), where $u^* = \frac{mh}{k-m}$ and $v^* = (1-u^*)(u^*+h)$. This steady state corresponds to the coexistence state, as both prey and predator densities are positive. Depending on the parameter values, the coexistence state can either be stable or unstable. It was determined that the critical value of h for which the steady state goes from being stable to unstable is given by $h_{cr} = \frac{1-p}{1+p}$, where $p = m/k$. This bifurcation is illustrated in figure 4.1, along with the curve $h = \frac{k-m}{m} = \frac{1-p}{p}$. For more details on this model, one can consult [23, 24].

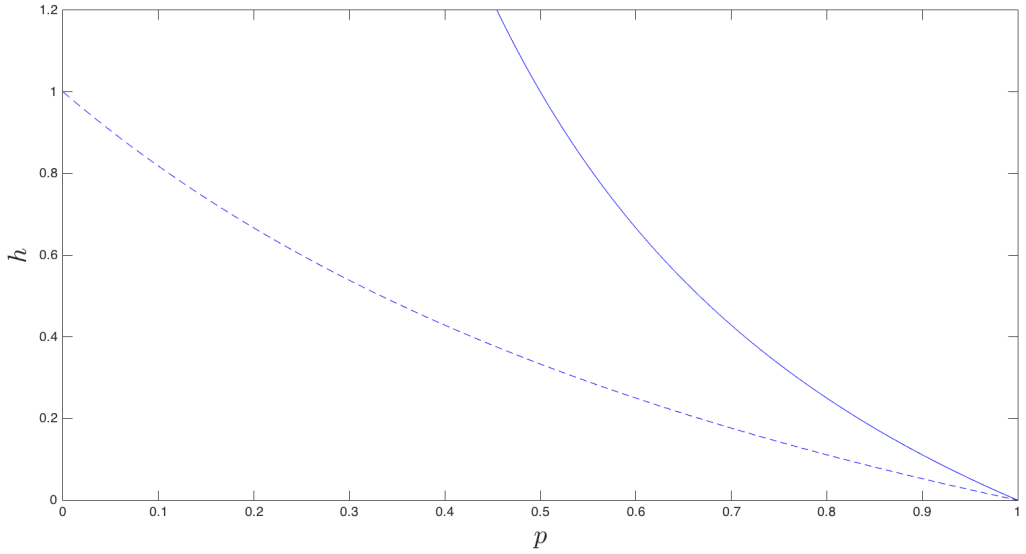

Figure 4.1: Bifurcation diagram for the steady state (u^*, v^*) as described in [19]. The coexistence state exists for parameter values under the curve of equation $h = \frac{1-p}{p}$ (full line). (u^*, v^*) is unstable under the curve of equation $h = \frac{1-p}{1+p}$ (dashed line).

In figure 4.1, we see that (u^*, v^*) is unstable for $h = 0.6$ and $p = 0.15$ ($k = 0.4$ and $m = 0.06$). We plot the vector field for system (4.1.2) for these parameter values in figure 4.2. We can see in this non-spatial model that solutions move away from the coexistence state.

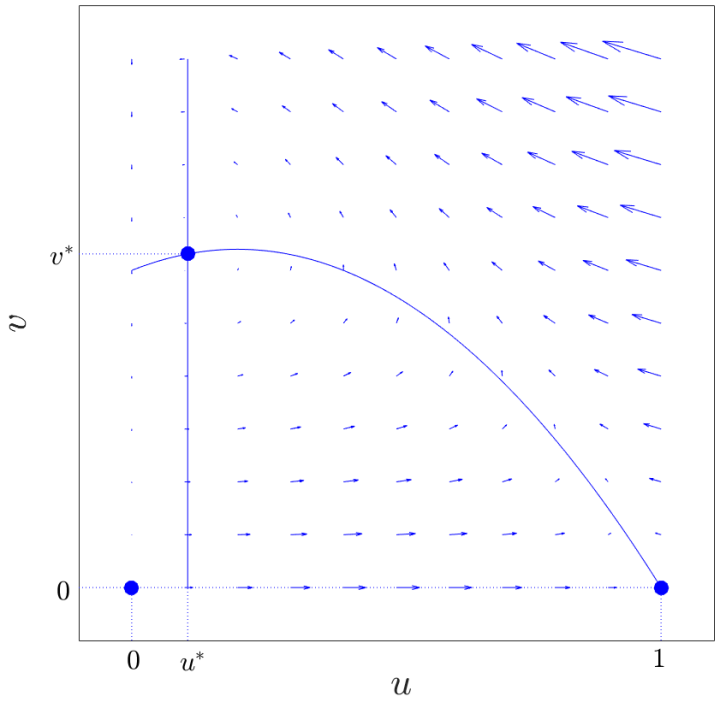

Figure 4.2: Vector field of the ordinary differential system (4.1.2), where $h = 0.6$, $k = 0.4$ and $m = 0.06$. The curves represent the non-trivial nullclines, $u = \frac{mh}{k-m}$ and $v = (1-u)(u+h)$, of the system.

When adding the spatial component, i.e. studying system (4.1.1), the solution does not behave as one would expect when (u^*, v^*) is unstable in the non-spatial model. The solution of (4.1.1), where $h = 0.6$ and $p = 0.15$ ($k = 0.4$ and $m = 0.06$), is illustrated in figure 4.3. In this figure, it almost seems like the steady state is stable in part of the solution, as portrayed by the plateau. We also have that as time increases, this region of said stability gets longer, as the length of the plateau increases. This spatial phenomenon was termed as dynamical stabilization. In the words of the authors [19], "a locally unstable equilibrium of the system can be made dynamically stable in the full diffusion-reaction system". We see in figure 4.3 that the spatial domain where dynamical stabilization takes place is bounded by two moving objects: the part of the solution preceeding the plateau in the movement, moving at some speed, say w, and the part following the plateau, moving at some speed, say z. It is clear that in the case where $w > z$, the length of the plateau will increase in time. If $w < z$, the plateau, if it even appears, will become absent after a while. Hence, it was concluded in [19] that a necessary condition for dynamical stabilization to occur is $w > z$.

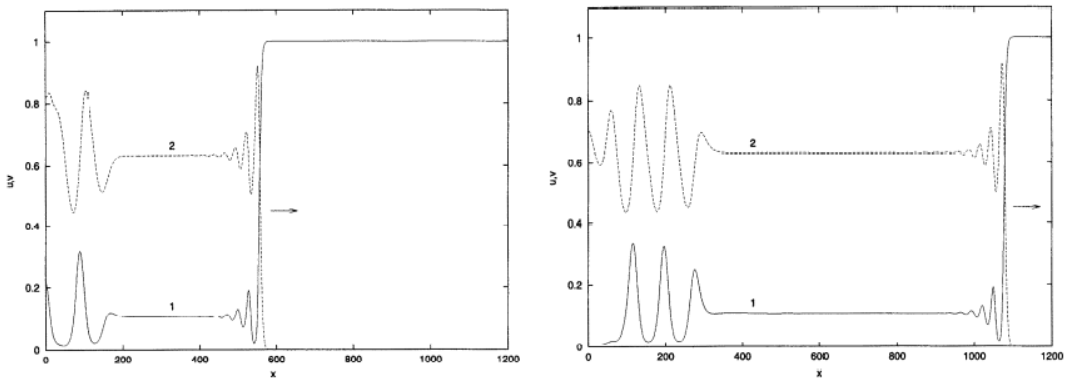

Figure 4.3: Figure 2 from [19] illustrating the concentration of prey u (Curve 1) and predator v (Curve 2) of system (4.1.1) at $t = 600$ (left) and $t = 1200$ (right), where $h = 0.6$, $k = 0.4$ and $m = 0.06$. The plateau observed in the solution corresponds to the locally unstable coexistence state (u^*, v^*).

4.2 Comparison of Speeds in the Second Iterate IDE

In this section, we relate the solution of the integrodifference equation with a stable 2-point cycle to the concept of dynamical stabilization. For the second iterate of such an integrodifference equation, we have calculated the spreading speed on both the intervals $[0, 1]$ and $[1, n_+]$. The formulas are computed in sections 2.4.3 and 3.2.3, respectively, with the Gaussian kernel and the Laplace kernel. Those spreading speeds correspond to the speeds observed in simulations, as explained in the beginning of section 3.2.3. We can thus compare the theoretical formulas to see if the necessary condition for dynamical stabilization is satisfied in the solutions generated by our simulations so far. More specifically, we will check whether the value $2c^*$ (2.4.5), which corresponds to the spreading speed of q on $[0, 1]$, is larger than $c^*_{[1,n_+]}$ (3.2.5).

In the case of the Gaussian kernel, we use equations (2.4.12) and (3.2.13):

$$\frac{2c^*}{c^*_{[1,n_+]}} = \sqrt{\frac{\log(F'(0))}{\log(r-1)}}.$$

Since $F'(0) > r - 1$ for the Ricker function and the logistic function, and since the logarithm is an increasing function, it follows that $2c^* > c^*_{[1,n_+]}$.

In the case of the Laplace kernel, we use equations (2.4.13), (2.4.15), (3.2.14)

and (3.2.16). The values for $2c^*$ and $c^*_{[1,n_+]}$ are determined by the equation

$$c = \frac{4s}{a^2 - s^2}, \tag{4.2.1}$$

where s is given by the expressions

$$s = s_1 = a\sqrt{\frac{2}{W_{-1}\left(-\frac{2}{F'(0)e^2}\right)} + 1}$$

and

$$s = s_2 = a\sqrt{\frac{2}{W_{-1}\left(-\frac{2}{|F'(1)|e^2}\right)} + 1},$$

respectively. Since $F'(0) > |F'(1)| = r - 1$, and since the Lambert W function is decreasing on the interval $[-1/e, 0]$ (see figure B.2), it follows that $s_1 > s_2$. Finally, equation (4.2.1) is increasing with respect to s, thus $2c^* > c^*_{[1,n_+]}$.

Note that the previous calculations are independent of the variance of the kernels. In all the considered cases, we conclude that the spreading speed of q on $[0, 1]$ is greater than the spreading speed on $[1, n_+]$ for $r > 2$. This comparison that is illustrated graphically in figure 4.4 for the Laplace kernel and the Ricker function. We obtain similar plots for the Laplace kernel and the logistic function, as well as for the Gaussian kernel and the Ricker and logistic functions. Those plots are illustrated in figures C.11, C.12 and C.13 in appendix C.

We also have that $N = 1$ is an unstable steady state of the map $N \mapsto F(N)$ when $r > 2$ in the Ricker function and the logistic function (see tables 2.1 and 2.2). Thus, the operator q satisfies the necessary condition for dynamical stabilization to occur at $N = 1$. This phenomenon is precisely what was observed during some simulations. In fact, looking at the top part of figure 4.5, we see the presence of a plateau at $N = 1$, whose length increases with time. We thus have an example of dynamical stabilization in the case of a discrete system.

As stated in section 10.2.2 of [20], having different spreading speeds within the solution does not guarantee dynamical stabilization, as it is not a sufficient condition. For example, when $r = 2.525$ in the Ricker function, the spreading speed on $[0, 1]$ is still greater than the spreading speed on $[1, n_+]$, but dynamical stabilization does not occur at $N = 1$. In fact, we notice the absence of a plateau in figure 4.6. We will discuss this observation further in section 5.6. In the following section, we will use a different approach that does not rely on the comparison of spreading speeds in order to determine the parameter values for which dynamical stabilization can occur in the solution of the integrodifference equation.

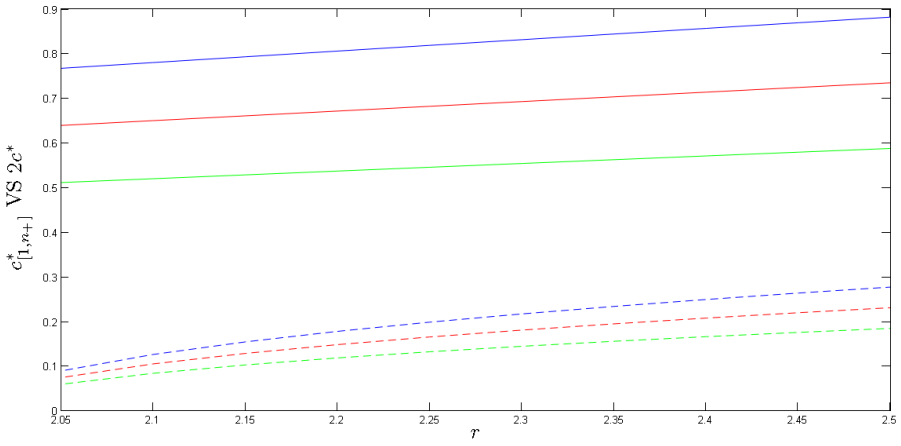

Figure 4.4: Theoretical spreading speed on $[0, 1]$ (full line) and $[1, n_+]$ (dashed line) for the operator q with the Ricker function and Laplace kernel for different values of a (top: $a = 10$, middle: $a = 12$, bottom: $a = 15$) with respect to r.

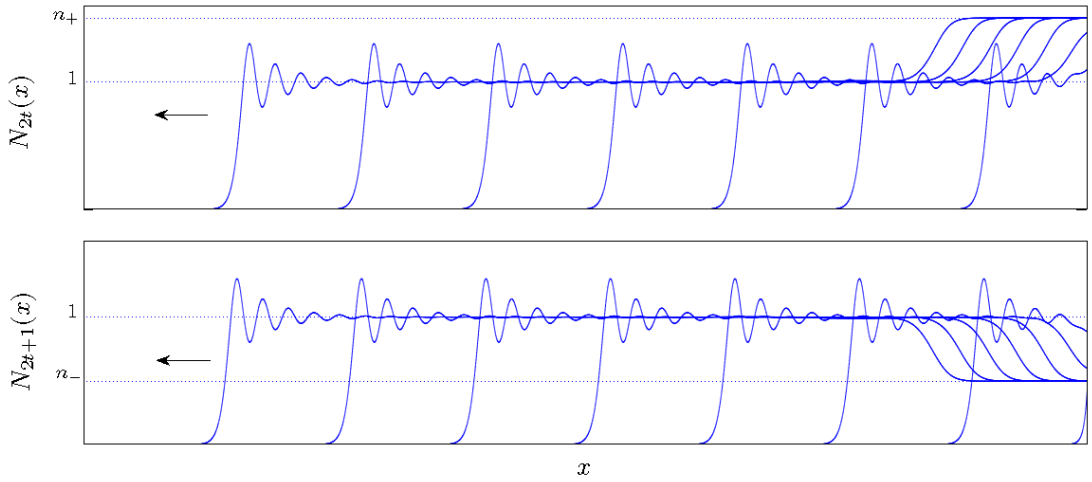

Figure 4.5: (Reminder of figure 3.1.) Solution of the integrodifference equation, where F is the Ricker function with $r = 2.2$, K is the Laplace kernel with $a = 15$ and $N_0 = n_+\chi_{[x\geq 10]}$, plotted for even (top panel) and odd (bottom panel) generations every 10 time steps. n_- and n_+ are the values that form the 2-point cycle.

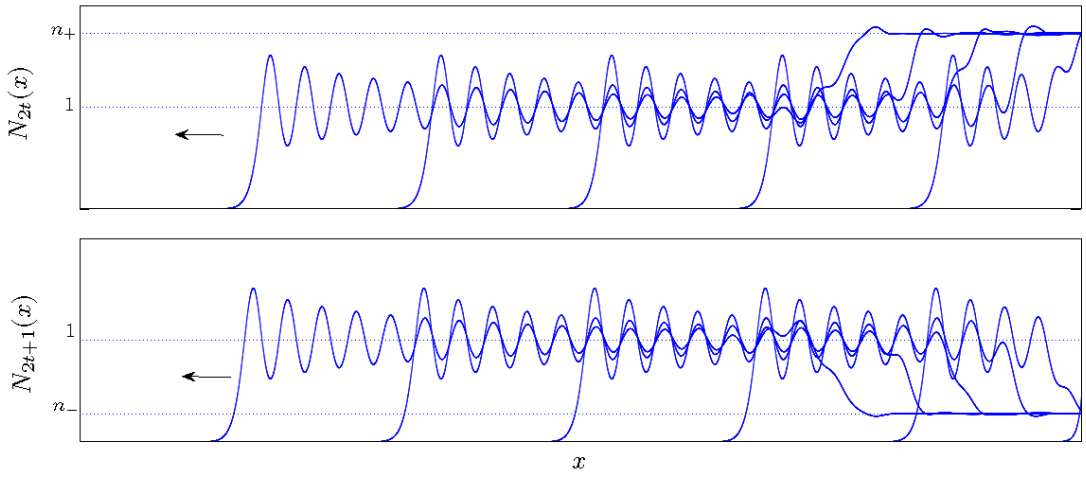

Figure 4.6: Solution of the integrodifference equation, where F is the Ricker function with $r = 2.525$, K is the Laplace kernel with $a = 15$ and $N_0 = n_+\chi_{[x\geq 10]}$, plotted for even (top panel) and odd (bottom panel) generations every 10 time steps. n_- and n_+ are the values that form the 2-point cycle.

4.3 Solution of the IDE with the Laplace Kernel

In this section, we study the shape of the solution for the integrodifference equation, where K is the Laplace kernel, and F is either the Ricker function or the logistic function. Using the Laplace kernel will allow us to relate operators Q (2.4.1) and q (3.2.1) to a system of delay differential equations [14]. Before we go into the details for the existence of the plateau observed in simulations, we first setup the system of delay differential equations that will be used in the analysis.

Define the following recursion

$$N_{t+1}(x) = \int K(x-y)G(N_t(y))dy,$$

where K and G are continuous and differentiable functions, and assume a solution in the form of a travelling wave with speed c. Then,

$$N_{t+1}(x) = N_t(x+c) = \int K(x-y)G(N_t(y))dy. \tag{4.3.1}$$

We shall omit the index t to simplify notation. When K is the Laplace kernel, we can differentiate equation (4.3.1) to obtain a second order delay differential equation,

as stated in [14]. In fact,

$$\begin{aligned} N(x+c) &= \int \frac{a}{2} e^{-a|x-y|} G(N(y))dy \\ &= \int_{-\infty}^{x} \frac{a}{2} e^{-a(x-y)} G(N(y))dy + \int_{x}^{\infty} \frac{a}{2} e^{a(x-y)} G(N(y))dy \\ &= \frac{a}{2} e^{-ax} \int_{-\infty}^{x} e^{ay} G(N(y))dy + \frac{a}{2} e^{ax} \int_{x}^{\infty} e^{-ay} G(N(y))dy. \end{aligned}$$

It then follows that

$$N'(x+c) = -\frac{a^2}{2} e^{-ax} \int_{-\infty}^{x} e^{ay} G(N(y))dy + \frac{a^2}{2} e^{ax} \int_{x}^{\infty} e^{-ay} G(N(y))dy$$

and

$$\begin{aligned} N''(x+c) &= a^2 \frac{a}{2} e^{-ax} \int_{\infty}^{x} e^{ay} G(N(y))dy + a^2 \frac{a}{2} e^{ax} \int_{x}^{\infty} e^{-ay} G(N(y))dy - a^2 G(N(x)) \\ &= a^2 \left[\int_{-\infty}^{x} \frac{a}{2} e^{-a(x-y)} G(N(y))dy + \int_{x}^{\infty} \frac{a}{2} e^{a(x-y)} G(N(y))dy \right] - a^2 G(N(x)). \end{aligned}$$

Thus, we obtain the following delay differential equation:

$$N''(x+c) = a^2 N(x+c) - a^2 G(N(x)).$$

By a change of variables, this equation is equivalent to

$$N''(y) = a^2 N(y) - a^2 G(N(y-c)).$$

By letting $n(y) = N'(y)$, we obtain a system of equations:

$$\begin{aligned} N'(y) &= n(y), \\ n'(y) &= a^2 N(y) - a^2 G(N(y-c)). \end{aligned} \tag{4.3.2}$$

The equilibrium points of this system are given by $(N^*, 0)$, where N^* denotes a fixed point of G. This system is expressed in terms of the spatial variable y. Therefore, the solution of (4.3.2) corresponds to the travelling wave solution of the integrodifference equation for some fixed t. A travelling wave solution connecting $N = N_1^*$ and $N = N_2^*$ in the integrodifference equation thus translates into a connection between the points

$(N_1^*, 0)$ and $(N_2^*, 0)$ in the phase plane of (4.3.2), where N_1^* and N_2^* denote two distinct fixed points of G. Hence, we are interested in studying the stability of the equilibrium points of (4.3.2). In fact, if $(N_1^*, 0)$ has an unstable direction and $(N_2^*, 0)$ has a stable direction, or vice versa, than a travelling wave solution can exist for the integrodifference equation.

We would like to justify the existence of the plateau at $N = 1$ in the solution of the integrodifference equation with a stable 2-point cycle through this framework. The presence of the plateau relies on the existence of the connection between 0 and 1, followed by a trajectory moving away from 1 in this solution. To study the connection from 0 to 1, we require the operator Q (2.4.1), which translates into setting $G = F$ in equation (4.3.1). For the connection from 1 to n_+, we use the operator q (3.2.1), which translates into setting $G = Q$ in equation (4.3.1). A necessary condition for dynamical stabilization to occur at $N = 1$ is thus the existence of a stable direction at $(1, 0)$ with $G = F$ in equation (4.3.1), and an unstable direction at $(1, 0)$ with $G = Q$ in equation (4.3.1).

4.3.1 Existence of a Stable Direction at $(1, 0)$

Now that we have established the required framework, we can start by studying the connection from 0 to 1 in the solution of the integrodifference equation. The recursion that defines our solution is thus obtained with the operator Q, and we assume it to be in the form of a travelling wave. The results in section 2.4 allow us to make such an assumption. Assuming the profile moves at speed c, we have

$$N(x + c) = Q[N](x) = \int K(x - y)F(N(y))dy. \tag{4.3.3}$$

From what precedes, differentiating (4.3.3) twice leads to the following system of delay differential equations (see system (4.3.2)):

$$\begin{aligned} N'(y) &= n(y), \\ n'(y) &= a^2 N(y) - a^2 F(N(y - c)). \end{aligned} \tag{4.3.4}$$

The equilibria of this system are $(0, 0)$ and $(1, 0)$. For a connection to exist from 0 to 1 in the solution of the integrodifference equation, we need the existence of a solution that moves away from $(0, 0)$ and towards $(1, 0)$ in system (4.3.4). A necessary condition for this behavior is the existence of an eigenvalue with positive real part at $(0, 0)$ and an eigenvalue with negative real part at $(1, 0)$.

To calculate the eigenvalues of (4.3.4), we linearize the system at $(N^*, 0)$ by letting $N(y) = N^* + M(y)$ to obtain a linear homogeneous system :

$$\begin{bmatrix} M'(y) \\ n'(y) \end{bmatrix} = \begin{bmatrix} 0 & 1 \\ a^2 & 0 \end{bmatrix} \begin{bmatrix} M(y) \\ n(y) \end{bmatrix} + \begin{bmatrix} 0 & 0 \\ -a^2 F'(N^*) & 0 \end{bmatrix} \begin{bmatrix} M(y-c) \\ n(y-c) \end{bmatrix}. \tag{4.3.5}$$

For a delay differential system of the form

$$\dot{x} = A_0 x(t) + A_1 x(t-\tau_1) + A_2 x(t-\tau_2) + ... + A_m x(t-\tau_m),$$

where $\dot{x}$ denotes the derivative of x, A_i are constant matrices and τ_i are constant delays for $i = 1, 2, \ldots, m$, the characteristic equation is given by [7]

$$\det(-\lambda I + A_0 + A_1 e^{-\tau_1 \lambda} + \cdots + A_m e^{-\tau_m \lambda}) = 0.$$

Hence, the characteristic equation of (4.3.5) is

$$\det \begin{bmatrix} -\lambda & 1 \\ a^2(1 - e^{-c\lambda} F'(N^*)) & -\lambda \end{bmatrix} = 0.$$

After scaling, this leads to the following transcendental eigenvalue problem:

$$1 - \frac{\lambda^2}{(ac)^2} = F'(N^*) e^{-\lambda}. \tag{4.3.6}$$

Note that equation (4.3.6) is independent of a when $c = c^*$ (see equation (2.4.16)).

$N^* = 0$: For $N^* = 0$, we have $F'(0) > 1$. In this case, equation (4.3.6) will not have solutions for $\lambda < 0$ (see figure 4.7). For $\lambda > 0$, there can be up to two positive real roots. If the functions on the left-hand side and right-hand side of equation (4.3.6) intersect for exactly one value of λ, then we also have

$$\frac{2\lambda}{(ac)^2} = F'(N^*) e^{-\lambda}. \tag{4.3.7}$$

Following the method of [14], we can combine (4.3.6) and (4.3.7) to obtain the following parametric representation for λ:

$$ac = \sqrt{\lambda^2 + 2\lambda}, \tag{4.3.8}$$

$$F'(0) = \frac{2e^{\lambda}}{2 + \lambda}. \tag{4.3.9}$$

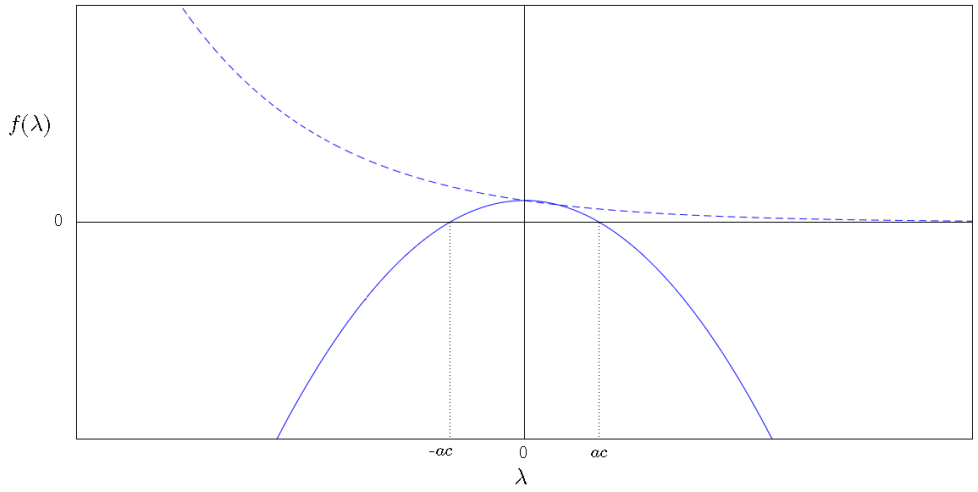

Figure 4.7: Figure illustrating the function $f(\lambda) = 1 - \frac{\lambda^2}{(ac)^2}$ (full line) and the function $f(\lambda) = e^{-\lambda}$ (dashed line).

This last representation corresponds specifically to the parametric representation of the spreading speed on $[0, 1]$ for $\lambda = \frac{2s^2}{a^2-s^2}$ (see equations (2.4.13) and (2.4.14)). Indeed,

$$c = \frac{1}{a}\sqrt{\lambda^2 + 2\lambda} = \frac{1}{a}\sqrt{\frac{4s^4}{(a^2-s^2)^2} + \frac{4s^2}{a^2-s^2}} = \frac{1}{a}\sqrt{\frac{4a^2s^2}{(a^2-s^2)^2}} = \frac{2s}{a^2-s^2}$$

and

$$F'(0) = \frac{2e^{\lambda}}{2+\lambda} = 2\exp\left(\frac{2s^2}{a^2-s^2}\right)\frac{1}{2+\frac{2s^2}{a^2-s^2}} = \frac{a^2-s^2}{s^2}\exp\left(\frac{2s^2}{a^2-s^2}\right).$$

Thus, we conclude that equation (4.3.6) has one positive real root for $c = c^*$, and two positive real roots for $c > c^*$ since $1 - \frac{\lambda^2}{(ac)^2} > 1 - \frac{\lambda^2}{(ac^*)^2}$ (see figure 4.8). Hence, a non-oscillating trajectory moving away from $(0, 0)$ for $c \geq c^*$ can exist in the delay differential system.

$N^* = 1$: When F is increasing on $[0, 1]$, i.e. $r < 1$ in the Ricker function or the logistic function (see sections 2.1.1 and 2.1.2), then $F'(1) > 0$. Also, since $F'(0) > 1$ and 0 and 1 are the only fixed point of F on $[0, 1]$, we have $F'(1) < 1$. In this case, we see from figure 4.7 that equation (4.3.6) will have one positive real root and one negative real root. The negative real root is a necessary condition for the existence of a non-oscillating trajectory going towards $(1, 0)$ in the solution of the delay differential

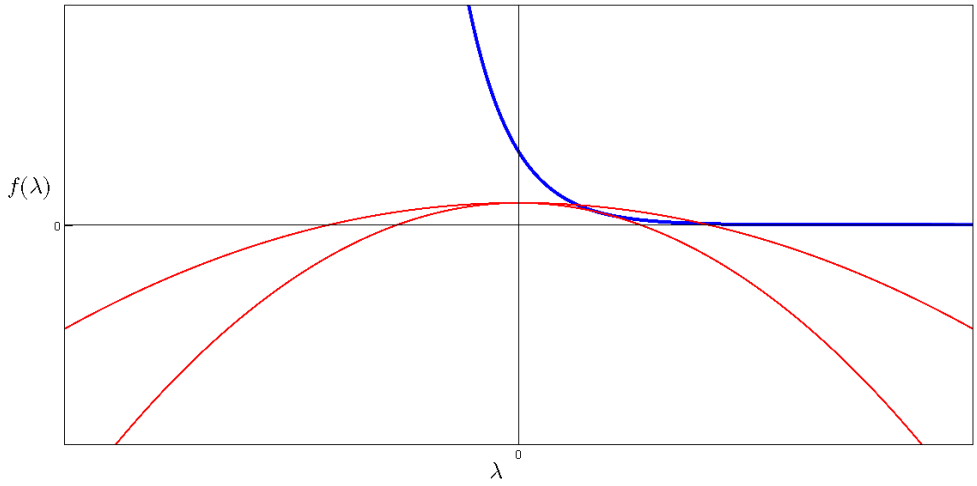

Figure 4.8: Figure illustrating the function $f(\lambda) = F'(0)e^{-\lambda}$ (thicker line) and the function $f(\lambda) = 1 - \frac{\lambda^2}{(ac)^2}$ for $c = c^*$ and $c > c^*$.

system. This result in combination with the analysis around $(0, 0)$ shows us that the necessary condition for the existence of a monotone connection between $(0, 0)$ and $(1, 0)$ is satisfied. In a phase plane, this connection corresponds to the plot shown in figure 4.9. Thus, a monotone profile from 0 to 1 in the solution of the integrodifference equation can exist for $c \geq c^*$, which agrees with the results of section 2.4.1.

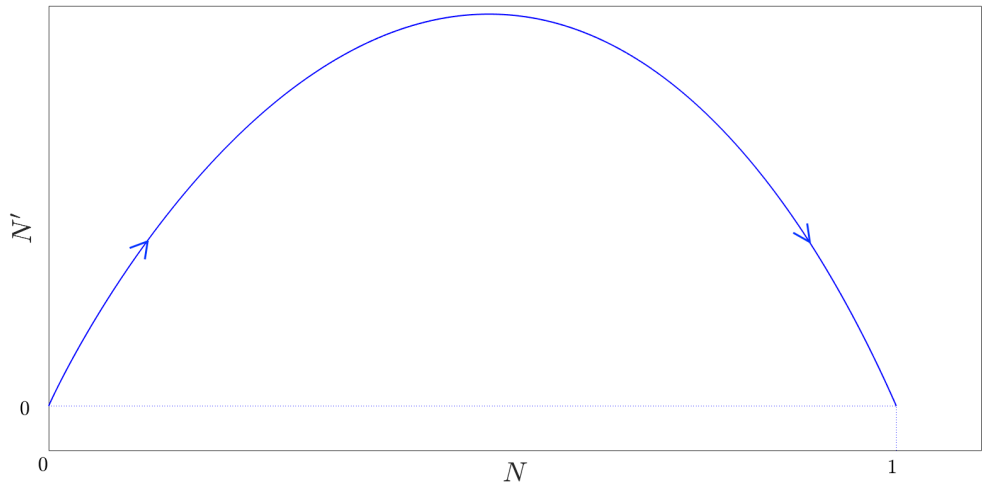

Figure 4.9: Phase plane for the solution of the integrodifference equation plotted in figure 2.13, where F is the Ricker function with $r = 0.8$ and K is the Laplace kernel with $a = 15$.

When F is the Ricker function or the logistic function, we have that $F'(1) < 0$ for $r > 1$ (see sections 2.1.1 and 2.1.2). In this case, equation (4.3.6) always has a positive real root and may have negative real roots (see figure 4.7). When there is a negative real root, we have the necessary condition for the existence of a monotone profile (as explained above). Using MATLAB®, we can find the smallest value of r for which equation (4.3.6) has no real negative root. This value is $r = 1.0327$ for the Ricker function and $r = 1.0686$ for the logistic function (see table D.6). The function $f(\lambda) = 1 - \frac{\lambda^2}{(ac^*)^2}$ is increasing with respect to c^* and c^* is increasing with respect to r (as mentioned in section 2.4.3). Also, the function $f(\lambda) = F'(1)e^{-\lambda} = (1-r)e^{-\lambda}$ decreases with respect to r. Thus, when r increases, the curves of these two functions cannot intersect for $\lambda < 0$, as illustrated in figure 4.10. We conclude that equation (4.3.6) with $c = c^*$ has a negative real root when $1 < r < 1.0327$ for the Ricker function and when $1 < r < 1.0686$ for the logistic function. Thus, the solution of the integrodifference equation observed during simulations (see figure 4.11) can still be in the form of a monotone travelling wave for those values of r, as the speed of the wave observed corresponds to c^* (see section 3.2.3).

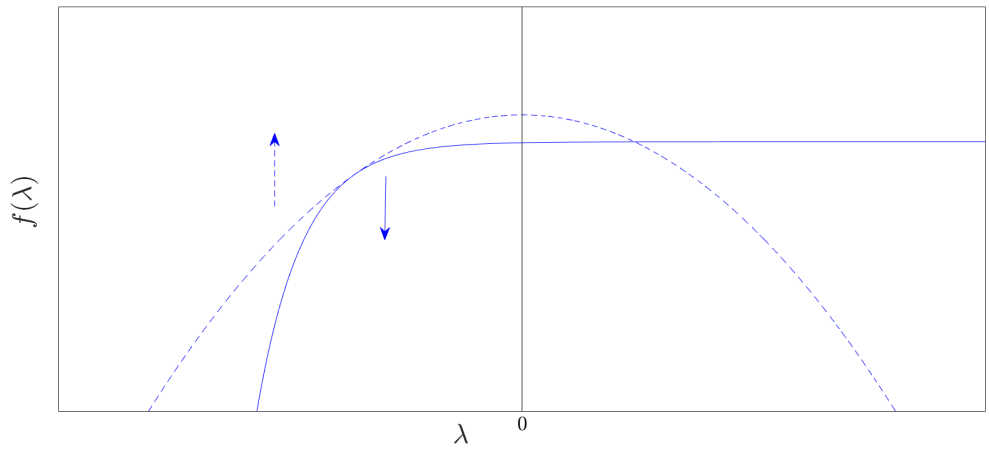

Figure 4.10: Plot of the functions $f(\lambda) = 1 - \frac{\lambda^2}{(ac)^2}$ (dashed line) and $f(\lambda) = F'(1)e^{-\lambda}$ for the Ricker function with $r = 1.0327$. The arrows indicate which way the curves move as r increases.

When no real negative roots exist, we look for the existence of complex-valued solutions with negative real part by letting $\lambda = \alpha + i\eta$ in equation (4.3.6):

$$1 - \frac{\alpha^2 - \eta^2}{(ac)^2} + \frac{2\alpha\eta i}{(ac)^2} = F'(1)e^{-\alpha}(\cos(\eta) - i\sin(\eta)).$$

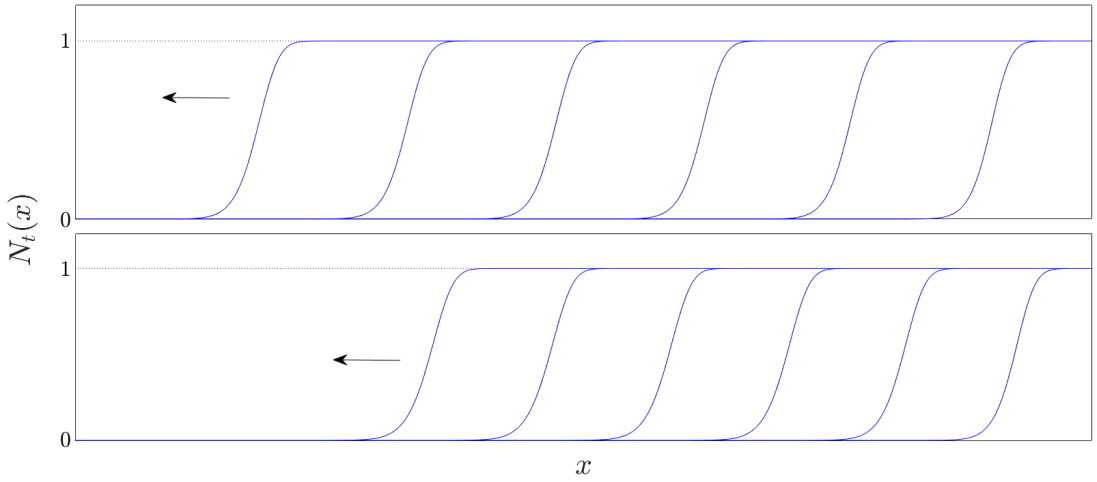

Figure 4.11: Monotone solution of the integrodifference equation, where K is the Laplace kernel with $a = 15$, F is the Ricker function with $r = 1.03$ (top) and the logistic function with $r = 1.06$ (bottom), and $N_0 = \chi_{[x\geq 10]}$ plotted every 10 time steps.

Thus, we have the following set of implicit equations:

$$1 - \frac{\alpha^2 - \eta^2}{(ac)^2} = F'(1)e^{-\alpha}\cos(\eta), \tag{4.3.10}$$

$$\frac{2\alpha\eta}{(ac)^2} = F'(1)e^{-\alpha}\sin(\eta). \tag{4.3.11}$$

Using MATLAB® (see table D.7), we plot those relations for the Ricker function and the logistic function with $c = c^*$ in figure 4.12. We observe that as r increases, the points of intersection move towards the right, with the exception of the point that represents the real positive eigenvalue.

The presence of complex eigenvalues with negative real part is a necessary condition for the existence of a trajectory that spirals towards $(1, 0)$. This would translate into damped oscillations in the solution of the integrodifference equation. When one of the complex eigenvalue reaches zero real part, then the solution could behave differently, as this represents a bifurcation.

We now find the value of r for which the real part of the eigenvalues reaches 0

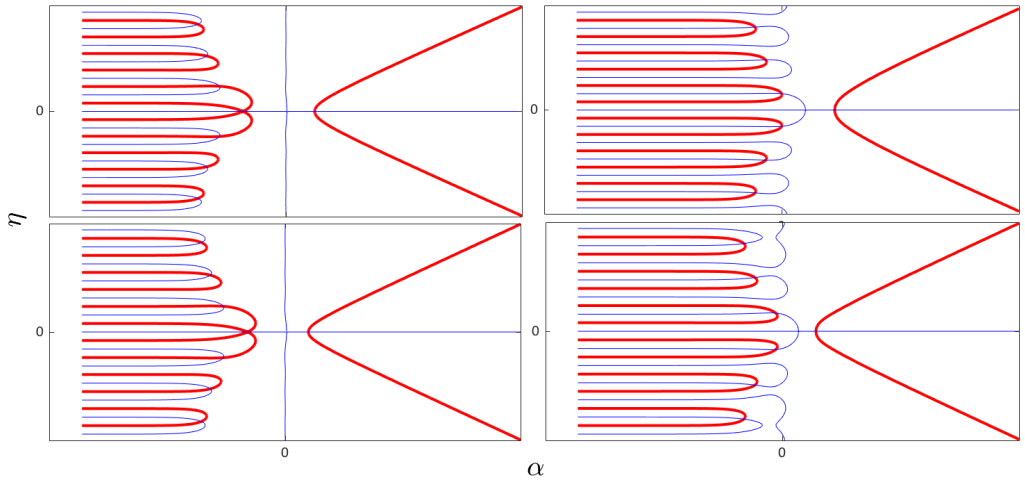

Figure 4.12: Plot of the implicit functions defined by equations (4.3.10) and (4.3.11) (thicker line) with $c = c^*$, the Ricker function for $r = 1.0327$ (top left) and $r = 2.526$ (top right), and the logistic function for $r = 1.0686$ (bottom left) and $r = 2.449$ (bottom right). Note that in all four plots, there are no negative real roots (this is more apparent after zooming in the plots).

when $c = c^*$. In order to do so, we substitute $\alpha = 0$ in equations (4.3.10) and (4.3.11):

$$1 + \frac{\eta^2}{(ac^*)^2} = F'(1)\cos\eta, \tag{4.3.12}$$

$$F'(1)\sin\eta = 0. \tag{4.3.13}$$

From equation (4.3.13), it follows that $\eta = k\pi$, $k \in \mathbb{Z}$. The value of $\eta = \pi$ will correspond to the rightmost pair of complex eigenvalues reaching 0 real part. Replacing this value of η into equation (4.3.12), we get

$$r - 1 = 1 + \frac{\pi^2}{(ac^*)^2}, \tag{4.3.14}$$

since $F'(1) = 1 - r$ in the case of the Ricker function and the logistic function. We can then find the root of this equation numerically with respect to r (see MATLAB® code in table D.8). Equation (4.3.14) has its root at $r = 2.5072$ for the Ricker function, and at $r = 3.1124$ for the logistic function.

We thus have the necessary condition for damped oscillations around $N = 1$ in the solution of the integrodifference equation, namely $1.0327 < r < 2.5072$ for the

Ricker function, and $1.0686 < r < 2.570$ for the logistic function. The simulations exhibit exactly this type of behavior. Also, the oscillations become more and more apparent as r increases. (compare figure 2.14 to figure 4.13 for the Ricker function). In the phase plane, the solution of the delay differential equation from $(0, 0)$ to $(1, 0)$ would correspond to the plot shown in figure 4.14. Having a stable direction at $(1, 0)$ in the delay differential system is a necessary condition for dynamical stabilization to occur.

For the Ricker function, when $r = 2.5072$, there is a bifurcation in the complex eigenvalues. We can thus expect a change of behavior in the solution. For $2.5072 < r < 2.692$, simulations reveal a cycle around $N = 1$ instead of damped oscillations, as shown in figure 4.6. Due to this cycle, dynamical stabilization is not observed at $N = 1$ for those values of r, as will be mentioned in section 4.4.

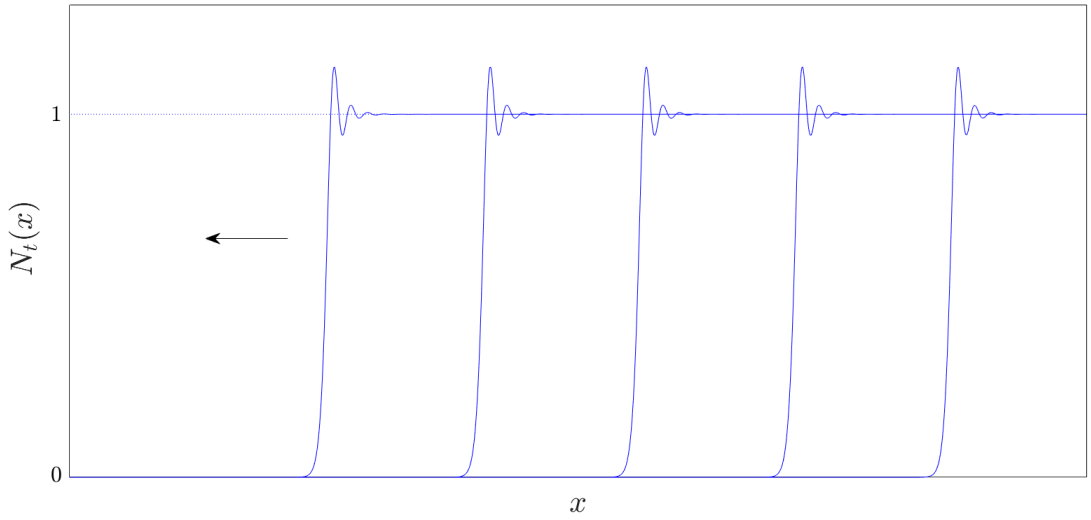

Figure 4.13: Solution of the integrodifference equation, where F is the Ricker function with $r = 1.8$, K is the Laplace kernel with $a = 15$ and $N_0 = \chi_{[x \geq 10]}$, plotted every 10 time steps.

4.3.2 Existence of an Unstable Direction at $(1, 0)$

For dynamical stabilization to occur at $N = 1$, we need the solution of the second iterate integrodifference equation to move towards $N = 1$ and then to move away from $N = 1$. The analysis in section 4.3.1 gives us the values of r for which the former condition is satisfied. In this section, we want to establish the values of r for which the latter condition is satisfied. We define the iteration that describes our

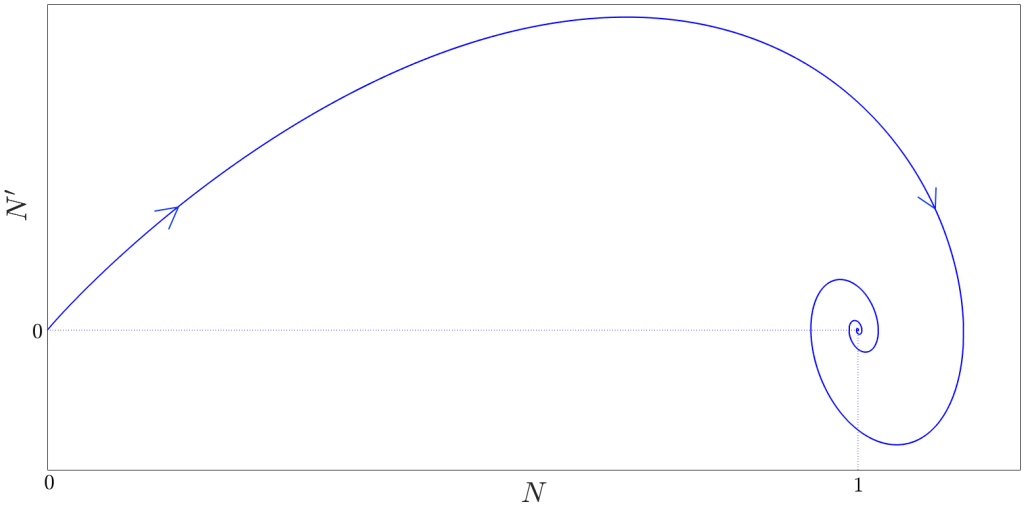

Figure 4.14: Phase plane for the solution of the integrodifference equation plotted in figure 4.13, where F is the Ricker function with $r = 1.8$ and K is the Laplace kernel with $a = 15$.

solution with the operator q to reflect the connection between 1 and n_+. We assume that the solution is in the form of a travelling wave, which we know exists for $r > 2$ from the results in section 3.2. Assuming that the profile moves at speed c, we have

$$N(x+c) = q[N](x) = \int K(x-y)F(Q[N](y))dy. \tag{4.3.15}$$

Similarly to (4.3.3), solutions of (4.3.15) can be described by the following system of delay differential equations:

$$\begin{aligned} N'(y) &= n(y), \\ n'(y) &= a^2 N(y) - a^2 F(Q[N](y-c)). \end{aligned} \tag{4.3.16}$$

The equilibrium points of this system are given by $(N^*, 0)$, where $N^* \in \{0, n_-, 1, n_+\}$ denotes a fixed point of q. For the solution of the second iterate integrodifference equation to move away from 1, we need the existence of a solution that moves away from $(1, 0)$ in system (4.3.16). A necessary condition for this is an eigenvalue with positive real part at $(1, 0)$. We thus linearize system (4.3.16) around $(N^*, 0)$ by letting $N(y) = N^* + M(y)$ to compute its eigenvalues:

$$\begin{aligned} n'(y) &= a^2(N^* + M(y)) - a^2 F\left(\int K(y-c-z)F(N^* + M(z))dz\right) \\ &\approx a^2 N^* + a^2 M(y) - a^2 F\left(\int K(y-c-z)[F(N^*) + F'(N^*)M(z)]dz\right) \end{aligned}$$

$$
\begin{aligned}
&= a^2N^* + a^2M(y) - a^2F\left(F(N^*) + F'(N^*)\int K(y-c-z)M(z)dz\right)\\
&\approx a^2N^* + a^2M(y) - a^2\left(F(F(N^*)) + F'(F(N^*))F'(N^*)\int K(y-c-z)M(z)dz\right)\\
&= a^2M(y) - a^2(F\circ F)'(N^*)\int K(y-c-z)M(z)dz
\end{aligned}
$$

Thus, we obtain the following delay differential system:

$$
\begin{aligned}
&M'(y) = n(y),\\
&n'(y) = a^2M(y) - a^2(F\circ F)'(N^*)\int K(y-c-z)M(z)dz.
\end{aligned}
\tag{4.3.17}
$$

Now, assume an exponential solution in (4.3.17) by letting $\begin{bmatrix} M(y)\\ n(y)\end{bmatrix} = \begin{bmatrix} C_1\\ C_2\end{bmatrix} e^{\lambda y}$, where C_1 and C_2 are constants. It follows that

$$
\lambda C_1 e^{\lambda y} = C_2 e^{\lambda y} \tag{4.3.18}
$$

and

$$
\lambda C_2 e^{\lambda y} = a^2C_1e^{\lambda y} - a^2C_1(F\circ F)'(N^*)\int K(y-c-z)e^{\lambda z}dz. \tag{4.3.19}
$$

We expand the integral term in (4.3.19):

$$
\begin{aligned}
\int K(y-c-z)e^{\lambda y}dz &= \int \frac{a}{2}e^{-a|y-c-z|}e^{\lambda z}dz\\
&= \frac{a}{2}\left[\int_{-\infty}^{y-c} e^{-a(y-c-z)+\lambda z}dz + \int_{y-c}^{\infty} e^{-a(-y+c+z)+\lambda z}\right]\\
&= \frac{a}{2}\left[\lim_{t\to-\infty}\frac{e^{-ay+ac+(a+\lambda)z}}{a+\lambda}\Big|_t^{y-c} + \lim_{s\to\infty}\frac{e^{ay-ac+(\lambda-a)z}}{\lambda-a}\Big|_{y-c}^{s}\right]\\
&= \frac{a}{2}\left[\frac{e^{\lambda(y-c)}}{a+\lambda} + \frac{e^{\lambda(y-c)}}{a-\lambda}\right]\\
&= \frac{a^2e^{\lambda(y-c)}}{a^2-\lambda^2},
\end{aligned}
\tag{4.3.20}
$$

provided that $-a < \mathrm{Re}(\lambda) < a$. From equation (4.3.18), we have that $\lambda C_1 = C_2$. Substituting this last expression in (4.3.19), along with (4.3.20), we obtain

$$
\lambda^2 = a^2 - (F\circ F)'(N^*)e^{-\lambda c}\frac{a^4}{a^2-\lambda^2}.
$$

Rearranging the terms in the previous expression leads to the following transcendental eigenvalue problem for delay differential system (4.3.17):

$$\left(\frac{a^2-\lambda^2}{a^2}\right)^2 = (F\circ F)'(N^*)e^{-\lambda c}. \tag{4.3.21}$$

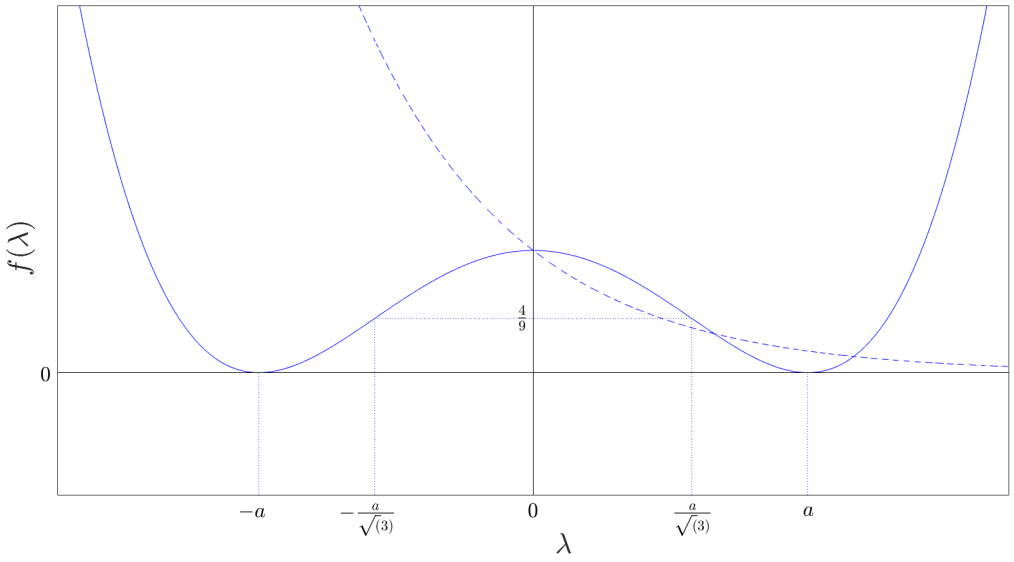

Figure 4.15: Figure illustrating the function $f(\lambda) = \left(\frac{a^2-\lambda^2}{a^2}\right)^2$ (full line) and the function $f(\lambda) = e^{-\lambda}$ (dashed line).

$N^* = 1$: For $N^* = 1$, we have $(F\circ F)'(1) = [F'(1)]^2 > 1$ for $r > 2$ since $F'(1) = 1-r$ for the Ricker function and the logistic function. In this case, equation (4.3.21) will not have solutions for $\lambda < 0$ (see figure 4.15). For $\lambda > 0$, there can be up to two positive real roots for $-a < \lambda < a$. If the functions on the left-hand side and right-hand side of equation (4.3.21) intersect for exactly one value of λ, then we also have

$$\frac{4\lambda(a^2-\lambda^2)}{a^4} = c(F\circ F)'(N^*)e^{-\lambda c}. \tag{4.3.22}$$

We combine (4.3.21) and (4.3.22) to obtain the following parametric representation for λ:

$$c = \frac{4\lambda}{a^2-\lambda^2}, \tag{4.3.23}$$

$$(F \circ F)'(1) = \left(\frac{a^2 - \lambda^2}{a^2}\right)^2. \tag{4.3.24}$$

This parametrization corresponds specifically to the minimal spreading speed $c^*_{[1,n_+]}$ for $\lambda = s$ (see equations (3.2.14) and (3.2.15)). Thus, we conclude that equation (4.3.21) has one positive real root for $c = c^*_{[1,n_+]}$, and will have two positive real roots for $c > c^*_{[1,n_+]}$, since $e^{-\lambda c^*_{[1,n_+]}} > e^{-\lambda c}$ for $\lambda > 0$ (see figure 4.16). Hence, a non-oscillating trajectory moving away from $(1, 0)$ for $c \geq c^*_{[1,n_+]}$ can exist in delay differential system (4.3.17). This agrees with the result that a travelling wave solution can only exist for $c \geq c^*_{[1,n_+]}$ (see section 3.2).

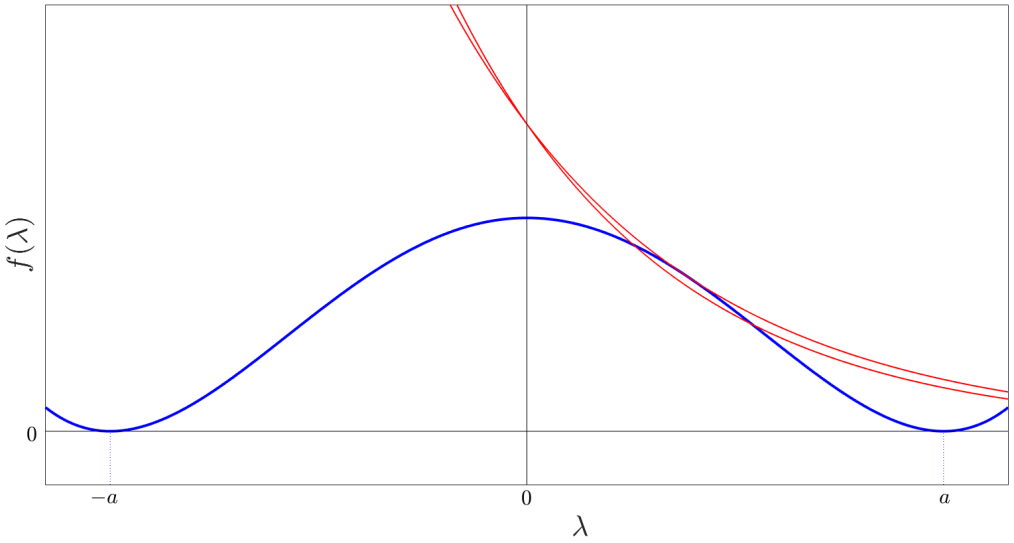

Figure 4.16: Figure illustrating the function $f(\lambda) = \left(\frac{a^2-\lambda^2}{a^2}\right)^2$ (thicker line) and the function $f(\lambda) = (F'(1))^2 e^{-\lambda c}$ for $c = c^*_{[1,n_+]}$ and $c > c^*_{[1,n_+]}$.

4.4 Summary

In sections 4.3.1 and 4.3.2, we studied the behavior at the steady state $(1, 0)$ for the corresponding delay differential equation describing the solution of the integrodifference equation on $[0, 1]$ and $[1, n_+]$, respectively. In this section, we put the pieces together in order to predict when dynamical stabilization occurs in the solution of the second iterate integrodifference equation with a stable 2-point cycle.

In section 4.2, we saw that the spreading speed on $[0, 1]$ of operator q is greater than the one on $[1, n_+]$ for $r > 2$ in the Ricker function and the logistic function. This relation is the necessary condition for dynamical stabilization to occur at $N = 1$. However, this condition is not sufficient. The information in table 4.1 sums up the results from section 4.3.1 and allows us to predict when dynamical stabilization can occur at $N = 1$. In fact, since section 4.3.2 shows the existence of a solution moving away from $N = 1$ for $r > 2$ in the second iterate integrodifference equation, we simply need the existence of a solution moving toward $N = 1$ in the first iterate integrodifference equation to ensure dynamical stabilization. In the case of the logistic function, dynamical stabilization is always observed at $N = 1$ for $2 < r < 2.570$. For the Ricker function, we observe dynamical stabilization at $N = 1$ when $2 < r < 2.5072$, but we observe cycles around $N = 1$ for $r > 2.5072$ (see figure 4.6).

Shape of the solution	Ricker function	Logistic function
Monotone on $[0, 1]$	$0 < r < 1.0327$	$0 < r < 1.0686$
Damped oscillations at $N = 1$	$1.0327 < r < 2.5072$	$1.0686 < r < 2.570$
Cycle at $N = 1$	$2.5072 < 2 < 2.692$	NA

Table 4.1: Shape of the solution from 0 to 1 generated by operator q with respect to r for the Ricker function and the logistic function.

We plot different phase planes for the solution of the second iterate integrodifference equation in figures 4.17, 4.18 and 4.19. The phenomenon of dynamical stabilization at $N = 1$ is illustrated by the presence of a trajectory moving towards $(1, 0)$ and another moving away from $(1, 0)$ in figures 4.17 and 4.18. In figure 4.19, we see the cycle around $(1, 0)$ in the case of the Ricker function for $r > 2.5072$, which translates into the absence of dynamical stabilization at $N = 1$.

The results of sections 4.3.1 and 4.3.2 allow us to argue the existence of two successive travelling objects within the solution of the integrodifference equation when there is a stable 2-point cycle. Having only studied the connections from 0 to 1 and 1 to n_+ independently in sections 2.4 and 3.2, we had no knowledge on how these two objects could coexist in the same solution. Note that we have only provided plausibility arguments for this coexistence, that are supported by numerical simulations.

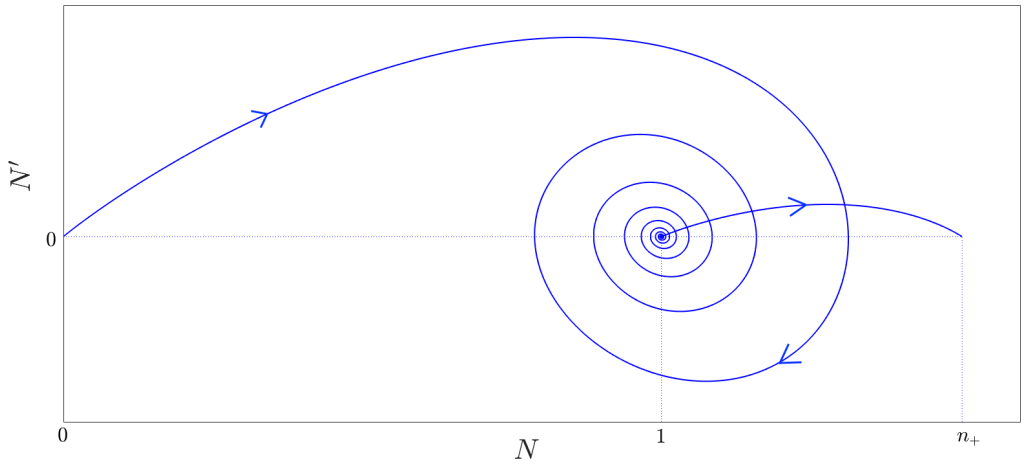

Figure 4.17: Phase plane for the solution of the integrodifference equation plotted in figure 4.5, where F is the Ricker function with $r = 2.2$ and K is the Laplace kernel with $a = 15$.

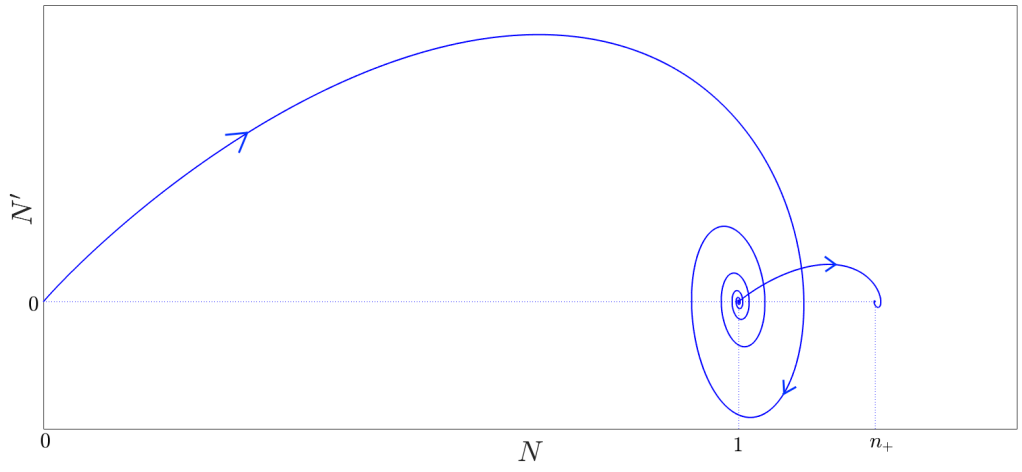

Figure 4.18: Phase plane for the solution of the integrodifference equation, where F is the logistic function with $r = 2.44$, K is the Laplace kernel for $a = 15$ and $N_0 = n_+\chi_{[x\geq 10]}$.

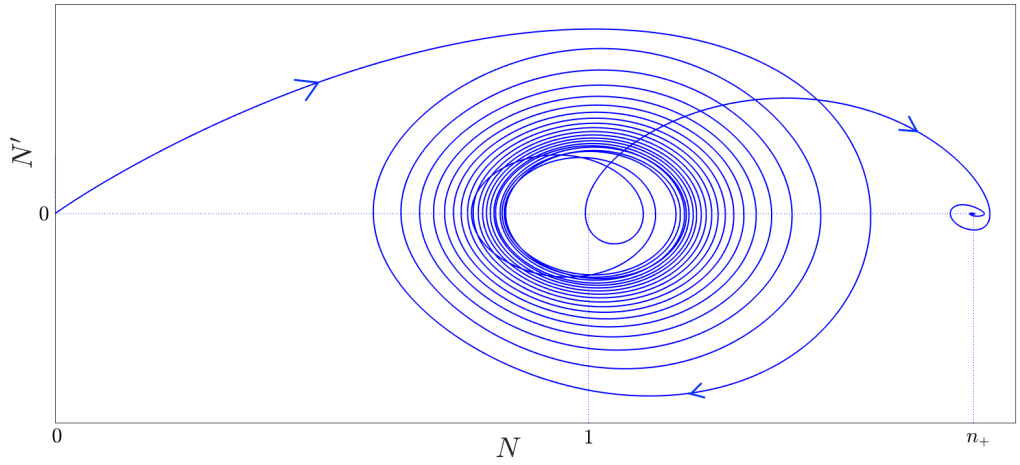

Figure 4.19: Phase plane for the solution of the integrodifference equation plotted in figure 4.6, where F is the Ricker function with $r = 2.525$ and K is the Laplace kernel for $a = 15$.

Chapter 5

Discussion

One of the goals of this thesis was to explain the spreading behavior of solutions for the integrodifference equation with a growth function that has a stable 2-point cycle. In this chapter, we will discuss the results we have obtained, and possible generalizations. We will also review the open questions to conclude with a description of future projects that relate to the concepts we have explored thus far.

5.1 Connection Between 1 and n_-

All throughout this thesis, we studied operator q on the interval $[1, n_+]$ to explain the connection seen in simulations between 1 and n_+. However, we can also observe a connection between 1 and n_- in the solution of the integrodifference equation with a stable 2-point cycle (see figure 5.1).

The results regarding the existence of a spreading speed and travelling wave solutions for operator q on $[1, n_+]$ from section 3.2 can also be applied to the interval $[n_-, 1]$. In fact, if a travelling wave between 1 and n_+ is observed in the solution of the recursion defined by operator q (3.2.1), then by applying operator Q (2.4.1) to this solution, we will observe a travelling wave between 1 and n_-. This relationship is illustrated in the bottom panels of figures 3.2 and 3.5.

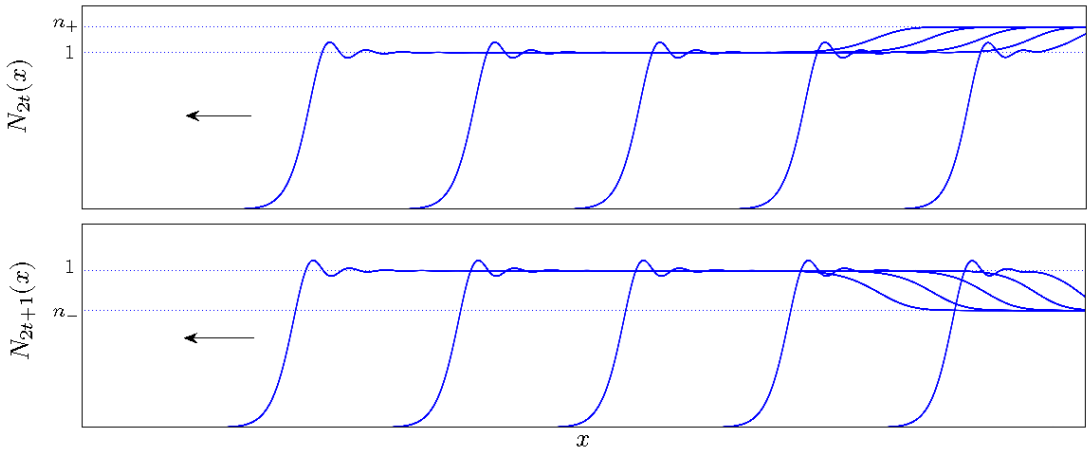

Figure 5.1: (Reminder of figure 1.2.) Solution of the integrodifference equation, where F is the logistic function with $r = 2.2$, K is the Laplace kernel with $a = 6$ and $N_0 = n_+\chi_{[x\geq 10]}$, plotted for even (top panel) and odd (bottom panel) generations every 10 time steps. n_- and n_+ are the values that form the 2-point cycle.

5.2 Generalization to 4-point Cycles, 8-point Cycles, Etc.

One of the natural questions that arises from the results on the growth function with a stable 2-cycle is what happens when this cycle becomes unstable? Can we say anything when the growth function has a stable 4-point cycle, stable 8-point cycle, etc? In [14], the authors plotted the solution of an integrodifference equation, where F is the logistic function with a stable 4-point cycle (see figure 5.2). They claimed that the solution alternates between four profiles while moving to the left, and described it as a travelling four-cycle. Replicating the simulations in MATLAB® in figure 5.3, we see an alternation in the profiles, but, just like in the case of the stable 2-point cycle, not all parts of the solution move at the same speed.

The techniques and results in this thesis can be applied to study the observed phenomenon. Let n_-^-, n_-^+, n_+^- and n_+^+ denote the values of the 4-point cycle in the growth function (see figures 2.6, 2.7, 2.11 and 2.12). The theory for the existence of a spreading speed on $[0, 1]$ and another on $[1, n_+]$ ($[1, n_-]$) was presented in sections 2.4 and 3.2, respectively. As for the spreading speed and travelling wave solutions on $[n_+, n_+^+]$ ($[n_+^-, n_+]$, $[n_-, n_-^+]$ and $[n_-^-, n_-]$), we must study the fourth iterate map of the integrodifference equation, which corresponds to the second iterate of the second

iterate map. Thus, the operator that defines the recursion for which we observe the connection between n^+ and n_+^+ is $(q \circ q)$, where q is as in (3.2.1).

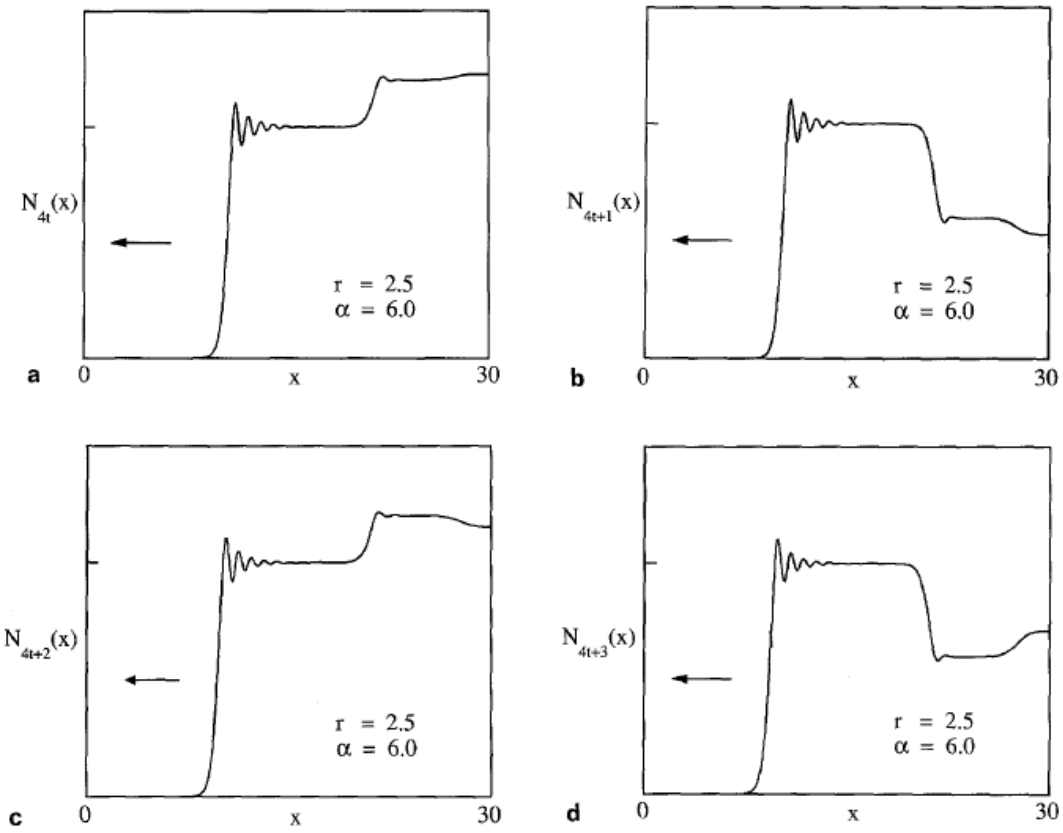

Figure 5.2: Fig. 10a-d from [14]. Solution of an integrodifference equation, where r is the parameter of the growth function and α is the parameter of the distribution kernel. Described as a travelling four-cycle.

As illustrated in figures 2.7 and 2.12, the stable 4-point cycle, in the case of the Ricker function and the logistic function, corresponds to two stable 2-point cycles, one around $N = n_-$ and the other around $N = n_+$. We illustrate the solutions obtained during simulations for the integrodifference equation with the stable 4-point cycle in figures 5.3 and 5.4 for initial conditions starting at 0 and 1, respectively. We see that the solution in figure 5.4 behaves just like the solution with a stable 2-point cycle for even and odd time steps.

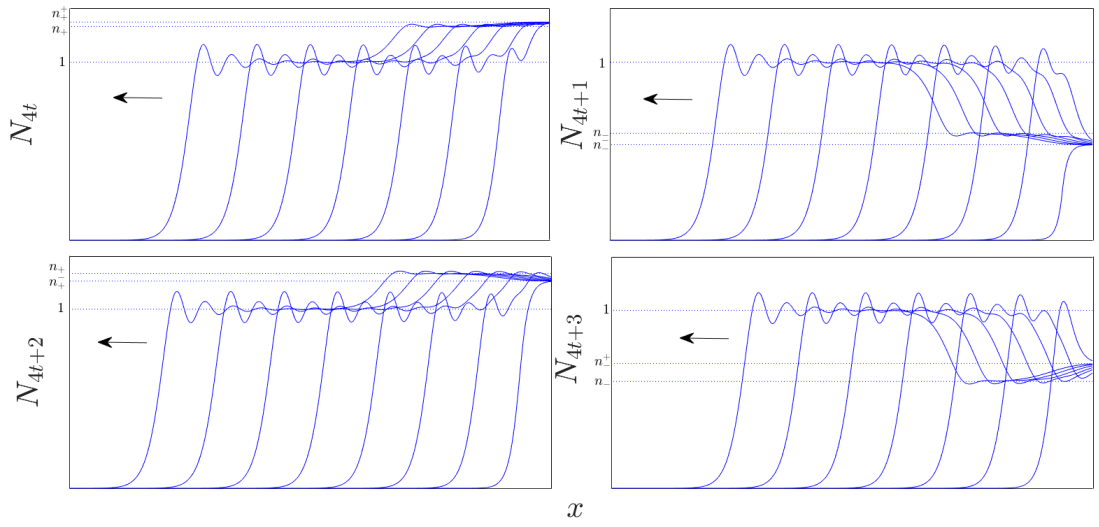

Figure 5.3: Solution of the integrodifference equation, where F the logistic function with $r = 2.5$, K is the Laplace kernel with $a = 6$ and $N_0 = n_+^+ \chi_{[x \geq 10]}$. n_- and n_+ are the values that form the 2-point cycle, and n_-^-, n_-^+, n_+^- and n_+^+ form the 4-point cycle.

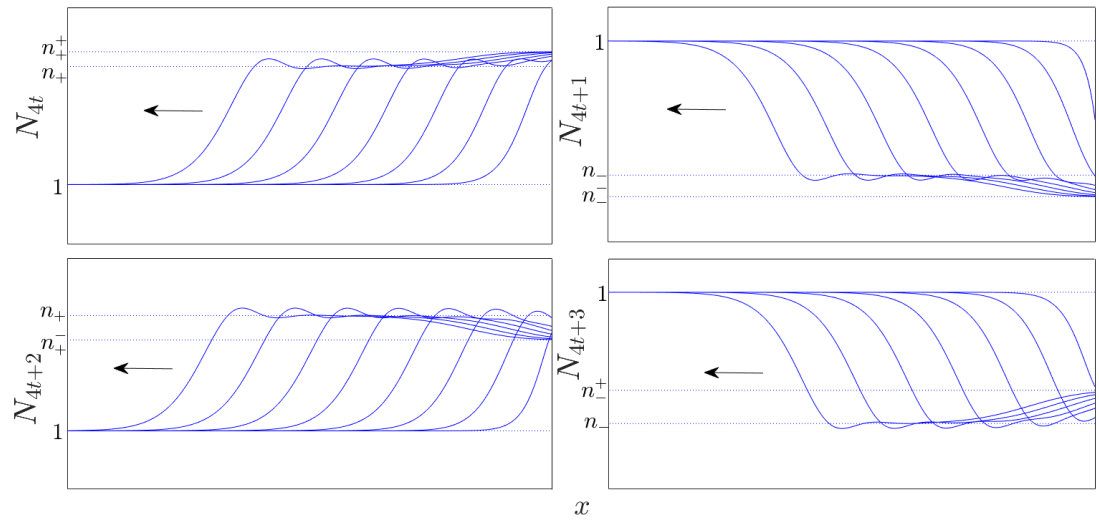

Figure 5.4: Solution of the integrodifference equation, where F the logistic function with $r = 2.5$, K is the Laplace kernel with $a = 6$ and $N_0 = \chi_{[x<10]} + n_+^+ \chi_{[x \geq 10]}$. n_- and n_+ are the values that form the 2-point cycle, and n_-^-, n_-^+, n_+^- and n_+^+ form the 4-point cycle.

Since operator q satisfies the continuity and compactness properties required for the existence of a spreading speed and travelling wave solutions, it follows that the operator $(q \circ q)$ will satisfy them as well, by the same arguments as Propositions 3.2.2 and 3.2.4. Also, similarly to Theorem 3.2.5, we can establish the other conditions for the existence of a spreading speed on $[n_+, n_+^+]$ (and also on $[n_+^-, n_+]$,$[n_-, n_-^+]$, and $[n_-^-, n_-]$ by application of operator Q), which are stated in the following theorem.

Theorem 5.2.1. *Let F be a growth function that respects the following conditions:*

i) F is bounded and Lipschitz continuous,

ii) F has exactly one stable 4-point cycle (n_+^+, n_-^-, n_+^-, n_-^+), which corresponds to two stable 2-point cycles in $(F \circ F)$, (n_-^-,n_-^+) and (n_+^-, n_+^+),

iii) $N = n_+$ is the only fixed point of $(F \circ F)$ on the interval $[n_+^-, n_+^+]$,

iv) $(F \circ F)'(n_+) < -1$,

v) F is non-increasing on $[n_+^-, n_+^+]$ and non-decreasing on $[n_-^-, n_-^+]$.

Then, there exists a spreading speed $c^*_{[n_+, n_+^+]}$ for the operator $(q \circ q)$ on the interval $[n_+, n_+^+]$.

In a similar manner, we could keep generalizing this result for 8-point cycles, and so on, up until the value of r for which chaotic behavior is observed in the growth function. We also notice in figures 5.3 and 5.4, that in addition to having dynamical stabilization at $N = 1$, we also observe it at $N = n_+$ ($N = n_-$). Since dynamical stabilization at $N = 1$ does not happen for $2.5072 < r < 2.692$ in the case of the Ricker function, we cannot observe dynamical stabilization both at $N = 1$ and $N = n_+$ ($N = n_-$) like in figure 5.3 (see figure 5.5). A similar analysis to the one done in chapter 4 could be done with the operator $(q \circ q)$ to make predictions regarding dynamical stabilization at $N = n_+$ ($N = n_-$).

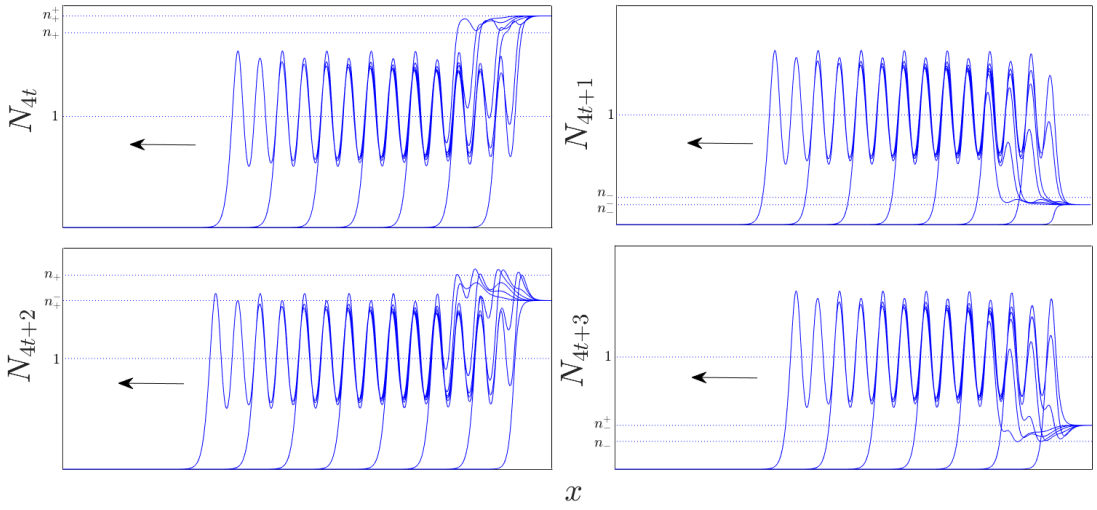

Figure 5.5: Solution of the integrodifference equation, where F is the Ricker function with $r = 2.6$, K is the Laplace kernel with $a = 15$ and $N_0 = n_+^+ \chi_{[x \geq 10]}$. n_- and n_+ are the values that form the 2-point cycle, and n_-^-, n_-^+, n_+^- and n_+^+ form the 4-point cycle.

5.3 Gaussian Kernel and Dynamical Stabilization

In section 4.3, we studied the shape of the solution for the integrodifference equation with the Laplace kernel. For the Gaussian kernel, it is difficult to do a similar analysis, as we cannot relate the operators Q and q to a system of delay differential equations, or even ordinary differential equations. Since the Gaussian kernel is also symmetric and unimodal, we can expect dynamical stabilization to occur. However, we cannot expect the solutions to necessarily have the same shape as for the Laplace kernel. The results from table 4.1 do not depend on the variance of the Laplace kernel. For the Gaussian kernel, the value of r for which the solution goes from being monotone to non-monotone on $[0, 1]$ is not predicted by this same table. In fact, we see in figure 5.6 that this change of behavior happens for smaller values of r for $\sigma^2 = 0.1$. Also, we do not observe cycles at $N = 1$ in the case of the Ricker function for $\sigma^2 = 0.1$, a result that was also independent of the variance in the case of the Laplace kernel (see figure 5.7). Thus, changing the distribution kernel has an impact on the shape of the solution. Hence, it is difficult to make predictions regarding dynamical stabilization when K is not the Laplace kernel.

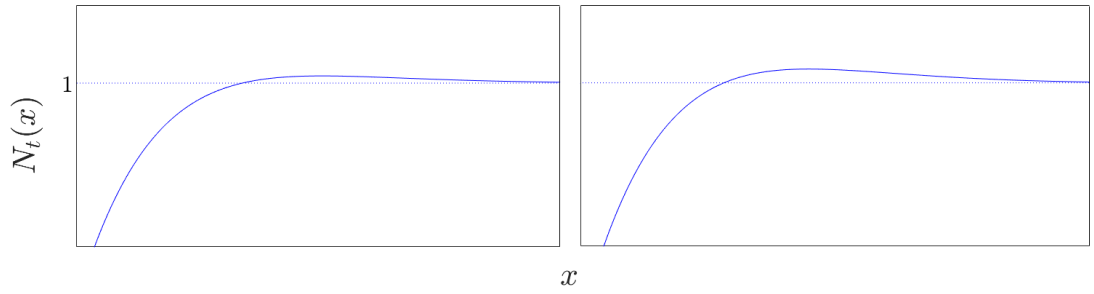

Figure 5.6: Close-up of the solution of the integrodifference equation, where K is the Gaussian kernel with $\sigma^2 = 0.1$ and F is the Ricker function with $r = 1.03$ (left), the logistic function with $r = 1.06$ (right) and $N_0 = \chi_{[x\geq 10]}$.

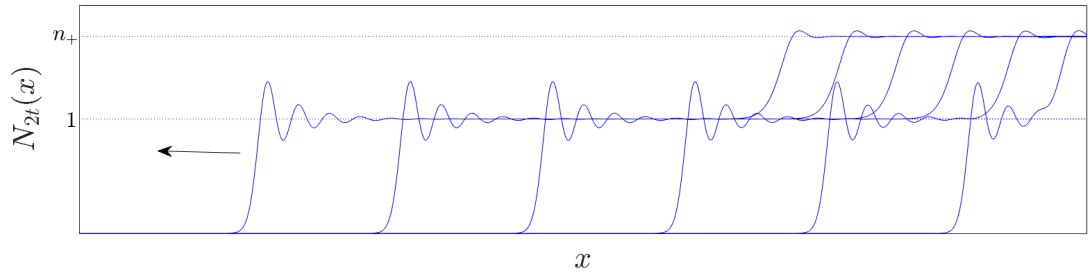

Figure 5.7: Solution of the integrodifference equation, where K is the Gaussian kernel with $\sigma^2 = 0.1$ and F is the Ricker function with $r = 2.525$ and $N_0 = n_+\chi_{[x\geq 10]}$, plotted every 10 time steps.

5.4 Symmetry of the Kernel

All throughout this work, we assumed that the distribution kernel is symmetric, i.e. $K(-x) = K(x)$. This assumption allowed us to apply the theory from [31] to left-moving travelling waves instead of right-moving travelling waves, all while keeping the same formulas for the spreading speed. In the case where the distribution kernel is not symmetric, we would have to define two spreading speeds, one in the positive direction and another in the negative direction.

The authors in [12] used symmetric kernels, while others only consider the rightward spreading speed [17]. Our work is based on their results. Others have generalized the theory to asymmetric kernels and defined directional spreading speeds accordingly [33]. We believe that our results on spreading speeds carry over to asymmetric kernels when these directional spreading speeds are used.

However, it is difficult to make predictions regarding dynamical stabilization in the solution of the integrodifference equation with an asymmetric distribution kernel. We have discussed earlier in section 5.3 that the results regarding dynamical stabilization were different for the Laplace kernel and the Gaussian kernel when considering the Ricker function. Since the outcome relies on the shape of the kernel, finding a general approach to predict dynamical stabilization given an arbitrary kernel would be very tedious.

5.5 Other Types of Solutions

Throughout this work, we have used step functions as the initial conditions during simulations. Although these functions are not continuous, we can still apply the results regarding spreading speeds and travelling waves for such initial conditions since $Q[N_0]$ is continuous. Could we observe different types of solutions with different initial conditions?

When $r > 2$ in the case of the Ricker function and the logistic function, Theorems 3.1 and 3.2 of [12] and Theorem 4.1 of [17] say that travelling wave solutions can still exist in the integrodifference equation. However, the solution we have been studying, that is obtained with a step function as the initial condition, is not a travelling wave. In [17], the authors ran simulations for $r = 2.1$ in the Ricker function, where the initial condition was a decaying exponential function. The results obtained by their numerical scheme is illustrated in figure 5.8.

The numerical scheme used to produce figure 5.8 in [17] relies on the FFT algorithm that we have also used. The authors in [17] treat the problem as a fixed point problem, $N(x + ct) = Q_c[N(x)]$, with the value of c obtained by the spreading speed formula. Using MATLAB®, we simulate the solution of the integrodifference equation, using our scheme from table D.4, with the same parameter values and a similar initial condition as [17]. Our result can be viewed in figure 5.9, where we show the spread in the positive direction for $N_0 = e^{-x}$.

The thicker curves plotted in figure 5.9, which correspond to the solution of the integrodifference equation at 20 and 21 time steps, resembles to the one in figure 5.8. However, the solution falls back on the values of the stable 2-point cycle shortly after. This behavior was not observed in [17]. Differences between our numerical methods and the ones from [17] thus need to be studied in future projects.

We also studied the existence of travelling wave solutions that connect an unstable steady state to a stable steady state of q. Another type of solution that

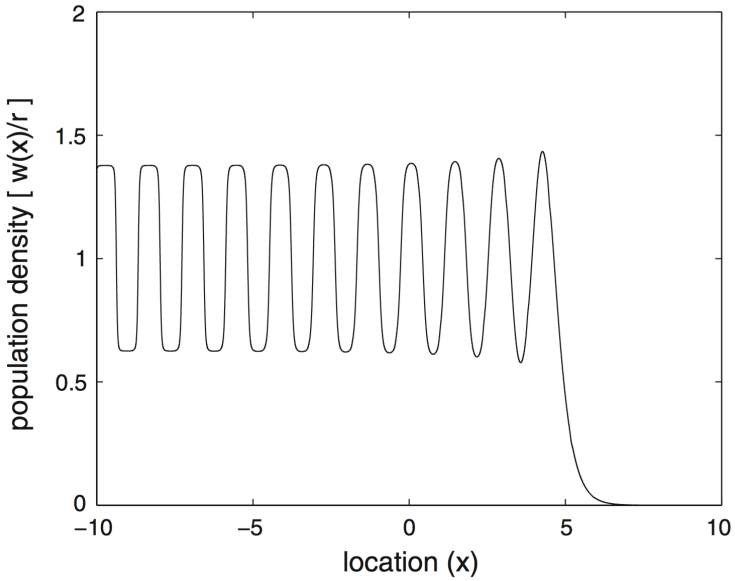

Figure 5.8: Fig. 3 from [17]. Travelling wave solution of the integrodifference equation, where F is the Ricker function with $r = 2.1$, K is the Laplace kernel with $a = 200$ and N_0 is a decaying exponential.

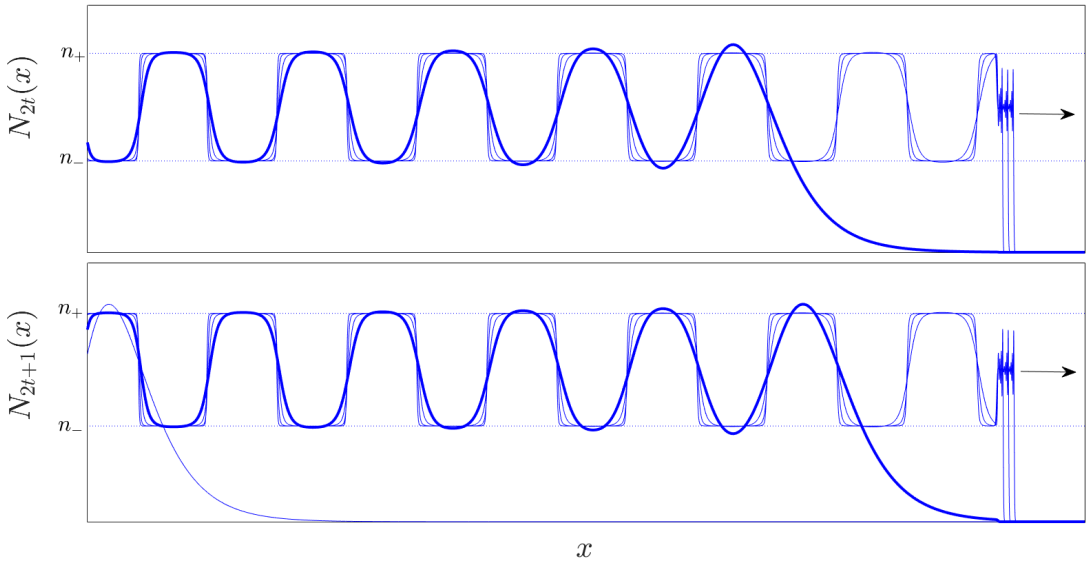

Figure 5.9: Solution of the integrodifference equation, where F is the Ricker function with $r = 2.1$, K is the Laplace kernel with $a = 200$ and $N_0 = e^{-x}$, plotted for even (top panel) and odd (bottom panel) generations every 10 time steps. Note that σ^2 is small since a is very large.

could exist in the system, as portrayed in figure 5.10, is a bistable wave, i.e. a travelling wave that connects two stable steady states, namely n_- and n_+. This idea is based on the results in [18], where the existence of a bistable wave was shown on $[0, 1]$ in the case where the growth function F in operator Q has two stable steady states, namely at $N = 0$ and $N = 1$, and one unstable steady state at $N = \alpha$, where $0 < \alpha < 1$. In other words, [18] establishes the existence of a bistable wave on $[0, 1]$ in the case of a strong Allee effect (see "Biological Terminology") at $N = 0$. When F is the Ricker function or the logistic function with a stable 2-point cycle in the growth function F, then $(F \circ F)$ has two stable steady states, $N = n_-$ and $N = n_+$, and an unstable steady state, $N = 1$, where $n_- < 1 < n_+$. Can we thus relate the results of [18] to operator q_2 (3.2.7) on $[n_-, n_+]$? Can the results of [18] also be applied to operator q, as the steady states are the same as q_2? In [29], the authors consider a strong Allee effect at $N = 0$ and provide a result for the spreading speed on $[0, 1]$. Since the function $(F \circ F)$ has a strong Allee effect at $N = n_-$, can we relate to the work in [29] to calculate the spreading speed, if it exists? Numerical simulations in figure 5.10 suggest the existence of a travelling wave connecting n_- to n_+ in operator q. A thorough analysis of this case is beyond the scope of this work and will be considered in the future.

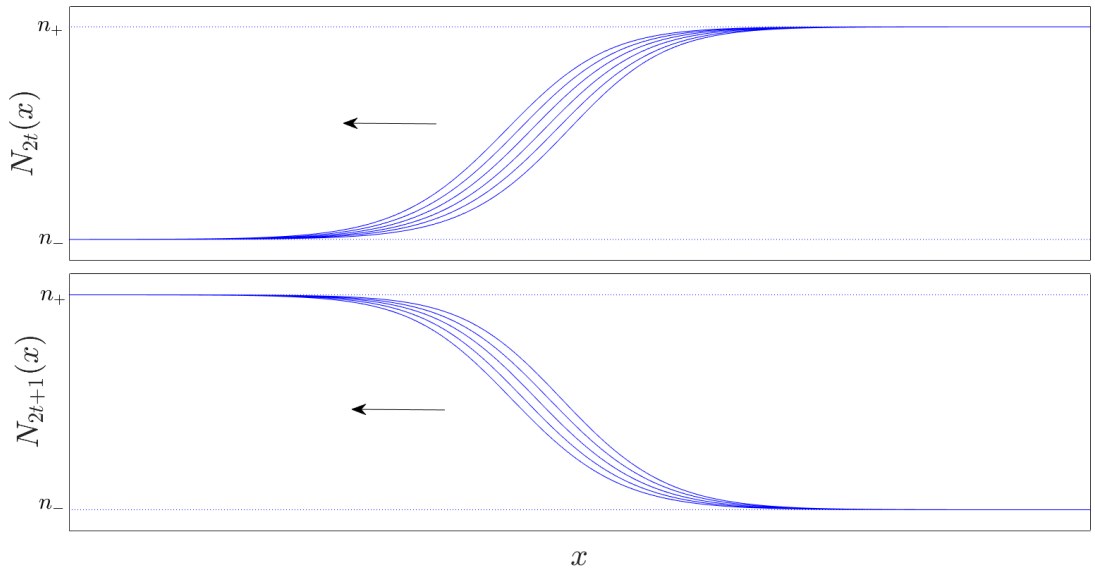

Figure 5.10: Solution of the integrodifference equation, where F is the Ricker function with $r = 2.2$, K is the Laplace kernel with $a = 15$ and $N_0 = n_-\chi_{[x<10]} + n_+\chi_{[x\geq 10]}$, plotted for even (top panel) and odd (bottom panel) generations every 10 time steps.n_- and n_+ are the values of the 2-point cycle.

5.6 Numerical Schemes

The integrodifference model is nothing but a convolution between the dispersal kernel K and the growth function $(F \circ N)$, calculated iteratively for each time step (see equation (2.2.1)). Throughout this work, we ran simulations based on two different numerical schemes to calculate this convolution product at each time step. The first scheme that we applied uses a fast Fourier transform (FFT), which is a discrete adaptation of the Fourier transform found in MATLAB® [25]. The scheme is based on the convolution theorem that states that the Fourier transform of a convolution product is the product of Fourier transforms. It is a highly efficient scheme. The fast Fourier transform and its inversion assume that the domain is periodic. Thus, we require a padding in the numerical simulation to avoid any kind of overlapping. The code for this scheme can be found in table D.4.

To provide some kind of robustness to our numerical analysis, we also developed an alternative scheme to see if it provided the same conclusions. This second scheme calculates the convolution by direct integration with the help of the trapezoid rule. The code can be found in table D.5. This last algorithm is very slow when the step size for discrete integration is small. Given that oscillations are observed for certain parameter values in the solution, we must keep the step size very small to ensure that the loss of precision is not too big during the integration.

In order to compare both of these methods, we can compare the relative error obtained between the theoretical and numerical values for the spreading speed. When doing so, there is not one that performs a lot better than the other, given the chosen step sizes. The method of direct integration could be more precise if the step size was increased, but this increase is very costly in time. That being said, we can be satisfied with the FFT algorithm, given its purpose in this thesis. We can also use these relative errors to compare the distribution kernels and the growth functions. When doing so, there is no particular distribution kernel or growth function that is better overall in terms of relative errors. In some instances, the Gaussian kernel seems to produce lower errors, and for others, it seems to produce higher errors. It is thus difficult to pin-point exactly what the error source is, given the many variables in play. For the majority of simulations, the errors are well below 5%, which gives us confidence in the theoretical formulas that we obtained.

In both numerical schemes, we have some limitations due to the fact that we cannot integrate over all real numbers. As a first consequence, the distribution kernel does not integrate to 1 numerically. However, we can easily fix this problem by normalizing the distribution kernel, as we did in the MATLAB® code. A more important consequence is that we are limited in the number of time steps that we

can simulate. In fact, the solution is compromised when it gets too close to the boundaries of the finite domain. This is because we lose a part of the distribution kernel when it is centered at a value near the boundary during the computation of the convolution product. In order to run a maximum number of time steps, the variance of the distribution kernel needs to be small enough, but not too small as to be lost in the step size, and the domain needs to be large enough. However, having a larger domain requires a smaller step size. Thus, there is always a compromise to make.

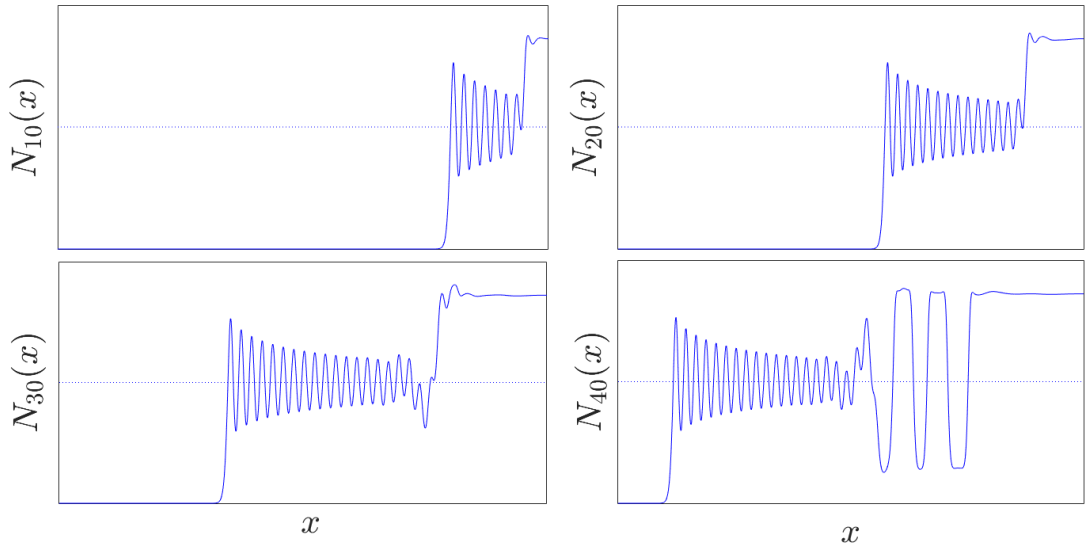

Figure 5.11: Solution of the integrodifference equation, where F is the Ricker function with $r = 2.525$, K is the Laplace kernel with $a = 100$ and $N_0 = n_+\chi_{[x\geq 10]}$.

It is also possible that this limitation is keeping us from seeing the actual long-term behavior of the solution in some cases. This leaves open questions regarding the results that we observed. Does the asymptotic behavior of the solution of the integrodifference equation in figure 5.9 resemble the dynamical stabilization observed in the solution where the initial condition is of the form $N_0 = \chi_{[x>0]}$? Can dynamical stabilization occur for any initial condition? Is there always dynamical stabilization at $N = 1$ in the case of the Ricker function? Is dynamical stabilization absent in the solution plotted in figure 4.6 because we cannot run the simulation long enough to observe the damped oscillations? We can run the simulation for smaller variance in the distribution kernel in an attempt to answer this last question (see figure 5.11), but we are still limited in the number of time steps we can simulate. In fact, since the rate of change of the solution is great due to the many oscillations, the error obtained at each iteration is significant and accumulates rapidly compared to more monotone

solutions, resulting in some very strange plots. We see in figure 5.11 that after less than 30 time steps, the solution becomes erratic, with $a = 100$ in the Laplace kernel.

5.7 Biological Implications

In section 2.2, We explained how integrodifference equations are models that describe the population density of a species in the environment. In chapter 1, we briefly introduced the problematic of invasive species. Being able to make accurate predictions regarding the speed of spatial spread of such species would allow one to implement prevention, management and control strategies to minimize the damages caused by invasion. Having a model such as an integrodifference equation allows us to do so, by studying the spreading speed and travelling wave solutions, when this model applies.

We see by our results that the choice of the growth function is very important when defining our model. In the case where the growth phase is described by the Ricker function or the logistic function, we can observe dynamical stabilization in the solution. In other words, it could seem like the population density of the invader would be stabilizing in the environment (corresponding to the state $N = 1$ in our solution), only to have another wave move in later. If the growth function is not well chosen, the analysis could overlook the possibility of this second wave, which would have consequences on the adopted management and control strategies. On the other hand, if one were making predictions based on empirical data without fitting an underlying model, one could think that the population is attaining a steady state. This could lead to a greater economical impact from the invasive species if the second event is not taken into consideration.

Also, even though the Ricker function and the logistic function exhibit a similar type of behavior as the parameter r changes, it is still important to make the distinction between these two growth functions. In fact, the results that we have obtained regarding dynamical stabilization show that the solution with the Ricker function is more erratic than the one with the logistic function, as we predict that for some range of r, the oscillations around $N = 1$ do not dampen, resulting in a cycle before the second wave moves in. We also observe that the choice of distribution kernel has an effect on the way dynamical stabilization occurs, as discussed in section 5.3. Thus, what we have shown via simulations could be possible outcomes in nature, and ecologists and biologists should be aware of these types of scenarios in order to make informed decisions.

5.8 Future Projects

In a recent paper [21], the authors highlight the need for mathematical theory on non-monotone operators. More specifically, they focus on the existence of stacked front solutions in an integrodifference model via numerical simulations. As stated by the authors of [21], "the profile of a stacked front solution looks like a staircase of traveling wave fronts". This profile is exactly the type of solution we studied in this thesis, through the concept of dynamical stabilization, in the integrodifference equation. To summarize our results, there are no travelling two-cycles from 0 to n_+ (n_-) for operator Q, but two cases of stacked front solutions for operator q, that correspond to the solutions with n_- and n_+ in the second travelling wave. The authors of [21] also mention that a theory for stacked fronts was developed, but only in the case of partial differential equations [3, 8, 13]. Thus, the work we have done in this thesis is a step towards closing the gap on non-monotone operators, and establishing a theory for stacked fronts for integrodifference equations. However, more advances need to be made in order to have a proper foundation for the subject.

Some questions have been left open for discussion during the course of this work. The first project that follows from this thesis is the proof of the formula for the spreading speed of q on $[1, n_+]$. At the moment, we only have a conjecture based on the analysis from section 3.2.3.

Conjecture 5.8.1. *Let q be the operator defined by expression (3.2.1). Assume F is the Ricker function or the logistic function. Then the spreading speed $c^*_{[1,n_+]}$ on $[1, n_+]$ is linearly determined, and is thus given by equation* (3.2.5).

Based on the work in section 3.2.3, we also have the following unanswered questions: If the spreading speed of the operator q_2, defined by (3.2.7), is linearly determined, is the spreading speed of the operator q also linearly determined? How does interchanging the order of the convolution with K and the application of F in the operator affect the value of the spreading speed? Could this interchangeability be applied to higher-order iterates of the integrodifference equation? Perhaps proving Conjecture 5.8.1 would provide some insight and serve as a starting point to answer these questions.

In section 2.4.2, we mention that the results from [12] allow to determine when there is an upward convergence, i.e. when we know precisely the values of the limits in the definition of the spreading speed, for solutions of an integrodifference equation with a non-monotone growth function on $[0, \beta]$. This result was stated in Theorem 2.4.14. We were not able to use the work of [12] to show the upward convergence in the case of a spreading speed and travelling waves on $[\beta, n_+]$. However,

we do observe it during simulations for $\beta = 1$ with the growth functions that we have studied. Thus, proving this upward convergence remains an open problem. We hope that the generalized approach provided in [33] to obtain the same results as [12] might allow us to determine the condition for which there is upward convergence on $[\beta, n_+]$.

A big part of this thesis was discussing the existence of two travelling objects in the same operator. However, the justification that those two objects can coexist in the solution at the same time is based purely on plausibility arguments in chapter 4. We have shown that the necessary conditions for such a solution to exist is satisfied, in the case where the integrodifference equation can be transformed into a system of delay differential equations. This method was only applied to an integrodifference equation with the Laplace kernel. Some additional research could be done in order to determine a more general approach that would allow to explain dynamical stabilization with various distribution kernels. Particularly, we could further explore the outcome of the solution given an asymmetric distribution kernel. Also, proving analytically that two travelling objects can coexist in the same solution is an open problem.

Finally, several other projects would include the improvement of the numerical scheme, as hinted by section 5.6, and the study of alternative solutions, as introduced in section 5.5.

Appendix A

Moment-generating Functions and Convolutions

A.1 Moment-generating Functions

Let f denote a continuous probability distribution of a random variable x. We will denote its moment-generating function by M_f, which is defined by

$$M_f(t) = \int_{\mathbb{R}} e^{tx} f(x) dx,$$

for all t where the integral converges. The moment-generating function uniquely defines the probability distribution, and we have that $M_f(0) = 1$ when M_f is defined at $t = 0$ [2].

A.1.1 Moment-generating Function of the Gaussian Kernel

Let K be defined by equation (2.2.2).

$$\begin{aligned} M_K(s) &= \int e^{sx} K(x) dx \\ &= \frac{1}{\sqrt{2\pi\sigma^2}} \int e^{-\frac{1}{2\sigma^2}\left(x^2 - 2\sigma^2 sx\right)} dx \\ &= \frac{1}{\sqrt{2\pi\sigma^2}} \int e^{-\frac{1}{2\sigma^2}\left[(x-\sigma^2 s)^2 - \sigma^4 s^2\right]} dx \end{aligned}$$

$$
\begin{aligned}
&= \frac{e^{\sigma^2 s^2/2}}{\sqrt{2\pi\sigma^2}} \int e^{-\left(\frac{1}{\sqrt{2\sigma^2}}(x-\sigma^2 s)\right)^2} \\
&= e^{\sigma^2 s^2/2} \frac{\sqrt{2\sigma^2}}{\sqrt{2\pi\sigma^2}} \int e^{-z^2} dz \\
M_K(s) &= e^{\sigma^2 s^2/2}.
\end{aligned}
$$

A.1.2 Moment-generating Function of the Laplace Kernel

Let K be defined by equation (2.2.3).

$$
\begin{aligned}
M_K(s) &= \int e^{sx} K(x) dx \\
&= \int_{-\infty}^{0} \frac{a}{2} e^{(a+s)x} dx + \int_{0}^{\infty} \frac{a}{2} e^{(s-a)x} dx \\
&= \frac{a}{2} \left(\lim_{t \to -\infty} \left[\frac{e^{(a+s)x}}{a+s} \right]_{-\infty}^{0} + \lim_{t \to \infty} \left[\frac{e^{(s-a)x}}{s-a} \right]_{0}^{\infty} \right) \\
&= \frac{a}{2} \left(\frac{1}{a+s} + \frac{1}{a-s} \right) \\
M_K(s) &= \frac{a^2}{a^2 - s^2},
\end{aligned}
$$

provided that $|s| < a$.

A.2 Convolutions

Let f and g be two probability distributions. We define the convolution of f and g by

$$
\begin{aligned}
(f * g)(x) &= \int_{\mathbb{R}} f(x-y) g(y) dy \\
&= \int_{\mathbb{R}} f(y) g(x-y) dy.
\end{aligned}
$$

A.2.1 Moment-generating Function of a Convolution

The moment-generating function of a convolution is given by

$$\begin{aligned}
M_{f*g} &= \int_{\mathbb{R}} e^{tx} f * g(x) dx \\
&= \int_{\mathbb{R}} e^{tx} \left[\int_{\mathbb{R}} f(x-y) g(y) dy \right] dx \\
&= \int_{\mathbb{R}} \int_{\mathbb{R}} e^{tx} f(x-y) g(y) dx dy \\
&= \int_{\mathbb{R}} \int_{\mathbb{R}} e^{t(z+y)} f(z) g(y) dz dy \text{ (by letting } z = x - y) \\
&= \int_{\mathbb{R}} e^{tz} f(z) dz \int_{\mathbb{R}} e^{yt} g(y) dy \\
&= M_f(t) M_g(t),
\end{aligned}$$

for all t where both M_f and M_g are defined.

Using induction, we can show that for a given finite sequence of probability distribution $\{f_1, f_2, ..., f_n\}$,

$$M_{f_1 * f_2 * \cdots * f_n}(t) = M_{f_1}(t) M_{f_2}(t) \cdots M_{f_n}(t),$$

for all t where $M_{f_1}, M_{f_2}, ..., M_{f_n}$ are defined.

A.2.2 Convolution of the Gaussian Kernel

Let K be defined by equation (2.2.2). From what precedes along with the result of appendix A.1.1, the moment-generating function of $K * K$ is given by

$$M_{K*K}(s) = e^{\sigma^2 s^2} = e^{2\sigma^2 s^2/2}.$$

This corresponds to the moment-generating function of a Gaussian kernel with variance $2\sigma^2$. Thus,

$$(K * K)(x) = \frac{1}{\sqrt{4\pi\sigma^2}} e^{-\frac{x}{4\sigma^2}}.$$

A.2.3 Convolution of the Laplace Kernel

Let K be defined by equation (2.2.3). We compute the convolution of the Laplace kernel by using the definition.

$$\begin{aligned}(K * K)(x) &= \int_{\mathbb{R}} K(x-y)K(y)dy \\ &= \frac{a^2}{4}\int_{\mathbb{R}} e^{-a(|x-y|+|y|)}dy.\end{aligned}$$

Assume $x \geq 0$, then

$$\begin{aligned}(K * K)(x) &= \frac{a^2}{4}\left(\int_{-\infty}^{x} e^{-a(x-y+|y|)}dy + \int_{x}^{\infty} e^{-a(y-x+|y|)}dy\right) \\ &= \frac{a^2}{4}\left(\int_{-\infty}^{0} e^{-a(x-2y)}dy + \int_{0}^{x} e^{-ax}dy + \int_{x}^{\infty} e^{-a(2y-x)}dy\right) \\ &= \frac{a^2}{4}e^{-ax}\left(\frac{e^{2ay}}{2a}\Big|_{-\infty}^{0} + y\Big|_{0}^{x} + \frac{e^{-2ay}}{-2a}\Big|_{x}^{\infty}\right) \\ &= \frac{a}{4}(a+1)e^{-ax}.\end{aligned}$$

Similarly, in the case where $x < 0$, we get

$$(K * K)(x) = \frac{a}{4}(-ax+1)e^{ax.}$$

Thus,

$$K * K(x) = \frac{a}{4}(a|x|+1)e^{-a|x|}.$$

Appendix B

Lambert W Function

The Lambert W function, also called the product logarithm, denoted by W, represents solutions of the equation

$$x = W(x)e^{W(x)}, \tag{B.0.1}$$

for all x in $\mathbb{C}$. We thus get the following relation:

$$y = xe^x \Leftrightarrow x = W(y). \tag{B.0.2}$$

Equation B.0.1 has infinitely many solutions in the complex plane, that we denote by $W_k(x)$, $k \in \mathbb{Z}$. In order to get the real-valued solutions of equation (B.0.1), i.e. $W(x) \in \mathbb{R}$, we must have $x \geq -\frac{1}{e}$. For $x \geq 0$ in $\mathbb{R}$ there is exactly one real solution, $W_0(x)$. For $-\frac{1}{e} < x < 0$, there are two distinct real solutions, the largest one being $W_0(x)$ and the smallest being $W_{-1}(x)$ [5] (see figures B.1 and B.2).

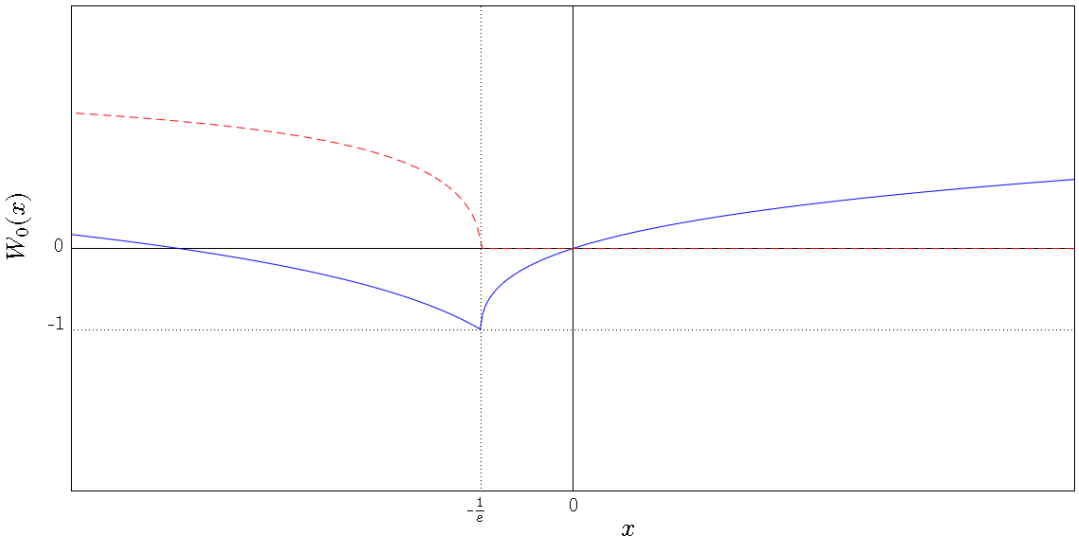

Figure B.1: Plot of the Lambert W function for $k = 0$. The solid line is the real part of the function and the dashed line is the imaginary part.

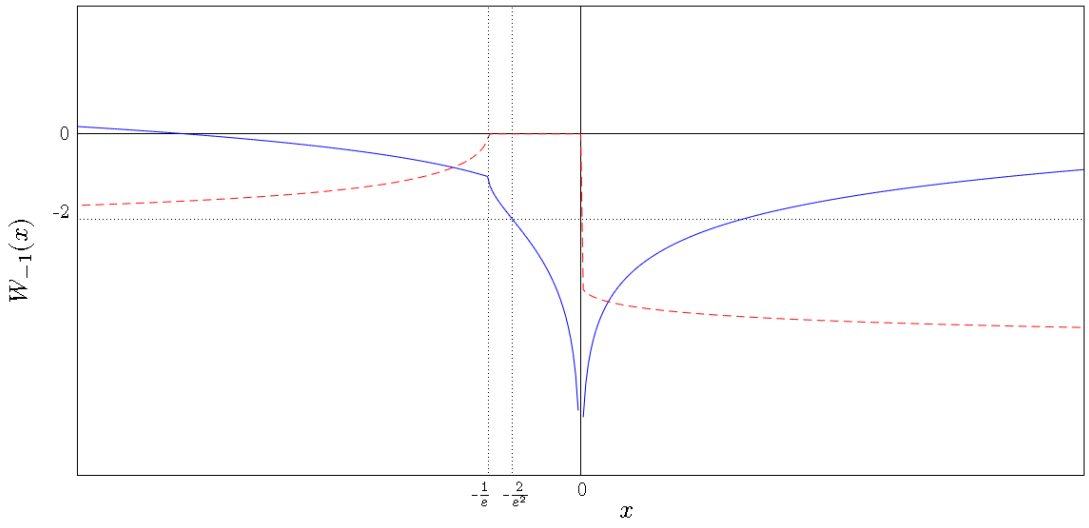

Figure B.2: Plot of the Lambert W function for $k = -1$. The solid line is the real part of the function and the dashed line is the imaginary part.

B.1 Solving Equations with the Lambert W Function

Using relation (B.0.2), we can use the Lambert W function to solve equations with an exponential term.

Solving $\rho x = e^x$, $\rho \neq 0$:

$$\begin{aligned} \rho x = e^x &\Rightarrow x e^{-x} = \frac{1}{\rho} \\ &\Rightarrow -x e^{-x} = -\frac{1}{\rho} \\ &\Rightarrow -x = W\left(-\frac{1}{\rho}\right) \\ &\Rightarrow x = -W\left(-\frac{1}{\rho}\right). \end{aligned} \tag{B.1.1}$$

Solving $\rho x^2 = e^x$, $\rho > 0$:

$$\begin{aligned} \rho x^2 = e^x &\Rightarrow \pm\sqrt{\rho} x = e^{\frac{x}{2}} \\ &\Rightarrow x e^{-\frac{x}{2}} = \pm\frac{1}{\sqrt{\rho}} \\ &\Rightarrow -\frac{x}{2} e^{-\frac{x}{2}} = \pm\frac{1}{2\sqrt{\rho}} \\ &\Rightarrow -\frac{x}{2} = W\left(\pm\frac{1}{2\sqrt{\rho}}\right) \\ &\Rightarrow x = -2W\left(\pm\frac{1}{2\sqrt{\rho}}\right). \end{aligned} \tag{B.1.2}$$

Appendix C

Additional Figures

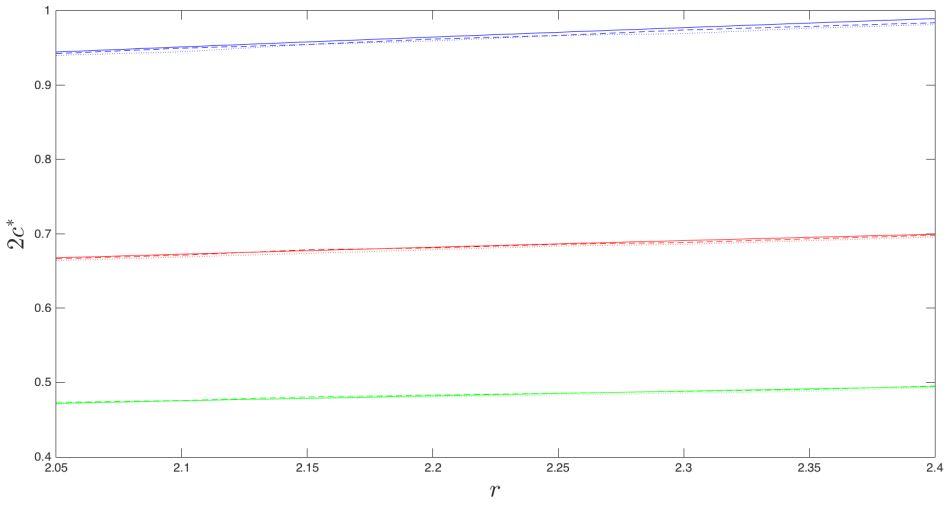

Figure C.1: Theoretical (full line) and numerical speed of operators q (dashed line) and q_2 (dotted line) on $[0, 1]$ with logistic function and Gaussian kernel for different values of σ^2 (top: $\sigma^2 = 0.1$, middle: $\sigma^2 = 0.05$, bottom: $\sigma^2 = 0.025$) with respect to the parameter r. The plot is generated with a scheme that uses the FFT algorithm, shown in table D.4, that is based on [25].

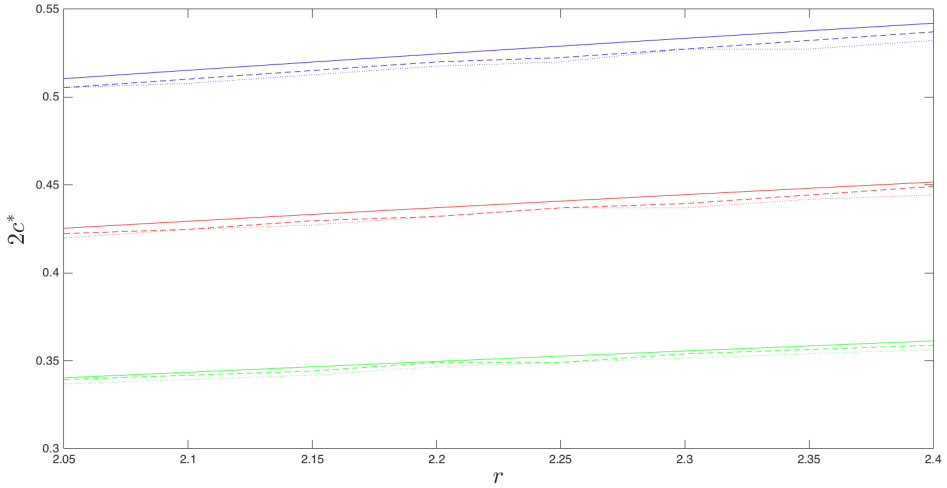

Figure C.2: Theoretical (full line) and numerical speed of operators q (dashed line) and q_2 (dotted line) on $[0, 1]$ with logistic function and Laplace kernel for different values of a (top: $a = 10$, middle: $a = 12$, bottom: $a = 15$) with respect to the parameter r. The plot is generated with a scheme that uses the FFT algorithm, shown in table D.4, that is based on [25].

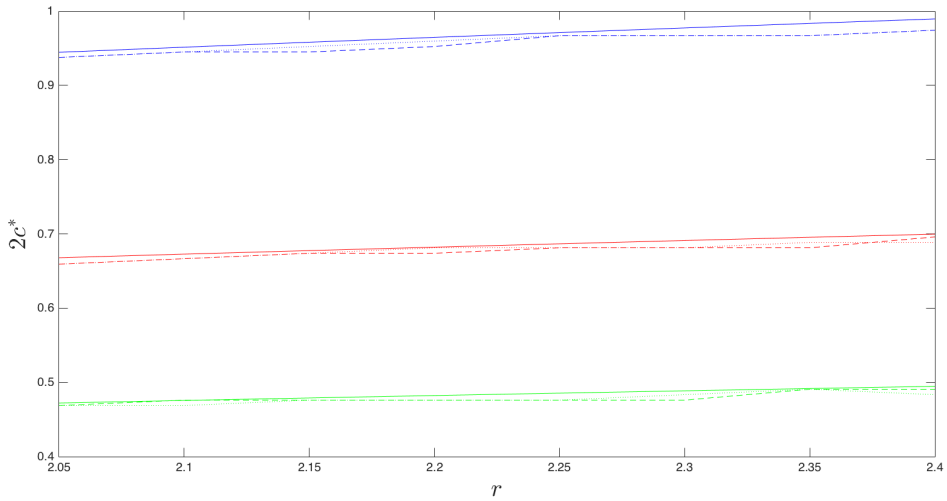

Figure C.3: Theoretical (full line) and numerical speed of operators q (dashed line) and q_2 (dotted line) on $[0, 1]$ with logistic function and Gaussian kernel for different values of σ^2 (top: $\sigma^2 = 0.1$, middle: $\sigma^2 = 0.05$, bottom: $\sigma^2 = 0.025$) with respect to the parameter r. The plot is generated with a scheme that uses the trapz algorithm, as shown in table D.5.

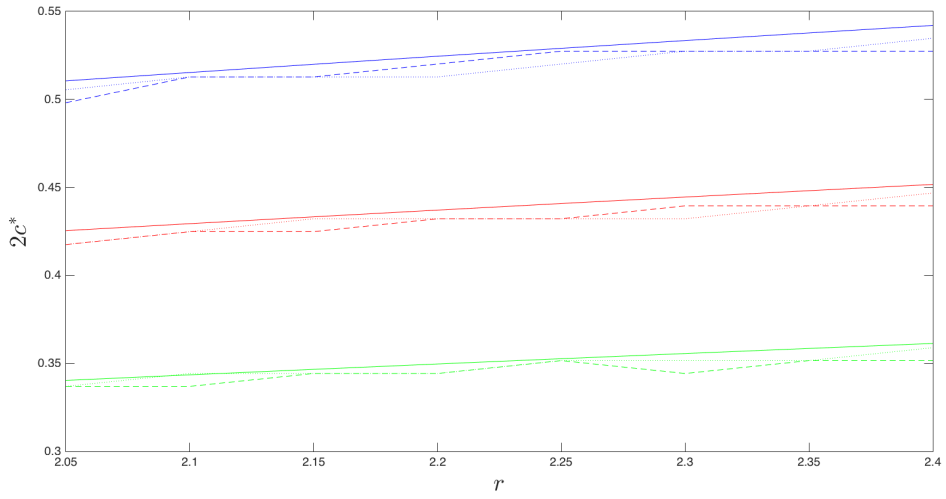

Figure C.4: Theoretical (full line) and numerical speed of operators q (dashed line) and q_2 (dotted line) on $[0, 1]$ with logistic function and Laplace kernel for different values of a (top: $a = 10$, middle: $a = 12$, bottom: $a = 15$) with respect to the parameter r. The plot is generated with a scheme that uses the trapz algorithm, as shown in table D.5.

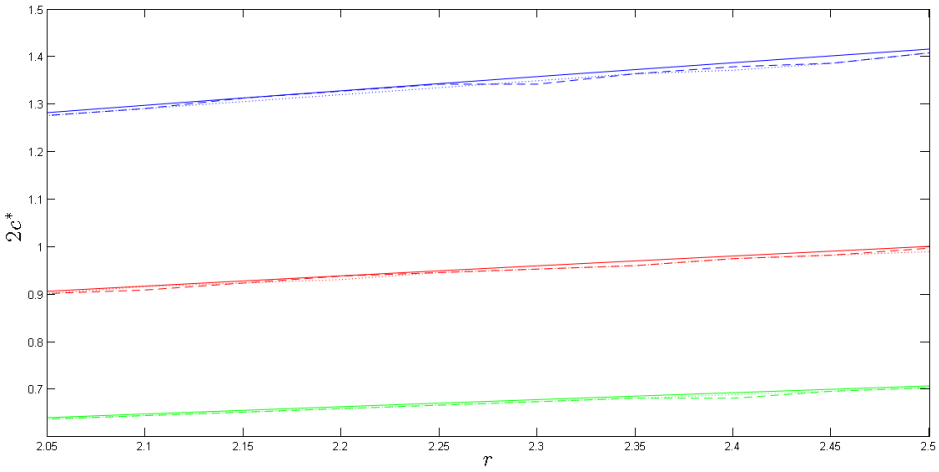

Figure C.5: Theoretical (full line) and numerical speed of operators q (dashed line) and q_2 (dotted line) on $[0, 1]$ with Ricker function and Gaussian kernel for different values of σ^2 (top: $\sigma^2 = 0.1$, middle: $\sigma^2 = 0.05$, bottom: $\sigma^2 = 0.025$) with respect to r. The plot is generated with a scheme that uses the trapz algorithm, as shown in table D.5.

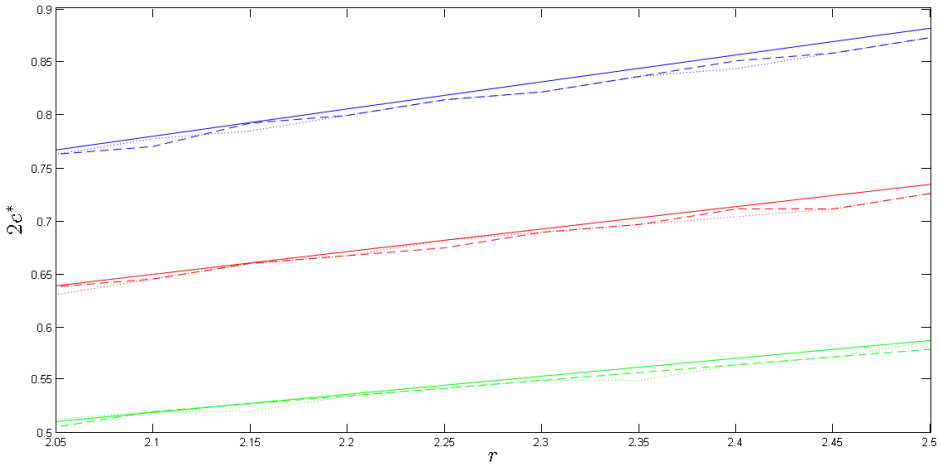

Figure C.6: Theoretical (full line) and numerical speed of operators q (dashed line) and q_2 (dotted line) on $[0, 1]$ with Ricker function and Laplace kernel for different values of a (top: $a = 10$, middle: $a = 12$, bottom: $a = 15$) with respect to r. The plot is generated with a scheme that uses the trapz algorithm, as shown in table D.5.

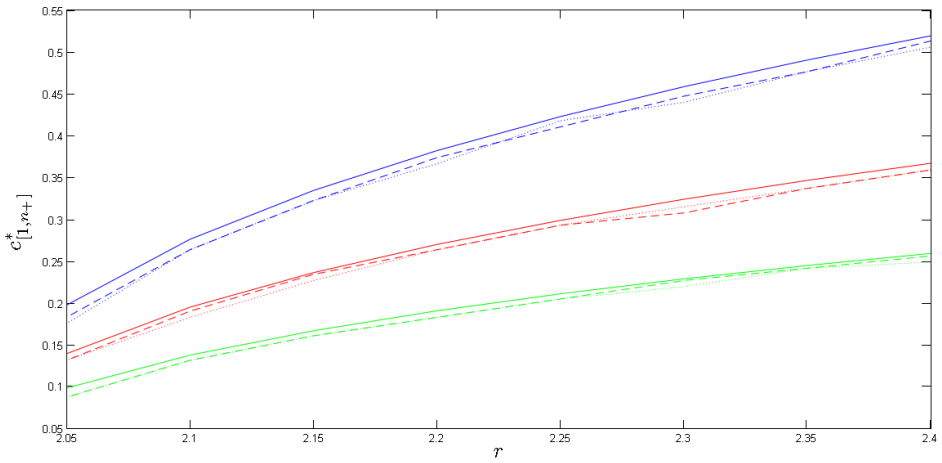

Figure C.7: Theoretical (full line) and numerical speed of operators q (dashed line) and q_2 (dotted line) on $[1, n_+]$ with logistic function and Gaussian kernel for different values of σ^2 (top: $\sigma^2 = 0.1$, middle: $\sigma^2 = 0.05$, bottom: $\sigma^2 = 0.025$) with respect to r. The plot is generated with a scheme that uses the trapz algorithm, as shown in table D.5..

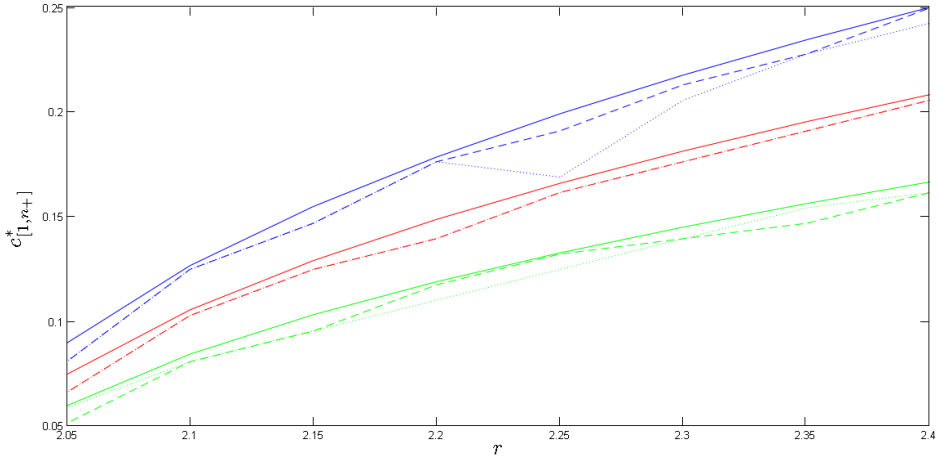

Figure C.8: Theoretical (full line) and numerical speed of operators q (dashed line) and q_2 (dotted line) on $[1, n_+]$ with logistic function and Laplace kernel for different values of a (top: $a = 10$, middle: $a = 12$, bottom: $a = 15$) with respect to r. The plot is generated with a scheme that uses the trapz algorithm, as shown in table D.5.

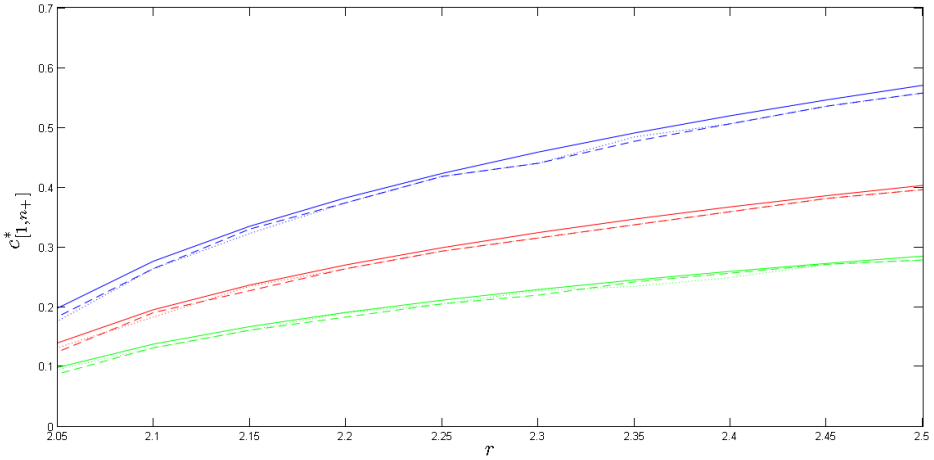

Figure C.9: Theoretical (full line) and numerical speed of operators q (dashed line) and q_2 (dotted line) on $[1, n_+]$ with Ricker function and Gaussian kernel for different values of σ^2 (top: $\sigma^2 = 0.1$, middle: $\sigma^2 = 0.05$, bottom: $\sigma^2 = 0.025$) with respect to the parameter r. The plot is generated with a scheme that uses the trapz algorithm, as shown in table D.5.

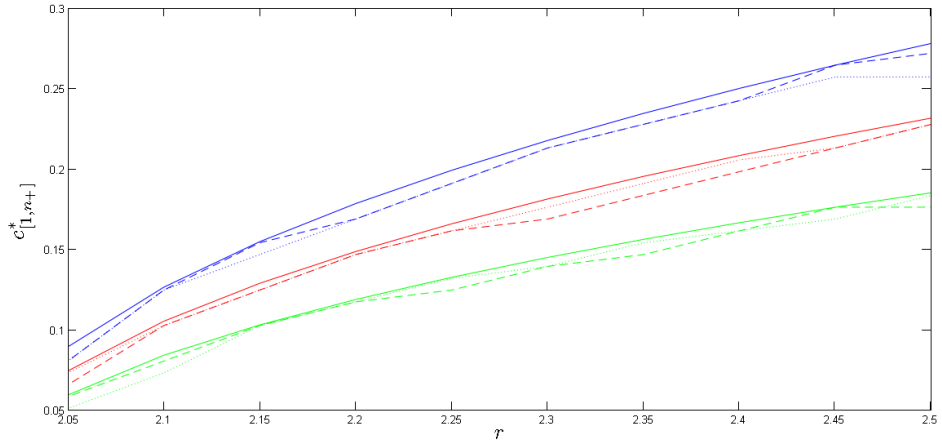

Figure C.10: Theoretical (full line) and numerical speed of operators q (dashed line) and q_2 (dotted line) on $[1, n_+]$ with Ricker function and Laplace kernel for different values of a (top: $a = 10$, middle: $a = 12$, bottom: $a = 15$) with respect to the parameter r. The plot is generated with a scheme that uses the trapz algorithm, as shown in table D.5.

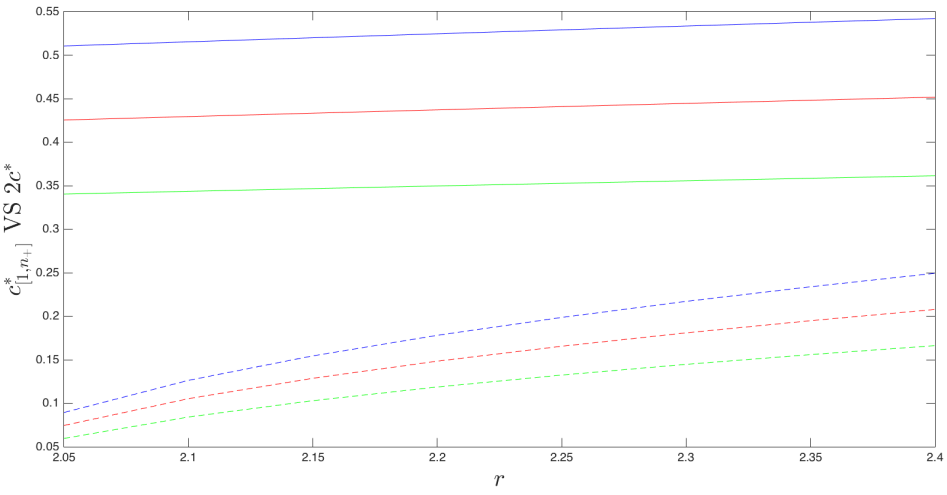

Figure C.11: Theoretical spreading speed on $[0, 1]$ (full line) and $[1, n_+]$ (dashed line) for operator q with the logistic function and Laplace kernel for different values of a (top: $a = 10$, middle: $a = 12$, bottom: $a = 15$) with respect to r.

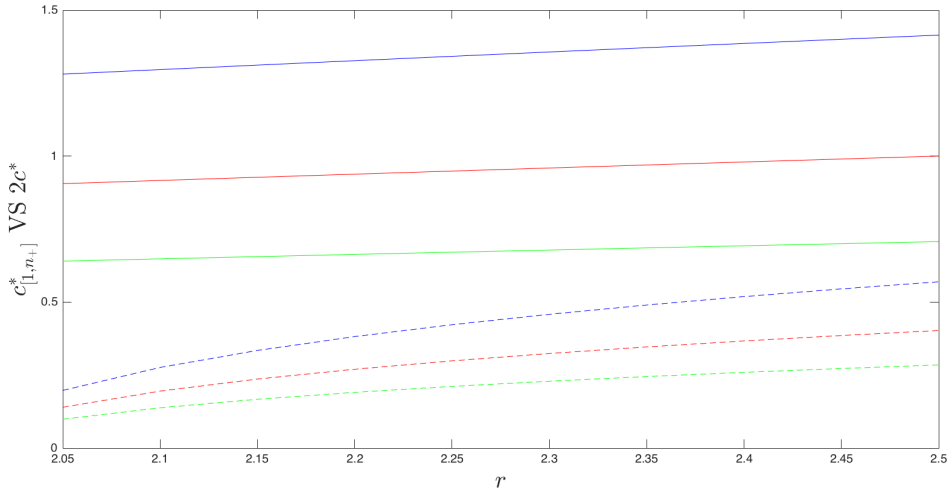

Figure C.12: Theoretical spreading speed on $[0, 1]$ (full line) and $[1, n_+]$ (dashed line) for operator q with the Ricker function and Gaussian kernel for different values of σ^2 (top: $\sigma^2 = 0.1$, middle: $\sigma^2 = 0.05$, bottom: $\sigma^2 = 0.025$) with respect to r.

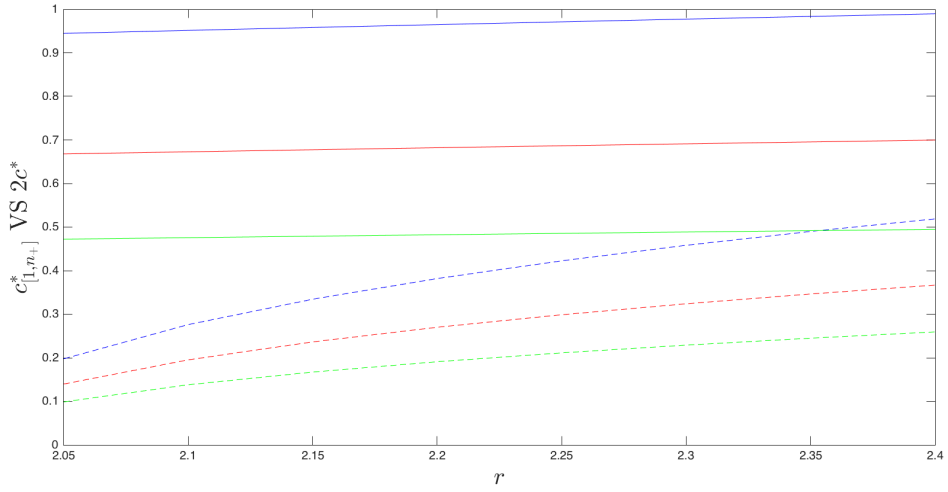

Figure C.13: Theoretical spreading speed on $[0, 1]$ (full line) and $[1, n_+]$ (dashed line) for operator q with the logistic function and Gaussian kernel for different values of σ^2 (top: $\sigma^2 = 0.1$, middle: $\sigma^2 = 0.05$, bottom: $\sigma^2 = 0.025$) with respect to r.

Appendix D

MATLAB® code

```
clear all

growth = 'r'; % must be either 'r' for ricker or 'l' for logistic
if growth ~= 'r' && growth ~= 'l'
    error('not a valid input for the growth function')
end

if growth == 'r'
    rmax = 2.526;
else
    rmax = 2.449;
end


r = 2.025 : 0.025 : rmax;

% Find values of cycle using Newton's method
for k = 1 : length(r)
    if growth == 'r'
        N = 0.2; % first guess for n-

        % Newton's method for finding roots
        for i = 1 : 10000
            f = N + N*exp( r(k)*( 1 - N ) ) - 2;
            df = exp( r(k)*( 1 - N ) )*( 1 - r(k)*N ) + 1;
            N = N - f/df;
        end

        nminus(k) = N;
        nplus(k) = 2 - N;    % n- + n+ = 2 for the Ricker function
```

```
    else
        nminus(k) = ( r(k) + 2 - sqrt( r(k)^2 - 4 ) )/( 2*r(k) );
        nplus(k)  = ( r(k) + 2 + sqrt( r(k)^2 - 4 ) )/( 2*r(k) );
    end

end
```

Table D.1: MATLAB® code to calculate the values of n_-, n_+, n_-^-, n_-^+, n_+^-, n_+^+ for the Ricker function for different values of r.

```
clear all

% Cobweb diagram for Ricker function

i = 5;       % p + 1 for p-cycle
r = 2.625;   % 2 < r < 2.526 for two-cycle
             % 2.526 < r < 2.656 for four-cycle

% Send error messages if input parameters are wrong
if i == 3 && ( r < 2 || r > 2.526 )
    error('For two-cycle, must select values of r in (2, 2.526).')
end

if i == 5 && ( r < 2.526 || r > 2.656 )
    error('For four-cycle, must select values of r in (2.526, 2.656).')
end

if i ~= 3 && i ~= 5
    error('Choose i = 3 or i = 5 to plot two-cycles or four-cycles.')
end

x = 0 : 0.01 : 3;
figure
y = x.*exp( r*( 1 - x ) );
plot( x, y, 'LineSmoothing', 'on' ), hold on
plot( x, x, 'LineSmoothing', 'on' )

% Draw cobweb
k(1) = 0.2;
plot( [ k(1) k(1) ], [ 0, k(1) ], 'r', 'LineSmoothing', 'on' )

for j = 2 : i
    k(j) = k(j-1)*exp( r*( 1 - k(j-1) ) );
    plot([ k(j-1) k(j-1)], [ k(j-1), k(j) ], 'r', 'LineSmoothing', 'on' )
    pause(0.1)
    plot( [ k(j-1) k(j) ], [ k(j) k(j) ], 'r', 'LineSmoothing', 'on' )
```

```
    pause(0.1)
end

j = i - 1;

% Loop until the p-cycle appears
while abs( k(i) - k(i-j) ) > 0.00001
    k(i+1) = k(i)*exp( r*( 1 - k(i) ) );
    plot( [ k(i) k(i) ], [ k(i) k(i+1) ], 'r', 'LineSmoothing', 'on' )
    pause(0.1)
    plot( [ k(i) k(i+1) ], [ k(i+1) k(i+1) ], 'r', 'LineSmoothing', 'on')
    i = i + 1;
    pause(0.1)
end

% return cycle points
for n = 1 : j
    stable(n) = k( length(k) -  n + 1 );
    plot( [ 0 stable(n) ], [ stable(n) stable(n) ], 'b--' )
    plot( [ stable(n) stable(n) ], [ stable(n) 0 ], 'b--' )
end

plot( [ 1 1 ], [ 1 0 ], 'b--' )
plot( [ 0 1 ], [ 1 1 ], 'b--' )

hold off
```

Table D.2: MATLAB® code to draw cobweb diagrams with two-cycles and four-cycles for the Ricker function.

```
clear all

growth = 'r'; % must be either 'r' for ricker or 'l' for logistic
if growth ~= 'r' && growth ~= 'l'
    error('not a valid input for the growth function')
end

if growth == 'r'
    rlast = 2.526;
else
    rlast = 2.449;
end

r = 2:0.0001:rlast;

rmin = r(1);
```

```
rmax = r( length(r) );

while rmax - rmin > 0.00005

    r0 = rmin + ( rmax - rmin )/2;

    if growth == 'r'

        x = 0.2;  % first guess for the value of n-

        % Newton's method for finding roots
        for i = 1 : 10000
            f = x*exp( r0*( 1 - x ) ) - 2 + x;
            df = exp( r0*( 1 - x ) )*( 1 - r0*x ) + 1;
            x = x - f/df;
        end

        criticalpoint = 1/r0;

    else
        x = ( r0 + 2 - sqrt( r0^2 - 4 ) )/( 2*r0 );

        criticalpoint = ( 1 + r0 )/( 2*r0 );

    end

    %define new rmin and rmax
    if x < criticalpoint
        rmax = r0;
    else
        rmin = r0;
    end

end

r0
```

Table D.3: MATLAB® code to find the values of r for which the Ricker function and the logistic function are non-increasing on $[n_-, n_+]$.

```
clear all

% Define domain and parameters
L = 80; np = 2^16; dx = 2*L/np;
x = linspace( -L, L, np + 1 );
```

```
kernel = 'g'; % must be either 'l' for laplace or 'g' for gauss
if kernel ~= 'l' && kernel ~= 'g'
    error('not a valid input for the kernel')
end

growth = 'r'; % must be either 'r' for ricker or 'l' for logistic
if growth ~= 'r' && growth ~= 'l'
    error('not a valid input for the growth function')
end

if growth == 'r'
    R = 2.05 : 0.05 : 2.526;
else
    R = 2.05 : 0.05 : 2.449;
end

Wave = 0;   % 0 if want wave from 0 and 1 for wave from 1

if kernel == 'l'
    a = [ 10, 12, 15 ];
else
    a = [ 0.1, 0.05, 0.025 ];
end

pad = ( x > -L/1.1 );

if Wave == 1
    pad2 = ( x <= -L/2 );
else
    pad2 = ( x < -L );
end

% calculate speeds for different values of a and r
for k = 1 : length(a)

    % Calculate functions K and K*K
    if kernel == 'l'
        Dist = a(k)/2*exp( -a(k)*abs(x) );
        ConvDist = a(k)/4*( a(k)*abs(x) + 1 ).*exp( -a(k)*abs(x) );
    else
        Dist = 1/sqrt( 2*pi*a(k) )*exp( -x.^2/( 2*a(k) ) );
        ConvDist = 1/sqrt( 4*pi*a(k) )*exp( -x.^2/( 4*a(k) ) );
    end

    % Normalize distribution kernels
    integral = trapz( x, Dist );
    NormDist = Dist/integral;
    intConv = trapz( x, ConvDist );
    NormConvDist = ConvDist/intConv;
```

```
FConvDist = fft( NormConvDist );
FDist = fft( NormDist );

for j = 1 : length(R)

    % May have to adjust the time steps in some cases..
    % convergence is slower for Wave = 1 for smaller values of R
    if j < 3
        Tsteps = 60;
    elseif j < 5
        Tsteps = 50;
    else
        Tsteps = 30;
    end

    % Get the value of n+ to generate initial connection for
    % connection between 1 and n+
    if Wave == 1

        if growth == 'l'
            nminus = ( R(j) + 2 - sqrt( R(j)^2 - 4 ) )/( 2*R(j) );
            nplus  = ( R(j) + 2 + sqrt( R(j)^2 - 4 ) )/( 2*R(j) );
        else
            n = 0.2; % first guess for n-

            % Newton's method for finding roots
            for i = 1 : 10000
                f = n + n*exp( R(j)*( 1 - n ) ) - 2;
                df = exp( R(j)*( 1 - n ) )*( 1 - R(j)*n ) + 1;
                n = n - f/df;
            end
            nminus = n;
            nplus = 2 - n; % property of the Ricker function

        end

        N_fft =  nplus*( x >= 10 );
    else
        N_fft = ( x > 10 );
    end

    M_fft = N_fft;

    N_fft1 = 0;
    M_fft1 = 0;
    N_fft2 = 0;
    M_fft2 = 0;
```

```
for i=1:Tsteps
    % keep track of progress
    a(k)
    R(j)
    i

    % Calculate K*F(N)
    if growth == 'r'
        N_fft = N_fft.*exp( R(j)*( 1 - N_fft ) );
    else
        N_fft = ( 1 + R(j) )*N_fft - R(j)*N_fft.^2;
    end
    FN = fft( N_fft );

    % convolute with FFT
    N_fft = dx*real( fftshift( ifft( FN.*FDist ) ) );

    % pad the extremities of the density
    N_fft = N_fft.*pad.*( N_fft > 0.00000000001 );
    N_fft = N_fft + pad2;

    % Calculate K*F(K*F(N))
    if growth == 'r'
        N_fft = N_fft.*exp( R(j)*( 1 - N_fft ) );
    else
        N_fft = ( 1 + R(j) )*N_fft - R(j)*N_fft.^2;
    end
    FN = fft( N_fft );

    % convolute with FFT
    N_fft = dx*real( fftshift( ifft( FN.*FDist ) ) );

    % pad the extremities of the density
    N_fft = N_fft.*pad.*( N_fft > 0.00000000001 );
    N_fft = N_fft + pad2;

    % Calculate K*K*F(F(N))
    if growth == 'r'
        M_fft = M_fft.*exp( R(j)*( 1 - M_fft ) );
        M_fft = M_fft.*exp( R(j)*( 1 - M_fft ) );
    else
        M_fft = ( 1 + R(j) )*M_fft - R(j)*M_fft.^2;
        M_fft = ( 1 + R(j) )*M_fft - R(j)*M_fft.^2;
    end
    FM = fft( M_fft );

    % convolute with FFT
    M_fft = dx*real( fftshift( ifft( FM.*FConvDist ) ) );
```

```
        % pad the extremities of the density
        M_fft = M_fft.*pad.*( M_fft > 0.00000000001 );
        M_fft = M_fft + pad2;

        % track a point on the solution for numerical speed
        if i == Tsteps - 1
            N_fft1 = x( find( N_fft > Wave + 0.05, 1 ) );
            M_fft1 = x( find( M_fft > Wave + 0.05, 1 ) );
        end

        if i == Tsteps
            N_fft2 = x( find( N_fft > Wave + 0.05, 1 ) );
            M_fft2 = x( find( M_fft > Wave + 0.05, 1 ) );
        end

    end

    speed_Nfft( j, k ) = abs( N_fft1 - N_fft2 );
    speed_Mfft( j, k ) = abs( M_fft1 - M_fft2 );

    % calculate theoretical speed
    if Wave == 1    % connection from 1 to n+
        if kernel == 'l'
            lambert = lambertw( -1, -2/( ( R(j) - 1 )*exp(2) ) );
            s = a(k)*sqrt( 2/lambert + 1 );
            speed_theo(j,k) =  4*s/( a(k)^2 - s^2 );
        else
            speed_theo(j,k) =  2*sqrt( a(k)*log( ( 1 - R(j) )^2 ) );
        end
    else    % connection from 0 to 1
        % result if 2 times the speed formula since second iterate
        if kernel == 'l'
            if growth == 'r'
                lambert = lambertw( -1, -2/exp( R(j) + 2 ) );
                s = a(k)*sqrt( 2/lambert + 1 );
            else
                lambert = lambertw( -1, -2/( ( 1 + R(j) )*exp(2) ) );
                s = a(k)*sqrt( 2/lambert + 1 );
            end
            speed_theo(j,k) = 4*s/( a(k)^2 - s^2 );
        else
            if growth == 'r'
                speed_theo(j,k) =  2*sqrt( 2*a(k)*R(j) );
            else
                speed_theo(j,k) =  2*sqrt(2*a(k)*log( 1 + R(j) ));
            end
        end
```

```
        end


    end
end

% calculate error between numerical and theoretical
diff_Nfft = abs( speed_theo - speed_Nfft )./speed_theo*100
diff_Mfft = abs( speed_theo - speed_Mfft )./speed_theo*100

% compare theoretical and numerical speeds
figure
plot( R, speed_theo( :, 1 ), 'b', 'LineSmoothing', 'on' ), hold on
plot( R, speed_theo( :, 2 ), 'r', 'LineSmoothing', 'on' )
plot( R, speed_theo( :, 3 ), 'g', 'LineSmoothing', 'on' )
plot( R, speed_Nfft( :, 1 ), '--b', 'LineSmoothing' ,'on' )
plot( R, speed_Nfft( :, 2 ), '--r', 'LineSmoothing' ,'on' )
plot( R, speed_Nfft( :, 3 ), '--g', 'LineSmoothing' ,'on' )
plot( R, speed_Mfft( :, 1 ), ':b',  'LineSmoothing' ,'on' )
plot( R, speed_Mfft( :, 2 ), ':r',  'LineSmoothing' ,'on' )
plot( R, speed_Mfft( :, 3 ), ':g',  'LineSmoothing' ,'on' ), hold off
```

Table D.4: FFT algorithm to calculate the numerical spreading speed of the IDE solution, where ConvDist is the convolution of the kernel calculated analytically in appendix A.2.

```
clear all

% Define the domain and parameters
L = 50; np = 2^12; dx = 2*L/np;
x = linspace( -L, 10, 2*np );

kernel = 'g'; % must be either 'l' for laplace or 'g' for gauss
if kernel ~= 'l' && kernel ~= 'g'
    error( 'not a valid input for the kernel' )
end

growth = 'r'; % must be either 'r' for ricker or 'l' for logistic
if growth ~= 'r' && growth ~= 'l'
    error( 'not a valid input for the growth function' )
end

if growth == 'r'
    r = 2.05 : 0.05 : 2.526;
else
```

```
    r = 2.05 : 0.05 : 2.449;
end

if kernel == 'l'
    a = [ 10, 12, 15 ];
else
    a = [ 0.1, 0.05, 0.025 ];
end


% generate the solution of the IDE for different values of r and a
for j = 1 : length(a)

    for k = 1 : length(r)

        % define number of Tsteps required before stabilization wave
        % (lowers as r increases)
        if r(k) < 2.3
            Tsteps = 70;
        else
            Tsteps = 40;
        end

        if growth == 'l'
            nminus = ( r(k) + 2 - sqrt( r(k)^2 - 4 ) )/( 2*r(k) );
            nplus  = ( r(k) + 2 + sqrt( r(k)^2 - 4 ) )/( 2*r(k) );
        else
            n = 0.2; % first guess for n-

            % Newton's method for finding roots
            for i = 1 : 10000
                f = n + n*exp( r(k)*( 1 - n ) ) - 2;
                df = exp( r(k)*( 1 - n ) )*( 1 - r(k)*n ) + 1;
                n = n - f/df;
            end
            nminus = n;
            nplus = 2 - n; % property of Ricker function
        end

        %Initial conditions for operator K*F(K*F(N))
        N1 = ( x <= 0 ) + nplus*( x > 0 );    % studying 1 to n+
        N2 = ( x > 0 );                       % studying at 0

        %Initial conditions for operator K*K*F(F(N))
        M1 = ( x <= 0 ) + nplus*( x > 0 );    % studying 1 to n+
        M2 = ( x > 0 );                       % studying at 0


        for t = 1 : Tsteps
```

```
%output to follow progress
a(j)
r(k)
t

% Calculate K*F(K*F(N))
if growth == 'r'
    func  = N1.*exp( r(k)*( 1 - N1 ) );
    func2 = N2.*exp(r(k)*(1 - N2));
else
    func  = ( 1 + r(k) )*N1 - r(k)*N1.^2;
    func2 = ( 1 + r(k) )*N2 - r(k)*N2.^2;
end

for i = 1 : length(x)

    % get K(x-y) = K(y-x)
    if kernel == 'l'
        dist = a(j)/2*exp( -a(j)*abs( x(i) - x ) );
    else
        expo = exp( -(( x(i) - x ).^2)./( 2*a(j) ) );
        dist = 1/sqrt( 2*pi*a(j) )*expo;
    end

    norm = trapz( x, dist );

    % normalize kernels and calculate K(x-y)F(N)
    integral  = ( dist/norm ).*func;
    integral2 = ( dist/norm ).*func2;

    % integrate with trapezoid rule for convolution
    Next1(i) = trapz( x, integral );
    Next2(i) = trapz( x, integral2 );
end

N1 = Next1;
N2 = Next2;

% Calculate K*F(K*F(N)) and K*K*F(F(N))
% iteration for K*F(K*F(N)) is done twice since the
% connection between 1 and n+ appears every second timestep
% whereas it appears every timestep for K*K*F(F(N))
if growth == 'r'
    func  = N1.*exp( r(k)*( 1 - N1 ) );
    func2 = N2.*exp( r(k)*( 1 - N2 ) );

    % second iterate functions
    func3 = M1.*exp( r(k)*( 1 - M1 ) );
    func3 = func3.*exp( r(k)*( 1 - func3 ) );
```

```
        func4 = M2.*exp( r(k)*( 1 - M2 ) );
        func4 = func4.*exp( r(k)*( 1 - func4 ) );
    else
        func  = ( 1 + r(k) )*N1 - r(k)*N1.^2;
        func2 = ( 1 + r(k) )*N2 - r(k)*N2.^2;

        % second iterate functions
        func3 = ( 1 + r(k) )*M1 - r(k)*M1.^2;
        func3 = ( 1 + r(k) )*func3 - r(k)*func3.^2;
        func4 = ( 1 + r(k) )*M2 - r(k)*M2.^2;
        func4 = ( 1 + r(k) )*func4 - r(k)*func4.^2;
    end

    for i = 1 : length(x)

        % get K(x-y) and K*K(x-y)
        if kernel == 'l'
            dist = a(j)/2*exp( -a(j)*abs( x(i) - x ) );
            expo = exp(-a(j)*abs( x(i) - x ) );
            convDist = a(j)/4*( a(j)*abs( x(i) - x) + 1 ).*expo;
        else
            expo1 = exp( -( ( x(i)-x ).^2 )./( 2*a(j) ) )
            dist = 1/sqrt( 2*pi*a(j) )*expo1;
            expo2 = exp( -( x(i) - x ).^2/( 4*a(j) ) )
            convDist = 1/sqrt( 4*pi*a(j) )*expo2;
        end

        norm = trapz( x, dist );
        normConv = trapz( x, convDist );

        % normalize kernels and calculate K(x-y)F(N)
        integral  = ( dist/norm ).*func;
        integral2 = ( dist/norm ).*func2;

        % normalize kernels and calculate K*K(x-y)F(F(N))
        integral3 = ( convDist/normConv ).*func3;
        integral4 = ( convDist/normConv ).*func4;

        % integrate with trapezoid rule for convolution
        Next1(i) = trapz( x, integral );
        Next2(i) = trapz( x, integral2 );
        Mext1(i) = trapz( x, integral3 );
        Mext2(i) = trapz( x, integral4 );
    end

    N1 = Next1;
    N2 = Next2;
    M1 = Mext1;
    M2 = Mext2;
```

```
        % define points on curve that will act as references to
        % calculate the wave speed

        % Track a positive point in the solution
        if t == Tsteps/2 - 1
            trackFirst1 = find( N2 > 0.01, 1 );
            trackFirstM = find( M2 > 0.01, 1 );
        elseif t == Tsteps/2
            trackFirst2  = find( N2 > 0.01, 1 );
            trackFirstM2 = find( M2 > 0.01, 1 );

        % Track the midpoint of 1 and n+ in the solution
        mid = ( nplus - 1 )/2;
        elseif t == Tsteps-1
            p = N1( 1:find( x > 0, 1 ) - 1 );
            trackSecond1 = find( p < 1 + mid, 1, 'last' );
            p2 = M1( 1:find( x > 0, 1 ) - 1 );
            trackSecondM = find( p2 < 1 + mid, 1, 'last' );
        elseif t == Tsteps
            p = N1( 1:find( x > 0, 1 ) - 1 );
            trackSecond2 = find( p < 1 + mid, 1, 'last' );
            p2 = M1( 1:find( x > 0, 1 ) - 1 );
            trackSecondM2 = find( p2 < 1 + mid, 1, 'last' );
        end

    end

    num_speed1( k, j )  = ( x( trackFirst1 )  - x( trackFirst2 ) );
    num_speed2( k, j )  = ( x( trackSecond1 ) - x( trackSecond2 ) );
    num_speedM1( k, j ) = ( x( trackFirstM )  - x( trackFirstM2 ) );
    num_speedM2( k, j ) = ( x( trackSecondM ) - x( trackSecondM2 ) );

    % Theoretical for first part of the wave
    % The formula is multiplied by 2 at the end since second iterate
    if kernel == 'l'
        if growth == 'r'
            lambert = lambertw( -1, -2/exp( r(k) + 2 ) );
            s = a(j)*sqrt( 2/lambert + 1 );
        else
            lambert = lambertw( -1, -2/( (1 + r(k))*exp(2) ) );
            s = a(j)*sqrt( 2/lambert + 1 );
        end
        theo_speed1( k, j ) = 4*s/( a(j)^2 - s^2 );
    else
        if growth == 'r'
            theo_speed1( k, j ) = 2*sqrt( 2*a(j)*r(k) );
        else
            theo_speed1( k, j ) = 2*sqrt( 2*a(j)*log( 1 + r(k) ) );
```

```
            end
        end

        % Theoretical for second part of the wave
        if kernel == '1'
            lambert = lambertw( -1, -2/( ( r(k)-1 )*exp(2) ) );
            s = a(j)*sqrt( 2/lambert + 1 );
            theo_speed2( k, j ) = 4*s/( a(j)^2-s^2 );
        else
            theo_speed2( k, j ) = 2*sqrt( a(j)*log( ( 1 - r(k) )^2 ) );
        end

    end

end

% compare  numerical speed on 0 to 1 of both operators with theoretical
figure
plot( r, theo_speed1( :, 1),  'b',   'LineSmoothing', 'on' ), hold on
plot( r, num_speed1( :, 1 ),  'b--', 'LineSmoothing', 'on' )
plot( r, num_speedM1( :, 1 ), 'b:',  'LineSmoothing', 'on' )
plot( r, theo_speed1( :, 2 ), 'r',   'LineSmoothing', 'on' )
plot( r, num_speed1( :, 2 ),  'r--', 'LineSmoothing', 'on' )
plot( r, num_speedM1( :, 2 ), 'r:',  'LineSmoothing', 'on' )
plot( r, theo_speed1( :, 3 ), 'g',   'LineSmoothing', 'on' )
plot( r, num_speed1( :, 3 ),  'g--', 'LineSmoothing', 'on' )
plot( r, num_speedM1( :, 3 ), 'g:',  'LineSmoothing', 'on' ), hold off

% compare numerical speed on 1 to n+ of both operators with theoretical
figure
plot( r, theo_speed2( :, 1),  'b',   'LineSmoothing', 'on' ), hold on
plot( r, num_speed2( :, 1 ),  'b--', 'LineSmoothing', 'on' )
plot( r, num_speedM2( :, 1 ), 'b:',  'LineSmoothing', 'on' )
plot( r, theo_speed2( :, 2 ), 'r',   'LineSmoothing', 'on' )
plot( r, num_speed2( :, 2 ),  'r--', 'LineSmoothing', 'on' )
plot( r, num_speedM2( :, 2 ), 'r:',  'LineSmoothing', 'on' )
plot( r, theo_speed2( :, 3 ), 'g',   'LineSmoothing', 'on' )
plot( r, num_speed2( :, 3 ),  'g--', 'LineSmoothing', 'on' )
plot( r, num_speedM2( :, 3 ), 'g:',  'LineSmoothing', 'on' ),hold off

% compare theoretical speeds of 0 to 1 and 1 to n+
figure
plot( r, theo_speed1( :, 1 ), 'b',   'LineSmoothing', 'on' ), hold on
plot( r, theo_speed2( :, 1 ), 'b--', 'LineSmoothing', 'on' )
plot( r, theo_speed1( :, 2 ), 'r',   'LineSmoothing', 'on' )
plot( r, theo_speed2( :, 2 ), 'r--', 'LineSmoothing', 'on' )
plot( r, theo_speed1( :, 3 ), 'g',   'LineSmoothing', 'on' )
plot( r, theo_speed2( :, 3 ), 'g--', 'LineSmoothing', 'on' ), hold off
```

```
% Compare theoretical and numerical speeds
error1 = ( abs( num_speed1-theo_speed1 )./theo_speed1 )*100
error2 = ( abs( num_speed2-theo_speed2 )./theo_speed2 )*100
error3 = ( abs( num_speedM1-theo_speed1)./theo_speed1 )*100
error4 = ( abs( num_speedM2-theo_speed2)./theo_speed2 )*100
```

Table D.5: Trapezoid method to calculate the numerical spreading speed of the IDE solution, where ConvDist is the convolution of the kernel calculated analytically in appendix A.2.

```
clear all

a = 15; % can be any value
r = 1.0001:0.0001:1.5;

rootRicker = 0;
rootLog = 0;
i = 1;
x = -10:0.0001:0; % look at lambda negative


while rootRicker == 0 || rootLog == 0

    % calculate right side of transcendental eigenvalue problem
    Fprime = 1 - r(i);
    y2 = Fprime*exp(-x);

    if rootRicker == 0
        % calculate the left side of transcendental eigenvalue problem
        sRicker = a*sqrt( 2/lambertw( -1, -2/exp( r(i) + 2 ) ) + 1 );
        cRicker = 2*sRicker/( a^2 - sRicker^2 );
        y1Ricker = 1 - x.^2./( a^2*cRicker^2 );

        yRicker = abs( y1Ricker - y2 );

        if all( yRicker > 0.0001 )   % no roots - keep iterating
            rootRicker = i;
        end
    end

    if rootLog == 0
        % calculate the left side of transcendental eigenvalue problem
        sLog = a*sqrt( 2/lambertw( -1, -2/( (r(i) + 1)*exp(2) ) ) + 1 );
        cLog = 2*sLog/( a^2 - sLog^2 );
        y1Log = 1 - x.^2./( a^2*cLog^2 );
```

```
        yLog = abs( y1Log - y2 );

        if all( yLog > 0.0001 )   % not roots - keep iterating
            rootLog = i;
        end
    end

    i = i + 1;
end

% return the first value of r for which there was no real root
r(rootRicker)
r(rootLog)
```

Table D.6: MATLAB® code to determine the values of r for which a negative real root exists in equation (4.3.6).

```
clear all
figure

a = 15;    % can be any value

% plots for Ricker function
r = [1.0327, 2.526];
for i = 1:length(r)

    s = a*sqrt( 2/lambertw( -1, -2/exp( r(i) + 2 ) ) + 1 );
    c = 2*s/( a^2 - s^2 );
    param = a^2*c^2;

    Fprime = 1 - r(i);

    % generate implicite functions
    func = @(x,y) 1 - (( x.^2 - y.^2 )./param) - Fprime*exp(-x).*cos(y);
    func2 = @(x,y) 2*x.*y./param + Fprime*exp(-x)*sin(y);

    subplot(2, 2, i)
    ez1 = ezplot( func, [-20, 20, -20, 20] ), hold on
    ez2 = ezplot( func2, [-20, 20, -20, 20] )
    set( ez1, 'color', 'red' )
    set( ez2, 'color', 'blue' )
    hold off

end

% plots for logistic equation
```

```
r = [1.0686, 2.449]
for i = 1:length(r)

    s = a*sqrt( 2/lambertw( -1, -2/( ( r(i) + 1 )*exp(2) ) ) + 1 );
    c = 2*s/( a^2 - s^2 );
    param = a^2*c^2;

    Fprime = 1 - r(i);

    % generate implicit functions
    func = @(x,y) 1 - (( x.^2 - y.^2 )./param) - Fprime*exp(-x).*cos(y);
    func2 = @(x,y) 2*x.*y./param + Fprime*exp(-x)*sin(y);

    subplot( 2, 2, i+2 )
    ez1 = ezplot( func, [-20, 20, -20, 20] ), hold on
    ez2 = ezplot( func2, [-20, 20, -20, 20] )
    set( ez1,'color','red')
    set( ez2, 'color', 'blue' )
    hold off

end
```

Table D.7: MATLAB® code to plot figure 4.12.

```
clear all

a = 15;     % can be any value
r = 2 : 0.0001 : 3.5;

% calculate the spreading speed
sRicker = a*sqrt( 2./lambertw( -1, -2./(exp( r + 2 )) ) + 1 );
cRicker = 2*sRicker./( a^2 - sRicker.^2 );
paramRicker = a^2*cRicker.^2;

sLog = a*sqrt(2./lambertw( -1, -2./( (r + 1)*exp(2) ) ) + 1 );
cLog = 2*sLog./( a^2 - sLog.^2 );
paramLog = a^2*cLog.^2;

% calculate left and right sides of implicit equation
y1 = r - 1;
y2Ricker = 1 + pi^2./paramRicker;
y2Log =    1 + pi^2./paramLog;

% find approximation of root
r(find( abs(y1 - y2Ricker) < 0.0001 ))
r(find( abs(y1 - y2Log) < 0.0001 ))
```

```
% plot to confirm graphically
plot( r, y1, 'r', 'LineSmoothing', 'on' ), hold on
plot( r, y2Ricker, 'LineSmoothing', 'on' )
plot( r, y2Log, 'LineSmoothing', 'on' )
hold off
```

Table D.8: MATLAB® code to find the root of equation (4.3.14).

```
clear all

% look at values of r where F is monotone on [n−,n+]
r = 2.0001 : 0.0001 : 2.2361;

for k=1:length(r)

    % calculate the value of n− and n+
    nminus = ( r(k) + 2 − sqrt( r(k)^2 − 4 ) )/( 2*r(k) );
    nplus  = ( r(k) + 2 + sqrt( r(k)^2 − 4 ) )/( 2*r(k) );

    % calculate F'(n−) and F'(n+)
    FprimeMinus = 1 + r(k) − 2*r(k)*nminus;
    FprimePlus = 1 + r(k) − 2*r(k)*nplus;

    y(k) = FprimeMinus*FprimePlus;

    test(k) = (FprimeMinus*FprimePlus < 1);

end

% see if any value of r violates the assumption
any(test == 0)

% plot to confirm graphically
plot(r,y)
```

Table D.9: MATLAB® code to verify if $0 < F'(n_-)F'(n_+) < 1$ for the logistic function when $2 < r < 2.2361$.

Bibliography

[1] Invasive Species Center. `http://www.invasivespeciescentre.ca/SitePages/default.aspx`. Accessed: 2016-01-19.

[2] Wolfram MathWorld: Moment-generating function. `http://mathworld.wolfram.com/Moment-GeneratingFunction.html`. Accessed: 2015-07-14.

[3] Global stability of traveling fronts and convergence towards stacked families of waves in monotone parabolic systems. *SIAM Journal on Mathematical Analysis*, 27:1261–1269, 1996.

[4] R. Colautti, S. Bailey, C. Overdijk, K. Amundsen, and H. MacIsaac. Characterised and projected costs of nonindigenous species in canada. *Biological Invasions*, 8(1):45–59, 2006.

[5] R.M. Corless, G.H. Gonnet, D.E.G. Hare, D.J. Jeffrey, and D.E. Knuth. On the Lambert W function. *Advances in Computational Mathematics*, 5:329–359, 1996.

[6] G. de Vries, T. Hillen, M. Lewis, J. Müller, and B. Schönfisch. *A Course in Mathematical Biology: Quantitative Modeling with Mathematical and Computational Methods*. Monographs on Mathematical Modeling and Computation. Society for Industrial and Applied Mathematics, 2006.

[7] R.D. Driver. *Ordinary and Delay Differential Equations*. Springer Science and Business Media, 2012.

[8] P.C. Fife and J.B. McLeod. The approach of solutions of nonlinear diffusion equations to travelling front solutions. *Archive for Rational Mechanics and Analysis*, 65:335–361, 1977.

[9] G.B. Folland. *Real analysis modern techniques and their applications*. John Wiley & Sons, Inc., 1999.

[10] O. Galor. *Discrete Dynamical Systems*. Springer Berlin Heidelberg, 2007.

[11] J.W. Green and F.A. Valentine. On the Arzela-Ascoli theorem. *Mathematics Magazine*, 34(4):199–202, 1961.

[12] S. Hsu and X. Zhao. Spreading speeds and traveling waves for nonmonotone integrodifference equations. *SIAM Journal on Mathematical Analysis*, 40(2):776–789, 2008.

[13] M. Iida, R. Lui, and H. Ninomiya. Stacked fronts for cooperative systems with equal diffusion coefficients. *SIAM Journal on Mathematical Analysis*, 43:1369–1389, 2011.

[14] M. Kot. Discrete-time traveling waves: Ecological examples. *Journal of Mathematical Biology*, 30:413–436, 1992.

[15] M. Kot and W.M. Schaffer. Discrete-time growth-dispersal models. *Mathematical Biosciences*, 80:109–136, 1986.

[16] J. Labelle and A. Mercier. *Introduction à l'analyse réelle*. Modulo Éditeur, 1993.

[17] B. Li, M.A. Lewis, and H.F. Weinberger. Existence of traveling waves for integral recursions with nonmonotone growth functions. *Journal of Mathematical Biology*, 58:323–338, 2009.

[18] R. Lui. Existence and stability of travelling wave solutions of a nonlinear integral operator. *Journal of Mathematical Biology*, 16:199–220, 1983.

[19] H. Malchow and S.V. Petrovskii. Dynamical stabilization of an unstable equilibrium in chemical and biological systems. *Mathematical and Computer Modelling*, 36:307–319, 2002.

[20] H. Malchow, S.V. Petrovskii, and E. Venturino. *Spatiotemporal Patterns in Ecology and Epidemiology*. Chapman and Hall CRC, 2008.

[21] N.G. Marculis and R. Lui. Modelling the biological invasion of Carcinus maenas (the European green crab). *Journal of Biological Dynamics*, 10(1):140–163, 2016.

[22] R.M. May. Biological populations obeying difference equations: Stable points, stable cycles, and chaos. *Journal of Theoretical Biology*, 51:511–524, 1975.

[23] S.V. Petrovskii and H. Malchow. A minimal model of pattern formation in a prey-predator system. *Mathematical and Computer Modelling*, 29(8):49–63, 1999.

[24] S.V. Petrovskii and H. Malchow. Critical phenomena in plankton communities: KISS model revisited. *Nonlinear Analysis: Real World Applications*, 1:37–51, 2000.

[25] J. Powell. Spatiotemporal models in ecology: an introduction to integro-difference equations. Technical report, Utah State University, 2009.

[26] W.E. Ricker. Stock and recruitment. *Journal of the Fisheries Board of Canada*, 11(5):559–623, 1954.

[27] H.R. Thieme. Density-dependent regulation of spatially distributed populations and their asymptotic speed of spread. *Journal of Mathematical Biology*, 8:173–187, 1979.

[28] M-H. Wang and M. Kot. Speeds of invasion in a model with strong or weak Allee effects. *Mathematical Biosciences*, 171:83–97, 2001.

[29] M-H. Wang, M. Kot, and M.G. Neubert. Integrodifference equations, Allee effects and invasions. *Journal of Mathematical Biology*, 44:150–168, 2002.

[30] H.F. Weinberger. Asymptotic behavior of a model in population genetics. *Nonlinear partial differential equations and applications*, 648:47–96, 1978.

[31] H.F. Weinberger. Long-time behavior of a class of biological models. *SIAM Journal on Mathematical Analysis*, 13(3):353–396, 1982.

[32] H.F. Weinberger and X-Q. Zhao. An extension of the formula for spreading speeds. *Mathematical Biosciences and Engineering*, 7(1):187–194, 2010.

[33] T. Yi and X. Zou. Asymptotic behavior, spreading speeds and traveling waves of nonmonotone dynamical systems. *SIAM Journal on Mathematical Analysis*, 47(3):3005–3034, 2015.